INVESTIGATING THE INTERACTIONS BETWEEN THE THIOLATE LIGAND AND MUTANTS OF A CONSERVED TRYPTOPHAN IN THE PROXIMAL HEME POCKET OF THE OXYGENASE DOMAINS OF ENDOTHELIAL AND *STAPHYLOCCUS AUREUS* NITRIC OXIDE SYNTHASES

by

Danelle Rae Driscoll

A thesis submitted to the Department of Chemistry

In conformity with the requirements for

the degree of Master of Science

Queen's University

Kingston, Ontario, Canada

(September, 2008)

Abstract

The electronegativity of thiolate ligation in the hemeprotein nitric oxide synthase (NOS) proteins has been identified as an influence on autoinhibition in this enzyme. The mutation of a conserved tryptophan residue, which hydrogen bonds to the coordinating thiolate ligand and therefore influences its electronegativity, to either phenylalanine or tyrosine has had various effects including heme loss and dimer disruption in the inducible isoforms, while hyperactivity occurs in the neuronal isoforms. I have performed the analogous mutations in W180 of $eNOS_{oxy}$, the endothelial isoform. UV/visible and resonance Raman spectroscopy have demonstrated that the mutants experienced increased basicity of the thiolate due to loss of the hydrogen bond between the mutated residue in the absence of the cofactor (6R)5,6,7,8-tetrahydrobiopterin (H_4B). The mutants also displayed relative rates of NO_2^- production that were comparable to the $nNOS_{oxy}$ mutants, which is consistent with the $nNOS_{oxy}$ results. The presence of H_4B alters porphyrin planarity, which enabled hydrogen bonding to occur in W180Y, thus restoring thiolate basicity to that of wild-type $eNOS_{oxy}$. Reduced overall activities by the proteins suggest that H_4B stabilizes the heme.

The analogous W56 mutants of saNOS, a NOS oxygenase domain-like protein from *Staphylococcus aureus* (saNOS), have been previously characterized using resonance Raman spectroscopy. These mutants also exhibit increased thiolate electronegativity over wild-type. As the homodimers had already been investigated, saNOS was an ideal system in which to explore heterodimers. Heterodimers were generated through the co-expression of one wild-type and one mutated subunit, enabling the examination of each subunit individually through resonance Raman spectroscopy. The subunits of the resulting proteins were shown to have heme environments that

resembled those of their corresponding homodimers. The activity of saNOS did not vary significantly for the various W56 mutants, suggesting that saNOS catalysis may be unaffected by thiolate electronegativity.

Acknowledgements

I would like to thank those who have provided encouragement and support over the course of my project. I could not have conducted my studies without my supervisor Dr. Steven Rafferty, and I must thank him for his guidance and inspiration, for letting me follow my own path, and for leading me back when I've gone astray.

I wish to thank my collaborator Dr. Manon Couture, and her students François Chartier, Jérôme Lang, and Stéphanie Gélinas, at Université Laval for their assistance, knowledge, patience (particularly with my French lessons), and for making me feel at home in their lab when I brought my protein samples to Québec for resonance Raman spectroscopy. I would also like to thank Jérôme for sharing his data on the saNOS W56 homodimeric proteins with me. I especially wish to acknowledge Dr. Couture and her family for their wonderful hospitality while I was working in her lab.

I am thankful for the support of my graduate supervisory committee members, Dr. Bruce Hill and Dr. Robert Campbell. Their insights into my research have been invaluable.

I also wish to thank Dr. Janet Yee and the members of the Rafferty and Yee labs, past and present, for sharing their knowledge and occasionally their protein samples. They have been a pleasure to work with, and have made this journey more fulfilling.

I would like to acknowledge the financial support provided by Queen's and Trent Universities.

Finally, I wish to thank my family and friends for their support. I could not have gotten through my studies without every last one of them.

For those who inspire me to inspire myself

Table of Contents

List of Figures

List of Tables

List of Abbreviations

AEBSF	4-(2-aminoethyl)-benzenesulfonyl fluoride hydrochloride
AEC	Anion exchange chromatography
ALA	5-aminolevulinic acid hydrochloride
CaM	Calmodulin
CO	Carbon monoxide
$\delta_{Fe\text{-}C\text{-}O}$	Fe(II)CO bending mode
$\delta_{Fe\text{-}N\text{-}O}$	Fe(III)NO bending mode
eNOS	Endothelial nitric oxide synthase
$eNOS_{oxy}$	Endothelial nitric oxide synthase oxygenase domain
FAD	Flavin adenine dinucleotide
Fe^{2+}	Ferrous heme iron
Fe^{3+}	Ferric heme iron
FMN	Flavin mononucleotide
$FMNH^{\cdot}$	Reduced flavin mononucleotide radical
$FMNH_2$	Fully reduced flavin mononucleotide
Glu_7	Polyglutamate tag
H_4B	(6R)5,6,7,8-tetrahydrobiopterin
HCl	Hydrochloric acid
HEPES	*N*-2-hydroxyethylpiperazine-*N'*-2-ethanesulfonic acid
His_6	Polyhistidine tag
HNS	Heme domain of NO Synthase-like protein
HPLC	High performance liquid chromatography
IMAC	Immobilized metal ion affinity chromatography
iNOS	Inducible nitric oxide synthase
$iNOS_{oxy}$	Inducible nitric oxide synthase oxygenase domain
ITU	Ethylisothiourea
L-Arg	L-arginine
LB	Luria Bertani Broth
L-NHA	$^{\omega}$N-Hydroxy-L-arginine
NAD^+	Nicotinamide adenine dinucleotide

NADPH	Nicotinamide adenine dinucleotide phosphate, reduced
$\nu_{Fe\text{-}CO}$	Fe(II)CO stretching mode
$\nu_{Fe\text{-}NO}$	Fe(III)NO stretching mode
Ni-NTA	Nickel-nitrilotriacetic acid
nNOS	Neuronal nitric oxide synthase
$nNOS_{oxy}$	Neuronal nitric oxide synthase oxygenase domain
NO	Nitric oxide
NO^-	Nitroxyl ion
NO_2^-	Nitrite
NO_3^-	Nitrate
NOS	Nitric oxide synthase
S	Spin state
saNOS	NOS oxygenase domain-like protein from *Staphylococcus aureus*
SDS-PAGE	Sodium dodecyl sulfate polyacrylamide gel electrophoresis
TB	Terrific Broth
Tris	Tris-(hydroxymethyl)aminomethane

Chapter 1. Introduction

Nitric oxide (NO) is a diatomic free radical gas. It is produced as a byproduct of combustion and is a highly toxic compound found in air pollution and cigarette smoke. Its toxicity is due to the reaction of NO with oxygen to produce highly reactive nitrogen-oxygen species that chemically damage proteins and DNA. It is thus surprising, with its high degree of toxicity and potency, that NO is also a biological signaling molecule. Its importance as a biological messenger was recognized in 1998, when three scientists were awarded the Nobel Prize in Physiology or Medicine for their research involving the role of NO as a signaling molecule in the cardiovascular system.[1] NO is active in many roles, including vasodilation, neurotransmission, and immune response, and it is carefully regulated as insufficient or excessive production leads to disease. Insufficient NO production has been associated with hypertension, atherosclerosis, and restenosis.[2] Overproduction of NO has been connected to rheumatic diseases, septic shock, diabetes mellitus, cerebral ischemia, Parkinson's disease, strokes, hypotension, neurotoxicity, Alzheimer's disease, tumours, and Multiple Sclerosis.[2; 3]

1.1. Nitric Oxide Synthase Proteins

Nitric oxide synthase (NOS) proteins are found in a wide variety of organisms, from bacteria to primates. Because the roles of nitric oxide are so diverse, there are many different isoforms of NOS proteins, both mammalian and bacterial. Despite these differences, some structural elements are conserved amongst all NOSs, and although there is some debate with respect to the bacterial isoforms, they are all thought to catalyze the synthesis of NO.

1.1.1. General Structure

NOS proteins belong to a family of heme-containing proteins that possess a thiolate as the proximal heme ligand. This family includes the heme chloroperoxidases and cytochrome P450 enzymes. NOS and P450 enzymes bind heme in the form of iron protoporphyrin IX (Figure 1A). NOS is unlike most of these enzymes as it contains both a heme-containing oxygenase domain and a reductase domain within one peptide (Figure 2). The cytochrome P450s, for example, are oxygenase proteins that interact with separate reductase proteins.

There are three mammalian isoforms of NOS: neuronal (nNOS, NOS-1), inducible (iNOS, NOS-2), and endothelial (eNOS, NOS-3), which share 51-57% sequence identity, and range in size from 131 to 161 kDa.[4] The eNOS and nNOS isoforms are named based on their primary tissue locations and related functions, but iNOS is found in a variety of tissues due to its role in immune response, and is named due to its difference in expression from the other two mammalian NOSs. The iNOS and nNOS isoforms are soluble proteins, but eNOS is membrane-anchored.[5] Both eNOS and nNOS are constitutively expressed, but iNOS expression requires induction by inflammatory agents, such as interferon γ.[6] Activation of eNOS and nNOS occurs in response to an increase in intracellular calcium ion (Ca^{2+}) levels, which stimulates the binding of calcium to calmodulin. The calcium-calmodulin (Ca/CaM) complex then binds to the calmodulin-binding region of NOS, which stimulates the reductase domain to initiate the transfer of electrons from NADPH.[7; 8; 9] The iNOS isoform is expressed with CaM bound to the protein, making it insensitive to intracellular Ca^{2+} concentration differences, and is thus always active.[10]

The mammalian NOS proteins are termed homodimeric, but they may be

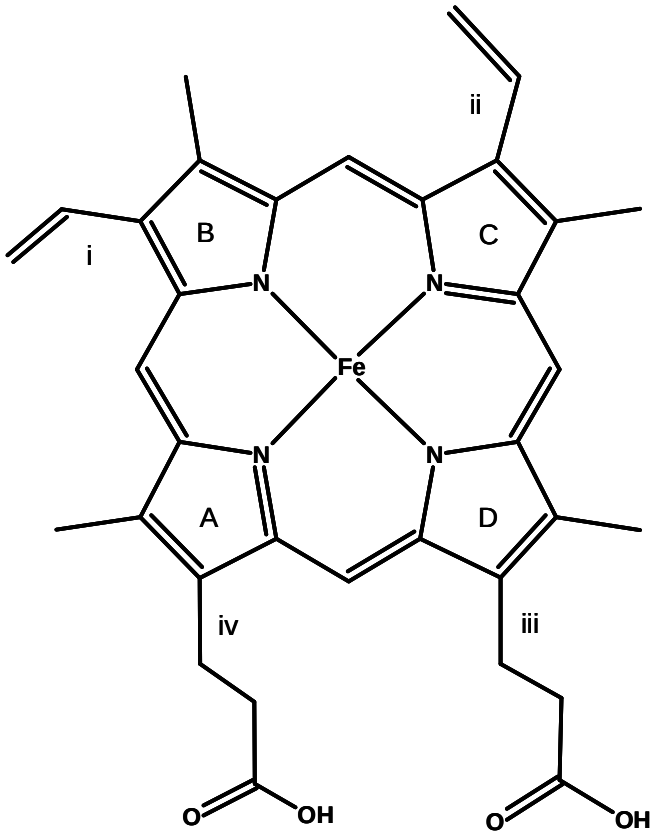

A

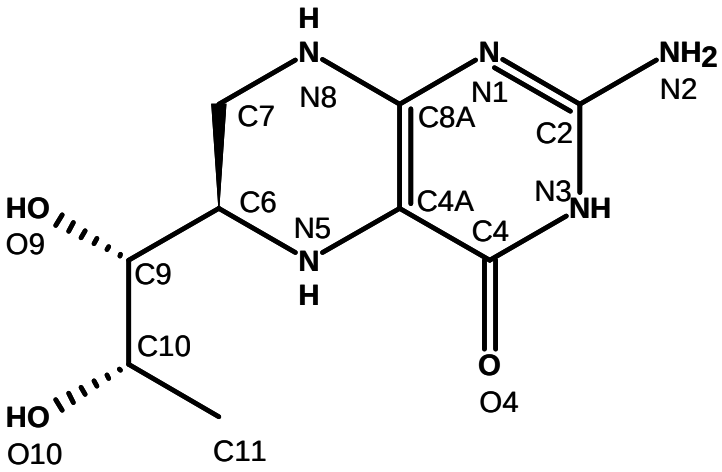

B

Figure 1. The cofactors of mammalian NOS oxygenase domains. The structures of iron protoporphyrin IX (A) and (6R)5,6,7,8-tetrahydrobiopterin, or H_4B (B).

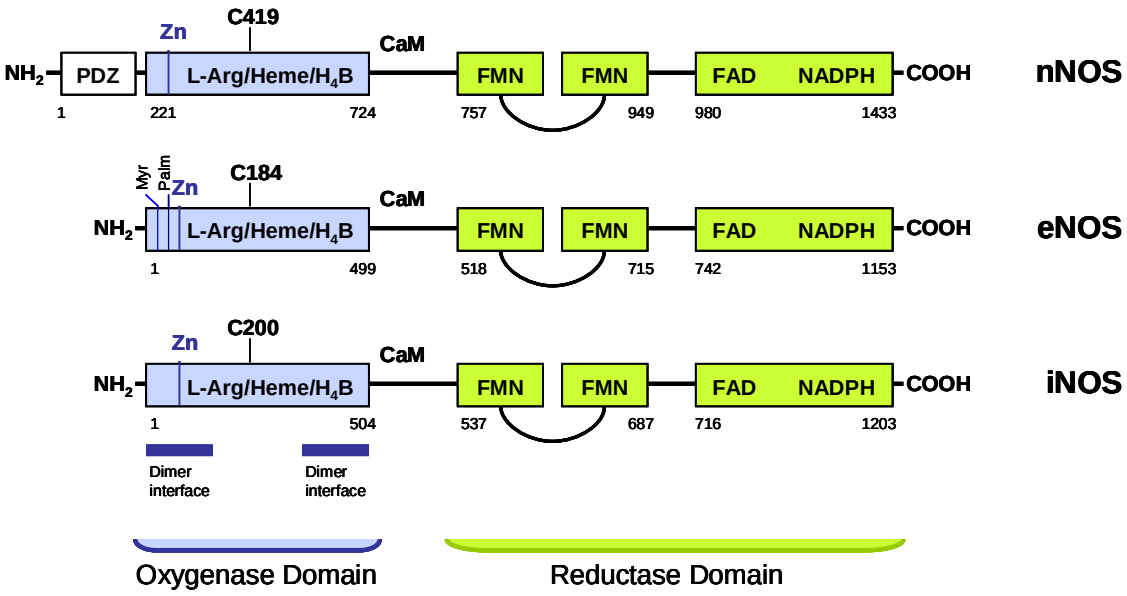

Figure 2. The structure of human nNOS, eNOS, and iNOS domains.[4] The oxygenase domains are shown in blue, with the locations of the dimer interface, Zn-ligating cysteine residues, and heme-ligating cysteine residues (C419, C186, C200). The PSD-95 discs large/zona occludens-1 domain of nNOS (PDZ) is involved in associating nNOS to synaptic sites in brain and skeletal muscle. eNOS undergoes dual acylation by myristate (G2) and palmitate (C15 and C26), which localizes the enzyme to the plasmalemmal caveolae of endothelial cells.

considered functional tetramers, as each subunit consists of an oxygenase and reductase domain that bind different cofactors and have different functions (Figure 3). The bacterial NOSs, also sometimes referred to as “Heme domain of NO Synthase-like proteins” (HNS), are truly dimeric in that they consist of dimerized oxygenase domains. They are believed to interact with a separate reductase protein like the other heme-thiolate proteins.

The C-terminal reductase domain of the mammalian NOS proteins binds the flavin mononucleotide (FMN) and flavin adenine dinucleotide (FAD) cofactors, and an electron donor, reduced nicotinamide adenine dinucleotide phosphate (NADPH). This domain contains between 635 and 681 residues, depending on the isoforms (Figure 2). The function of this domain is to transfer electrons from NADPH to the heme iron, of the opposite subunit’s oxygenase domain (Figure 3). Paired electrons are transferred from NADPH to FAD, from which they are transferred individually to FMN, which provides a single electron to reduce the heme iron. Isolated reductase domains are able to transfer electrons from NADPH, thus reducing proteins such cytochrome c.[11; 12]

The mammalian NOSs also have sequences between the reductase and oxygenase domains for the binding of calmodulin (CaM). As mentioned above, the binding of CaM to NOS enables electron transfer from NADPH, probably due to a conformational change in the protein, which brings the oxygenase and reductase domains in contact such that electron transfer is favourable.[13]

The oxygenase domains have been well characterized as they are the domains directly involved in dimerization and catalysis, and they can be expressed as recombinant proteins with retention of structure and some functions. The size of the

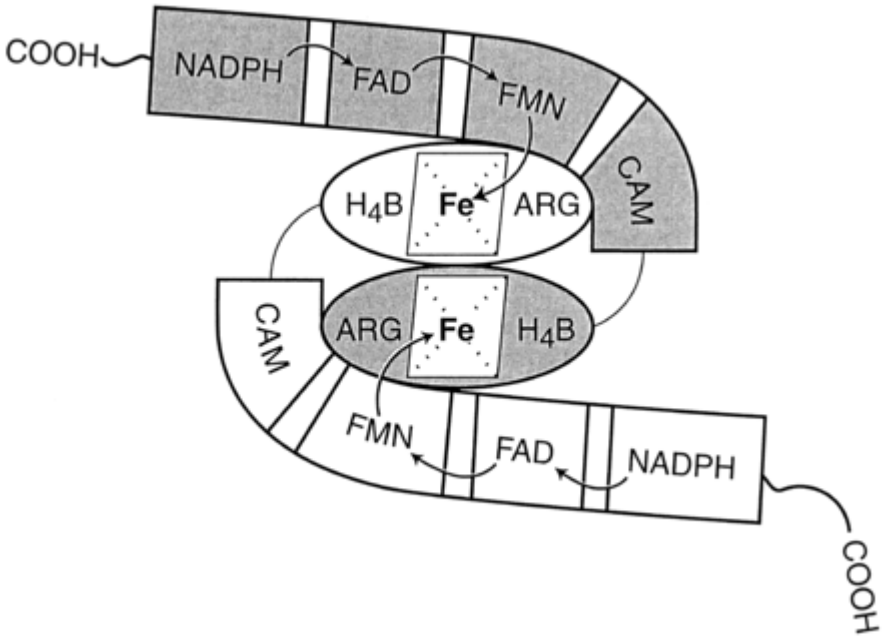

Figure 3. Schematic representation of the NOS apoenzyme.[14] Electrons are transferred from the reductase domain of one subunit to the oxygenase domain of the adjacent subunit.

mammalian N-terminal oxygenase domains vary between 499 and 504 residues (Figure 2). The oxygenase domains have a novel α/β fold with an elongated curved shape that is said to resemble a left-handed baseball catcher's mitt with the heme centered in the β sheet palm of the mitt, such that the distal surface of the heme is directed towards a large cavity (Figure 4).[15] There are 10 α helices and 12 anti-parallel β sheets found within the oxygenase domain. The distal heme pocket consists primarily of a continuous web of winged β sheets, which is unusual, as cytochrome P450s possess distal pockets consisting mostly of α helices.[15] The distal pocket is also hydrophobic, containing no hydrogen-donating residues; however, there are polar residues near the edge of the pocket.[15] The majority of protein interactions with the proximal heme surface involve the α3-β2 loop, composed of residues 181-195 (eNOS) which contains the cysteine residue that forms a thiolate ligation to the heme iron (Figure 4).[15]

The oxygenase domain binds domain-specific cofactors, heme (Figure 1A) and (6R)5,6,7,8-tetrahydrobiopterin (H_4B) (Figure 1B), and the substrate L-arginine. Heme must be bound within the oxygenase domain for dimerization and subsequent catalysis to occur, and is also required for the binding of H_4B and L-arginine, which also play a role in dimer formation.[16; 17; 18] Heme is ligated axially to the protein via the thiolate group of a cysteine residue (C186 in eNOS), and is stabilized within the binding pocket via π-stacking between tryptophan (W180 in eNOS) and phenylalanine (F355 in eNOS) residues. The D ring propionate group of the heme also forms hydrogen bonds with both H_4B and L- arginine (Figure 5A).[19]

The cofactor H_4B binds to the oxygenase domain on the proximal side of the heme. It is bound near the dimer interface, and is stabilized by hydrogen bonds

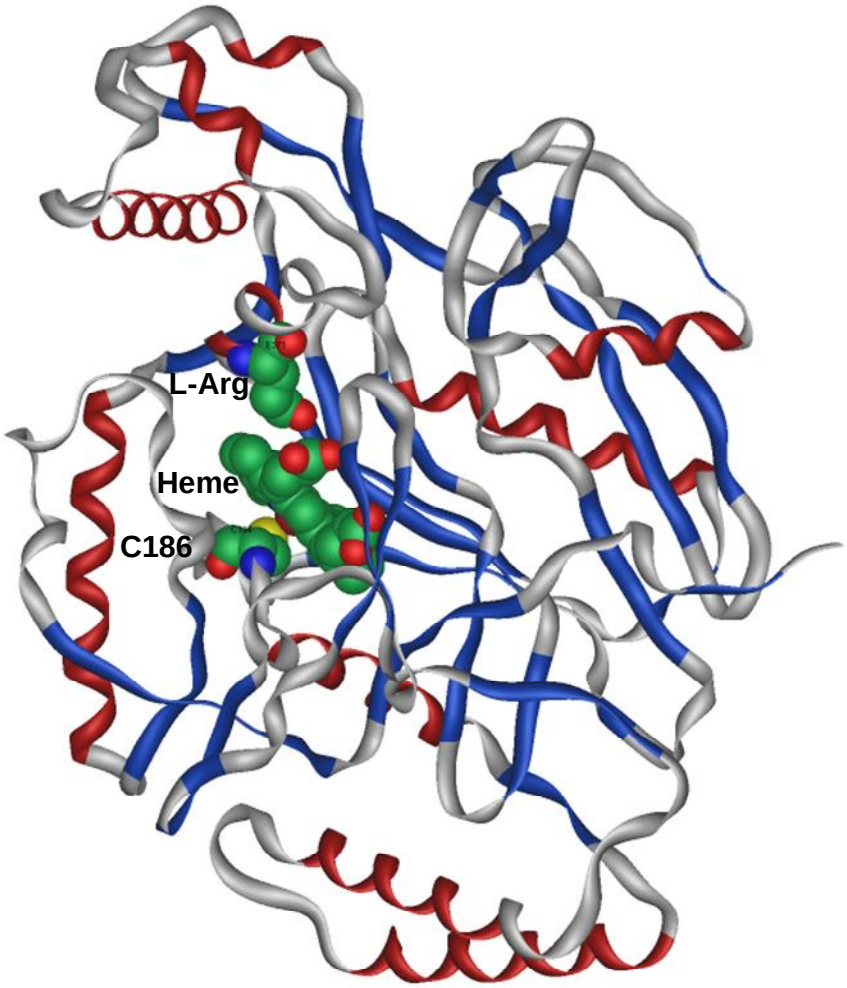

Figure 4. The structure of the oxygenase domain of eNOS. There are 10 α helices (red) and 12 anti-parallel β sheets (blue) within the domain. The heme-binding domain thus consists primarily of β sheets. The heme is held within the pocket by α3, β2, and the sequence connecting them (residues 181-195). Also visible are the proximal ligand to the heme (C186) and the L-arginine binding site (E363). The cofactors heme and H_4B, and the substrate L-arginine, are represented by space-filling molecules.

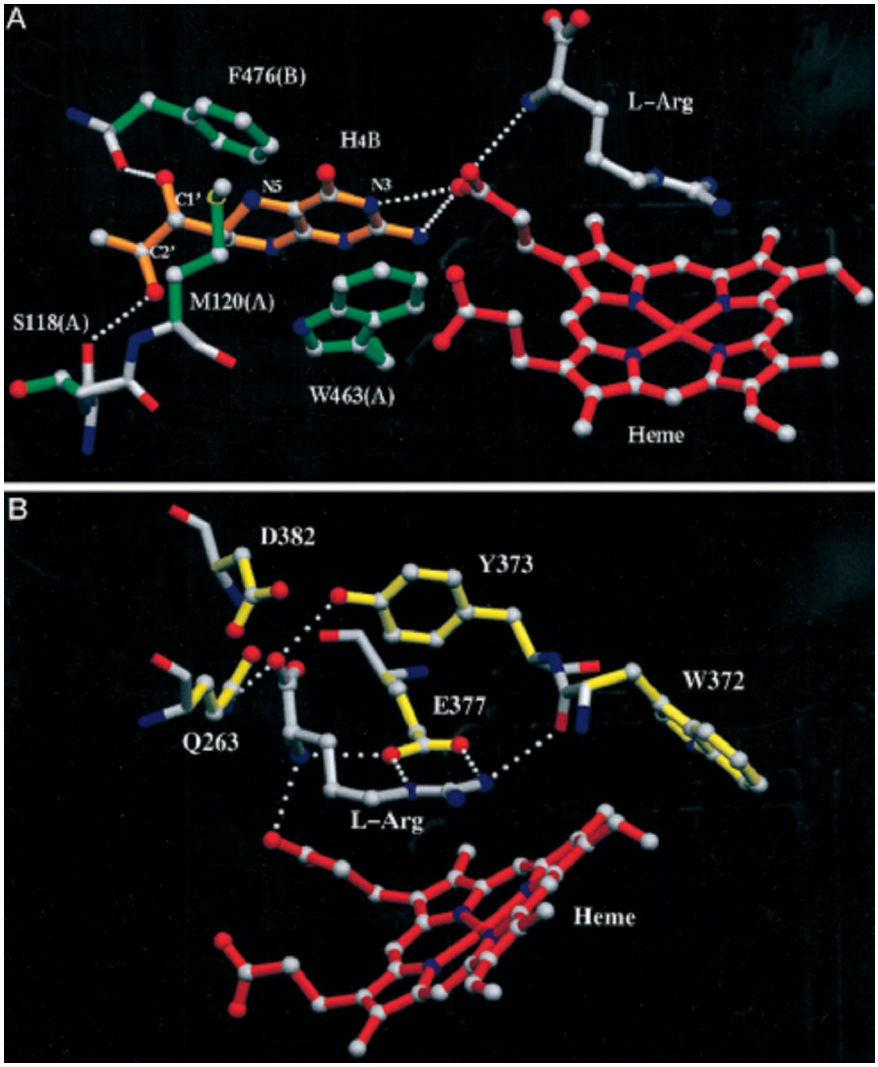

Figure 5. Interactions between heme, L-arginine, and H_4B in iNOS.[19] The residues involved in these interactions are conserved between iNOS and eNOS, with the exception of M120, which is a valine residue in eNOS. Both L-arginine and H_4B form hydrogen bonds to the same propionate group of the heme (A). H_4B is also stabilized by interactions with several nearby residues. L-arginine makes several hydrogen bonds to the protein (B), and the guanidinium nitrogen involved in catalysis is positioned above the heme iron.

between the cofactor and nearby residues, as well as through π–stacking with the side chain of a tryptophan residue (W463 in iNOS, W449 in eNOS) (Figure 5A). It has also been suggested that residues from the reductase domain are involved in H_4B binding near the heme.[20; 21] There is a hydrogen bond formed between N3 of H_4B and the D ring propionate of the heme, which enables electron transfer from H_4B to the heme during catalysis (Figure 5A). [22] Fully reduced H_4B remains tightly bound to NOS during catalysis, and is involved in catalysis through the donation of an electron to the oxyferrous complex, which may travel along the propionate.[23] H_4B is later regenerated by the donation of an electron from the reductase domain.[23] H_4B is positioned perpendicular to the heme, such that its dihydroxy-propyl side chain is aimed at the N-terminal hook (discussed below), which is believed to provide additional hydrogen bonds to stabilize H_4B binding.[21] The presence of H_4B increases the affinity for L-arginine binding and vice versa, and thus it has a structural role in addition to a catalytic function.

The substrate L-arginine binds to the distal pocket, such that the guanidinium nitrogen is positioned directly above the heme iron.[15] It is stabilized by hydrogen bonds with several nearby residues (Figure 5B). During catalysis, an oxygen atom from the oxyferrous complex is incorporated in the substrate through interaction with the guanidinium nitrogen. It has been observed that the presence of certain inhibitors causes L-arginine to bind to the pterin binding site, which may indicate that the H_4B binding site, which is unique to NOS, may have evolved from a binding site for L-arginine.[20] Within the oxygenase domain of mammalian NOSs, there are also two cysteine residues supplied from each monomer, that coordinate a zinc atom to the dimer interface.[20] The resulting zinc tetrathiolate center is a structural feature, promoting and

stabilizing dimer formation and the H_4B binding site, and does not appear to be involved in catalysis.[20]

The oxygenase domain can be isolated from the enzyme, either by limited proteolysis or by recombinant expression, and is capable of binding heme, H_4B, and L-arginine.[12] As such, isolated oxygenase domains are also able to dimerize. Isolated dimerized oxygenase domains undergo heme dissociation more easily than the intact enzyme, as it is not very stable in the weaker isoforms.[24] Although it cannot catalyze the full NOS reaction, dimerized oxygenase domains, with the appropriate cofactors, will synthesize L-citrulline and NO from the NOS reaction intermediate, $^{\omega}$*N*-hydroxy-L-arginine, and hydrogen peroxide, with hydrogen peroxide donating the required oxygen atoms and electrons.[25]

1.1.2. Dimerization

All NOS proteins are dimeric, and dimerization is required for catalytic activity. H_4B and L-arginine are involved in dimer stability; however, heme is the only required cofactor for dimerization to occur. Approximately 14% of the surface area of each monomer comprises the dimer interface (Figure 6).[19] It was reported that this exposed surface area, which is primarily hydrophobic, is much larger than that observed for cytochrome P450, and over 90% of this area borders the concave face of the oxygenase that contains the distal heme pocket.[19]

Dimer formation does not perturb most of the monomeric structure; however, the regions that are buried upon dimerization undergo conformational changes to create the binding sites for H_4B and L-arginine.[15; 21] The distal heme pocket in $iNOS_{oxy}$ is only 10 Å deep in the monomer, but dimerization creates a funnel-shaped 30 Å deep pocket that

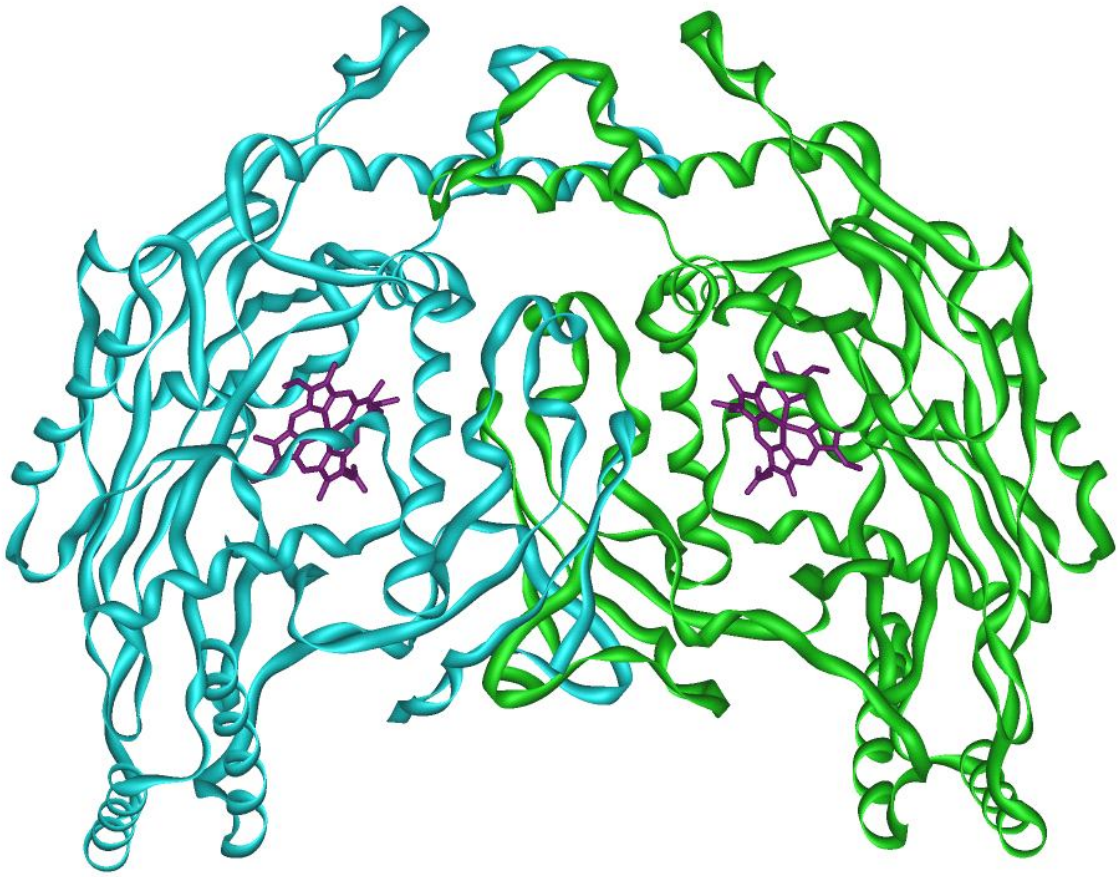

Figure 6. The homodimeric eNOS oxygenase domain (2nse). The individual subunits are denoted in blue and green, respectively. The heme (purple) is present in each oxygenase domain, within the active site.

terminates above the heme iron.[21] The shallowness of the distal pocket in the NOS_{oxy} monomer differs from cytochrome P450s, which bury the heme within the protein core, modulating heme activity through its limited accessibility to solvent.[26]

In mammalian NOSs, the N-terminal extension is involved in stabilization of the dimer. The extensions, which are like hooks, can take on either a swapped or unswapped conformation. Swapping implies that the N-terminal extensions interact with the adjacent subunit, whereas unswapped extensions interact with their own subunit.[27] Unswapped N-terminal extensions utilize two symmetry related cysteine residues from each subunit with a C-X_4-C motif (C96 and C101 in eNOS) to tetrahedrally coordinate a zinc ion, forming a zinc-tetrathiolate at the dimer interface.[20] Swapped N-terminal extensions engage in intersubunit disulfide bonding between the C101 residues, preventing zinc ion binding.[27] The presence of zinc-tetrathiolate increases dimer stability by reducing the surface area of the dimer interface exposed to solvent.[27] The absence of this structure through the swapped conformation results in an altered H_4B binding site, which negatively affects heme and L-arginine binding, resulting in reduced protein stability and catalysis.[20]

The H_4B binding site is located near the dimer interface. The helical lariats from each subunit sandwich H_4B via π-stacking, with W449 and F462 (eNOS), and hydrogen bonding with nearby residues and the porphyrin ring.[21] The extensive network of H_4B interactions aids in dimer stabilization and facilitates L-arginine binding.[21; 22]

The creation of a deep substrate pocket in the distal heme environment reduces exposure to solvent, and stabilizes L-arginine near the heme. The guanidinium nitrogens of L-arginine hydrogen bond with the carboxylate oxygens of E363.[21] L-

arginine also interacts with a network of hydrophilic side chains, which are associated with structural components of dimer formation.[21]

The mammalian NOS isoforms differ in terms of dimer stability, and the role of H_4B appears to be a key factor in this. Dimerization of iNOS involves interactions only between oxygenase domains, whereas for nNOS and eNOS there are more extensive interactions between reductase domains and between reductase and oxygenase domains, although these are not required for dimer stability.[28; 29; 30] The reduced number of subunit interactions in iNOS may explain why in the presence of H_4B iNOS forms catalytically active dimers, but tend to be monomeric when H_4B is absent.[31] Heme is required for dimerization in all isoforms, and is required for H_4B binding. H_4B stabilizes heme binding and dimerization in iNOS through its extensive interactions with the oxygenase domains. The nNOS isoform is not dependent on the presence of H_4B for heme incorporation and dimerization, although H_4B stabilizes the dimer once it has formed.[16; 17] Dimer stability is even less dependent on H_4B in eNOS, which forms the most stable dimers in the absence of H_4B or L-arginine.[28; 32]

1.1.3. Comparison of $eNOS_{oxy}$ and saNOS

My project focuses primarily on the oxygenase domain of the eNOS isoform, which will be discussed next. I have also examined a bacterial NOS_{oxy}-like protein from *Staphylococcus aureus*, saNOS, which will be described afterwards.

1.1.3.1. eNOS

The eNOS isoform is a 1205 amino acid protein with a molecular mass of 133 kDa.[33] Bovine eNOS possesses a 58% sequence identity with rat nNOS and a 51% sequence identity with murine iNOS, with the C-terminal two-thirds of the proteins being

highly similar and the N-termini being distinct to the respective isoforms.[33] eNOS is distinct from the other isoforms, however, as it is associated with the cellular membrane, whereas nNOS and iNOS are present in the cytosol.[5] It is thought that this localization enables endothelial cells to release NO in response to increased blood flow and shear stress, and thus facilitates the extracellular transport of NO, mediating its cytotoxic effects.[5; 34] Analysis of eNOS revealed that it does not possess any hydrophobic regions that could function as a membrane binding domain.[35] Instead, it is the co-translational, irreversible myristoylation of eNOS at position G2 that enables membrane attachment – nNOS and iNOS do not possess a consensus sequence for N-myristoylation.[5; 36] eNOS also undergoes post-translational acylation by palmitate, at positions C15 and C26, which is thought to play a role in orienting the enzyme on the membrane.[37; 38] Both modifications are required, however, to target eNOS to the plasmalemmal caveolae, which are small domains that contain calcium channels and protein kinase C.[39] Serine, threonine, and tyrosine residues are present that can be phosphorylated, causing eNOS to become cytosolic.[40] The myristoylation and palmitoylation domains are not required for catalysis, although NO production is reduced in palmitoylation-deficient eNOS.[41; 42]

1.1.3.2. saNOS, a Bacterial NOS

Although considerable study has been given to the mammalian isoforms of NOS, the more recently discovered bacterial NOS isoforms are also garnering attention. There has been some debate over whether these proteins are true NOSs, and the role NO could play in bacteria. The NOS_{oxy} isolated from *Bacillus subtilis* has been proven to generate NO, suggesting it is a functional NOS protein.[43] The role of NO in bacteria may be to protect the bacteria from oxidative stress, or could be involved in pathogenicity.[44; 45]

It has been observed that NHS proteins have only been identified in Gram-positive bacteria.[44] Among these is the NOS enzyme isolated from methicillin-resistant *Staphylococcus aureus* (MRSA) also known as saNOS. *S. aureus* is a common source of bacterial infections. Like other bacterial NOSs, and the cytochrome P450s, there is no reductase domain in saNOS. These proteins are believed to interact with separate reductase proteins, although the corresponding partner for saNOS has yet to be identified.

The saNOS protein has an approximate molecular mass of 80-90 kDa, indicating that it is slightly smaller than dimerized $eNOS_{oxy}$.[46] saNOS consists of dimerized oxygenase domains, each containing 345 residues, and shares a similar structure to that of the oxygenase dimers of mammalian NOSs, particularly $eNOS_{oxy}$.[46] The similarity is such that it can be superimposed with residues 125-491 of bovine eNOS, although the symmetry axis is slightly offset between the proteins and the saNOS dimer is more open to solvent by 5.3˚ (Figure 7).[46] The ligand binding sites within saNOS are comparable with those of mammalian NOSs. At the heme binding site are residues that are conserved within mammalian NOSs: W56, R51, C62, P104, F222, Asn223, G224, W225, M227, Glu230, W316, F342, and Y344.[46] This conservation of residues indicates that saNOS functions as an active oxygenase domain.[46]

The structure of saNOS differs from mammalian NOSs in that it is lacking the N-terminal extension that includes the zinc binding site found in eNOS and other mammalian NOSs.[46] As the N-terminal extension of mammalian NOSs, required for dimerization in these proteins, interacts with other residues along the dimer interface, alterations in these residues in the bacterial isoforms may serve to overcome the absence of the N-terminal hook by stabilizing the structure such that dimerization can

Figure 7. The overlapped $eNOS_{oxy}$ and saNOS dimers.[46] The saNOS subunits are coloured blue and green, and the $eNOS_{oxy}$ subunits are coloured red and orange. The angle between saNOS monomers is greater than that of $eNOS_{oxy}$ monomers by 5.3˚. The heme iron is present as a grey sphere, and the zinc atom of eNOS is displayed as a pink sphere. Note the absence of the N-terminal extensions in saNOS.

occur.[46]

Also unique to saNOS is a complete independence regarding the presence of H_4B.[46] There is conservation of many of the residues involved in H_4B binding; however, in saNOS there is an absence of two residues key for the specific binding of H_4B in mammalian NOSs. Bacteria are not believed to synthesize H_4B, and it is thought that another pterin, such as tetrahydrofolate (THF) may be the native cofactor, even though the crystal structure of saNOS was resolved with added NAD^+ bound at this site.[46]

1.1.4. NOS Active Sites

As stated previously, the active site of NOS proteins resides within the oxygenase domain. Heme is buried within the interior of each monomer. The heme is pulled out of plane due to its being ligated to a cysteine residue (C196 in eNOS, C62 in saNOS). This cysteine residue is hydrogen bonded to a tryptophan residue (W180 in eNOS, W56 in saNOS) (Figure 8). This tryptophan residue and a phenylalanine residue (F355, F222) engage in π-stacking with the heme, sandwiching the heme, and stabilizing it within the binding pocket. The D ring propionate group of the heme forms hydrogen bonds with both the N3 of H_4B and the α-amino group of L-arginine (Figure 5 and Figure 8).[19] Also within the active site is the glutamic acid residue (E363, E230) that hydrogen bonds to the L-arginine substrate.

1.2. Nitric Oxide Synthesis

The nitric oxide radical (NO) is synthesized biologically during the amino acid conversion of L-arginine to L-citrulline (Figure 9). The NOS reaction is a two-step reaction, requiring a total of two molecules of dioxygen and three electrons donated from one and a half molecules of NADPH.[25] The electrons are stripped from NADPH in pairs,

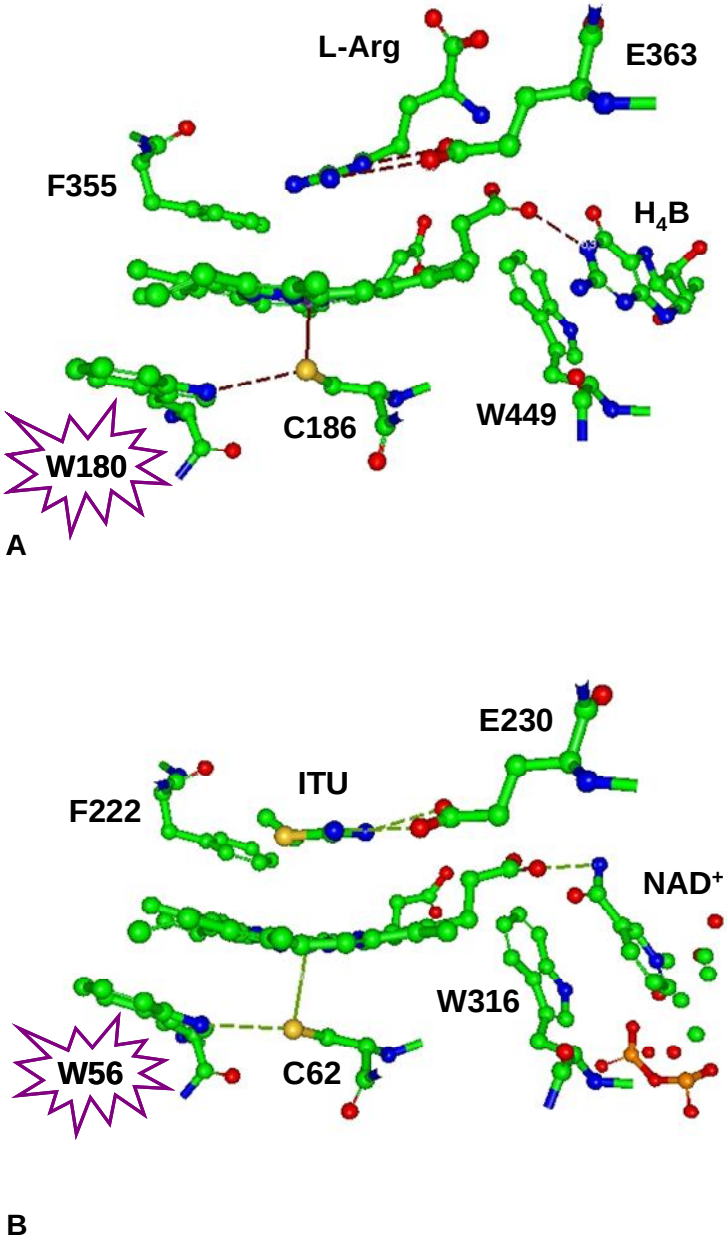

Figure 8. The active sites of (A) eNOS (2nse) and (B) saNOS (1mjt). A cysteine residue ligates to the proximal side of the heme (C186, C62). Tryptophan (W180, W56) and phenylalanine (F355, F222) residues sandwich the heme within the binding pocket, stabilizing the porphyrin ring. A glutamic acid residue (E363, E230) is responsible for hydrogen bonding to L-arginine, and to either H_4B or NADPH. The L-arginine binding site in saNOS (B) is shown with ethylisothiourea (ITU) bound.

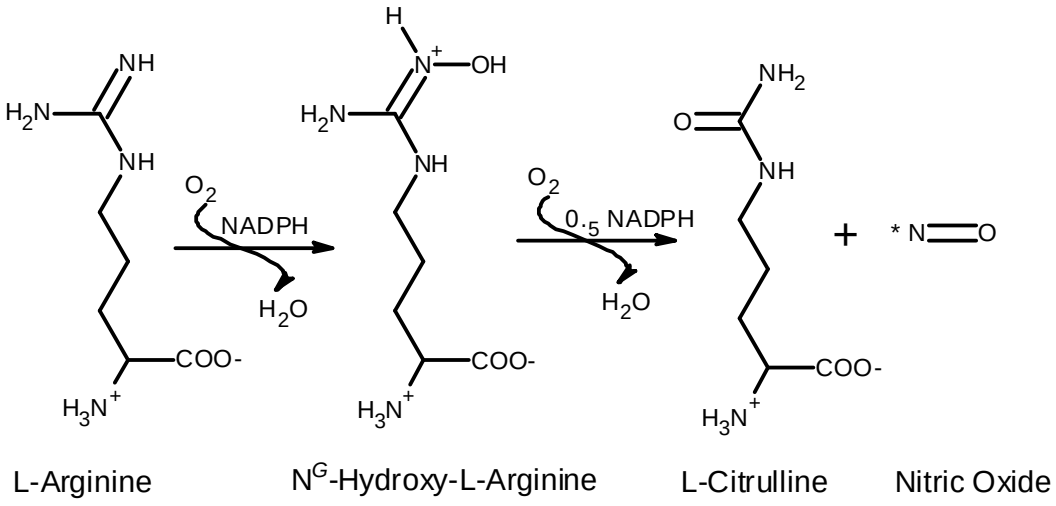

Figure 9. The NOS-catalyzed reaction.[25]

and thus the reaction occurs twice in a cycle. The electrons are then passed through the flavin cofactors, flavin adenine dinucleotide (FAD) and flavin mononucleotide ($FMNH_2$), individually.

In the first step of nitric oxide synthesis, an electron is donated from NADPH via $FMNH_2$, reducing the heme iron (Figure 10A).[4] O_2 binds to the heme iron, generating the ferrous-oxy complex.[47] The addition of a proton and an electron from H_4B, or the second electron from NADPH via FMNH when H_4B is absent, generates a heme-peroxy species.[48] Protonation of this species by L-arginine results in cleavage of the O-O bond, releasing OH^-.[21] The freed hydroxyl group picks up an additional proton from L-arginine, and is removed from the active site as water, leaving an ferryl-oxy species.[7; 21] This complex is highly reactive, and will rapidly oxygenate L-arginine to L-NHA, regenerating ferric heme.

In the second step of the reaction (Figure 10B), ferric heme is reduced with the addition of one electron from the second molecule of NADPH via $FMNH_2$.[4] O_2 binds to the heme iron, generating the ferrous-oxy complex. L-NHA reacts with ferrous-oxy to produce the heme-peroxy complex and an L-NHA radical, which react with each other to generate L-citrulline, NO, and to regenerate ferric heme.[4]

Once NO is generated, it binds to the heme iron. The heme iron-NO complex can then take one of three pathways (Figure 11).[49] NO can bind to and be quickly released from the ferric heme and allowed to diffuse out of the enzyme regenerating the heme for the next catalytic cycle.[49; 50] Alternatively, the ferric heme-NO complex can be reduced or NO can bind to ferrous heme, from which NO will be slowly released or the ferrous heme-NO complex will have to react with O_2 to regenerate ferric heme and

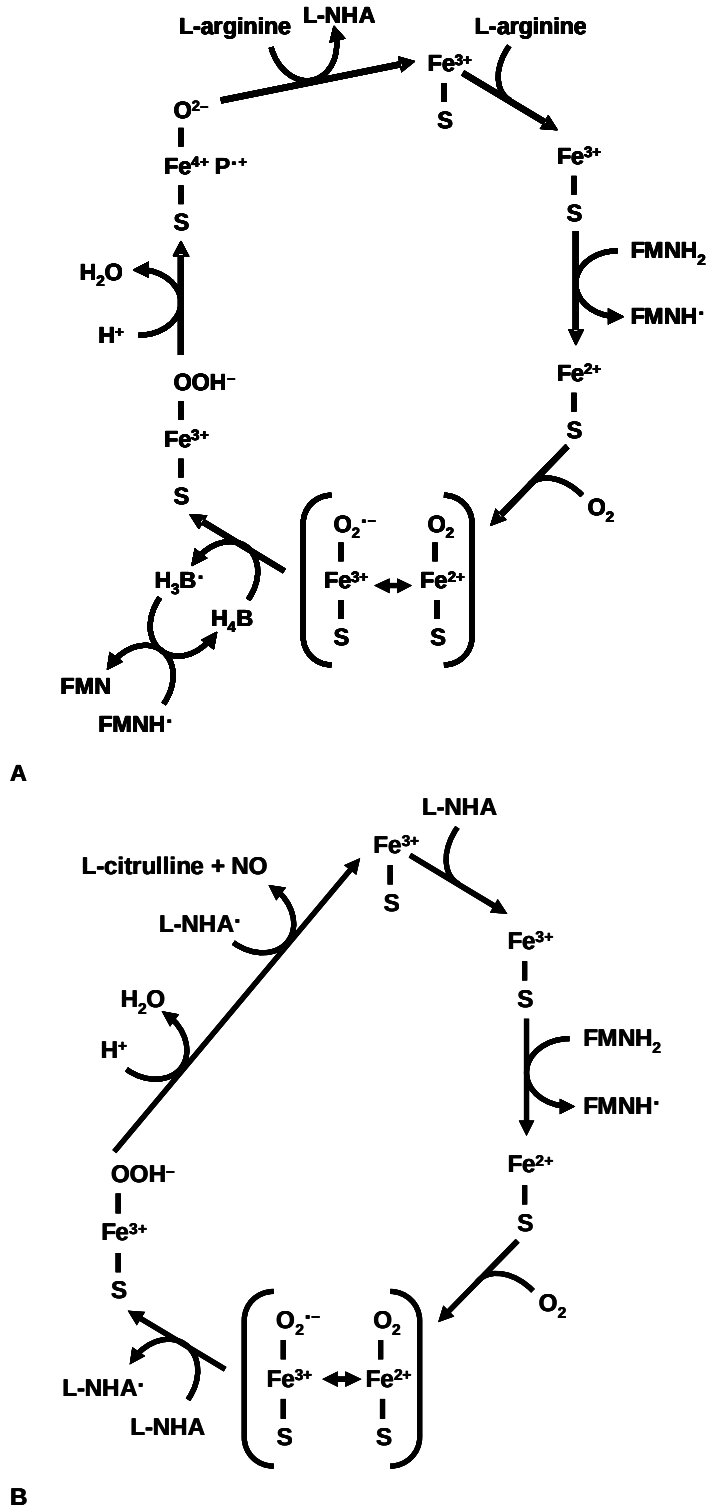

Figure 10. The proposed NOS reaction scheme.[4] In step one (A), L-arginine is hydroxylated to L-NHA. In the second step (B), L-NHA is oxidized to L-citrulline and NO.

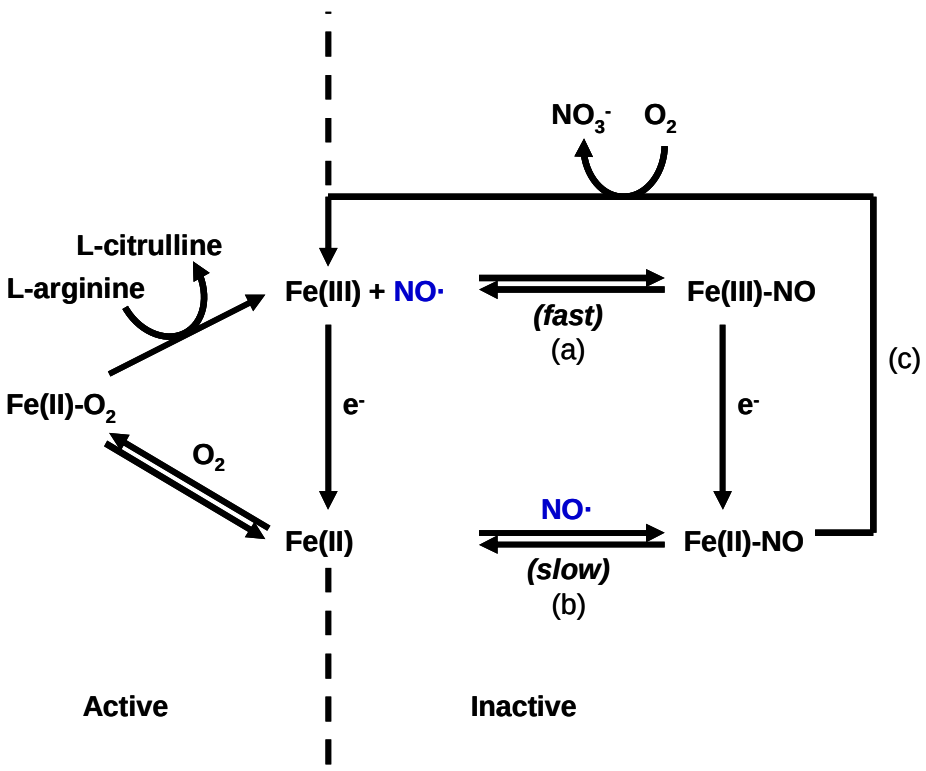

Figure 11. Once generated, NO has three fates.[49] (a) A ferric heme-NO complex can form, which quickly dissociates. (b) A ferrous heme-NO complex can be formed, from which NO slowly dissociates. (c) A ferrous heme-NO complex can be formed, which reacts with O_2 to produce nitrate.

release NO_3^-.[50]

The rates of NO synthesis in the mammalian isoforms are governed by three parameters: the rate of ferric heme reduction, the rate of dissociation of the Fe(III)NO complex, and the rate of oxidation of the Fe(II)NO complex.[51] The rate of NO synthesis in nNOS is regulated by the rate of Fe(II)NO complex formation, as the heme in nNOS is quickly reduced, and the NO dissociates from ferrous heme slowly, which partitions most of the nNOS heme in the inactive state.[50] In iNOS, reduction of the heme and the dissociation of the Fe(III)NO complex occur more slowly than in nNOS, which also partitions most of the iNOS heme into the inactive state.[51] The oxidation rate of the Fe(II)NO is much higher than that for nNOS, which results in higher steady state NO production than nNOS.[51] In eNOS, reduction of the heme is much slower than either nNOS or iNOS, and its rate of Fe(III)NO dissociation occurs much faster, which results in little to no accumulation of the Fe(II)NO complex.[51; 52] The overall activity of eNOS is still much lower than that observed for nNOS, as steady state NO synthesis by eNOS occurs at a rate very similar to the initial rates of NO production, whereas nNOS exhibits much slower steady-state NO synthesis than it does initially.[51] Therefore, eNOS does not experience the same autoinhibitory effect of NO binding that nNOS does.

1.3. Mutagenic Studies

Generating point mutations within the conserved residues of the active site can be an important tool for defining the roles of these residues in the active site, as their modifications can alter the protein's structure and/or function.

Previous studies have involved mutating the tryptophan residue that hydrogen bonds to the proximal cysteine ligand to another aromatic amino acid, either

phenylalanine or tyrosine. These studies have been conducted on the neuronal (W409) and inducible (W188) isoforms of the mammalian NOSs and also on saNOS (W56), and have had significant, although distinct, effects on the active site of the enzyme (Figure 8). Mutating the tryptophan residue to phenylalanine would eliminate the hydrogen bond observed between the cysteine ligand and the tryptophan residue. Mutating the tryptophan residue to tyrosine may allow for hydrogen bonding to occur, as there is a hydroxyl group on the residue that could form a hydrogen bond. Tyrosine is less bulky than tryptophan and also a stronger acid, making it a likely hydrogen bond donor.

1.3.1. nNOS

The aromatic substitutions were made to W409 in Dennis Stuehr's laboratory. The resulting mutants were both observed to be hyperactive, as demonstrated by increased rates of NO production, and a corresponding increase in the consumption of NADPH by 3- and 2-fold for W409F and W409Y, respectively, over the wild type protein.[53] This hyperactivity was thought to be attributed to a slower accumulation of the ferriheme-NO complex, which resulted from slower formation of the NO complex and faster reaction between the heme-NO complex and molecular oxygen.[54] The loss of the hydrogen bond between the indole nitrogen of the tryptophan residue and the heme cysteine thiolate ligand was thought to contribute to the hyperactive state of the mutants, because this strengthens the bond between the ferriheme and the thiolate ligand, which weakens the ferriheme-NO bond.[54]

1.3.2. iNOS

Performing the analogous mutation in iNOS generated very different results from those observed for nNOS. In $iNOS_{oxy}$, the conserved W188 residue was mutated to

phenylalanine, and the resulting W188F protein was heme-deficient and lacking in some secondary structure.[55] This was verified by reduced CO spectroscopy, which produced a small Soret band at 420 nm in response to the trace amounts of heme present, consistent with unstable cysteine-heme ligation.[55] In addition, mass spectrometry analysis confirmed that the W188F mutant was monomeric and heme-deficient.[56] The Rafferty lab also performed the W188Y substitution, which was shown by UV/visible spectroscopy to also be heme-deficient (Driscoll and Rafferty, unpublished data). These results indicate that the conserved tryptophan residue has both structural and catalytic roles in NOS.

1.3.3. saNOS

The mutations of W56 to both tyrosine and phenylalanine were conducted by the Couture laboratory at Université Laval. Both of these mutants were observed to bind heme and to be catalytically active. (Lang and Couture, unpublished; Driscoll and Rafferty, unpublished) The presence of the Soret band at 420 nm for the saNOS mutants indicates loss of the axial thiolate bond. As there is no histidine residue near the heme pocket of saNOS, it is unlikely that this state is due to proximal ligation of the heme to histidine.[46] Some P450 enzymes are able to transition from the P450 state to the P420 state, due to thiolate protonation, which is one hypothesis for the loss of thiolate ligation to the heme.[57]

1.4. Mixed Dimer System

As NOS oxygenase domains form homodimers, it is also possible to construct a dimer that contains two unique oxygenase domains, which is known as a mixed dimer, or heterodimer. Mixed dimers enable the study of each subunit individually, which can

enhance structure-function studies, by generating a protein where only one subunit carries the desired mutation, but the effects of the mutation can be studied throughout the protein. Mixed dimers of NOS can be produced through the co-expression of two versions of the plasmid encoding for the NOS oxygenase domain, but each bearing a unique affinity tag and selectable marker.

Mixed dimer systems are not a new concept in studying NOS. Xie *et al.* reported the construction of heterodimers in iNOS, with one wild-type truncated subunit, and the other a full-length subunit bearing a mutation at the position of the heme thiolate ligand.[58] Similar heterodimers were constructed using truncated wild-type or thiolate-deficient subunits and subunits that carried a mutation at a residue critical for H_4B binding.[58] The resulting mixed dimers showed that both subunits must possess functional heme-binding sites to dimerize and be active, and that only one H_4B-binding domain is necessary for dimerization and catalysis.[58]

Jennifer McDonald was successful in characterizing mixed dimers of the oxygenase domains of iNOS, by co-expressing plasmids where each subunit possessed a different C-terminal tag – either a 6-histidine or 7-glutamic acid repeat, both of which are small and hydrophilic (Figure 12). These do not significantly alter the structural or functional properties of the protein, although the Glu_7 tag does alter the *pI* of the protein due to the *pKa* (4.3) of the glutamic acid residues.[59] As each vector confers resistance to a different antibiotic, culturing the cells under double selective conditions should result in the growth of only bacteria that possess both plasmids. Three dimer species result from this expression: His_6-tagged homodimers, Glu_7-tagged homodimers, and His_6/Glu_7-tagged heterodimers. The His_6 tag possesses an affinity for nickel (II), and the use of a Ni-NTA chromatography column will bind His_6-tagged homodimers and dimers bearing

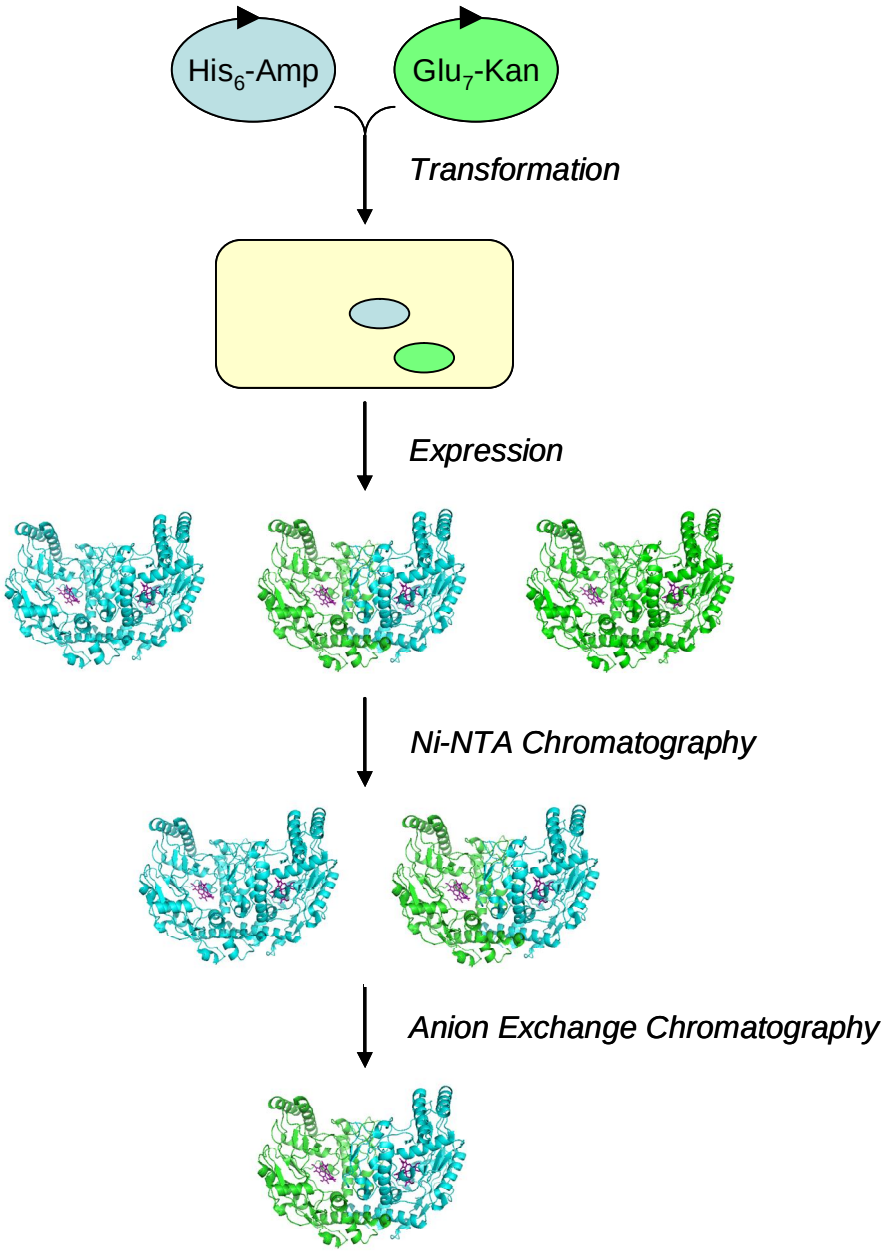

Figure 12. The expression and purification scheme for NOS_{oxy} mixed dimers. *E. coli* cells are co-transformed with two expression vectors, each encoding for the NOS oxygenase domain, but possessing a unique affinity tag and antibiotic resistance.

only one His_6 tag, and removes homodimeric protein possessing Glu_7 tags. Following nickel affinity chromatography, an anion exchange resin isolates the mixed dimer from the His_6-tagged homodimer based on its more negative charge and thus higher affinity for the resin.

1.5. UV/Visible spectroscopy of Heme Proteins

UV/visible spectroscopy is a form of electronic spectroscopy, which uses the ability of ultraviolet and visible light to promote an electron from a low energy state to a higher energy orbital – invoking an electronic transition.[60] This transition requires different amounts of energy depending on the structure of the molecule, with absorbance in the ultraviolet light range (180-400 nm) corresponding to a higher energy than that for visible light (400-780 nm).[60] Within the ultraviolet region, at 280 nm, the aromatic amino acids tryptophan, tyrosine, and to a lesser extent phenylalanine, strongly absorb.[61] This is due to a π to π^* transition of an electron in the bonding molecular orbital of the aromatic ring.[60] The absorbance at 280 nm corresponds to the transition for all three aromatic residues combined, and can be used to determine the concentration of protein present, provided the protein contains aromatic residues.[62]

UV/visible spectroscopy can also be used to characterize the heme iron within the protein sample. This is indicated by the Soret band, which is associated with π to π^* transitions of the porphyrin ring of the heme group. The position of the Soret band is sensitive to the oxidation, coordination, and spin states of the heme iron, as well as the environment surrounding the heme. The iron within the center of the porphyrin ring is present primarily in either the Fe(III) (ferric) or Fe(II) (ferrous) states, although Fe(IV) is also present transiently, and can be coordinated to six ligands: four planar ligands from

the porphyrin ring nitrogens, one proximal ligand to a cysteine residue (C186 in eNOS, C62 in saNOS), and one distal ligand that is provided externally.

The presence and nature of axial ligands influence the ligand field splitting and spin pairing in the heme iron, which determine the distribution of the *d* orbital electrons of the iron. Although the *d* orbitals all have different energy levels, they can be grouped into lower energy (the d_{xy}, d_{xz}, and d_{yz} orbitals) and higher energy (d_{z^2} and $d_{x^2-y^2}$) levels (Figure 13).[63] The spin state depends on whether the spin pairing energy can overcome the energy separation between these groups. The electrons within the *d* orbitals typically adopt one of two conformations: low-spin or high-spin. High-spin iron is the preferred state, as it is more energetically favorable for electrons to be unpaired (Figure 13, A and C). If the energy required to pair electrons is less than that required to promote electrons to a higher energy orbital, then a low-spin state occurs with the electrons being maximally paired (Figure 13, B and D). Unpaired electrons have a spin of 1/2, and spin-state (S) is often referred to by the number of unpaired electrons, or 1/2's. For example, five-coordinate high-spin iron possesses five *d* electrons that are all unpaired, and as such its spin state can be denoted as 5/2.

The porphyrin ring nitrogens, which lie along the *x* and *y* axes, bind to the iron with approximately the same strength. It is the axial ligands, which lie along the *z* axis, that have the greatest effect on spin state. The presence of axial ligands affects the energy difference between lower and higher energy orbitals through ligand field splitting. If six-coordinate heme iron is weakly bonded to an axial ligand, such as water, or if the iron is five- coordinate, the energy separation between the low energy and high energy orbitals will be small, enabling the promotion of to the higher energy orbitals, resulting in a high-spin iron.[63] Interactions between the iron and axial ligands generating a strong

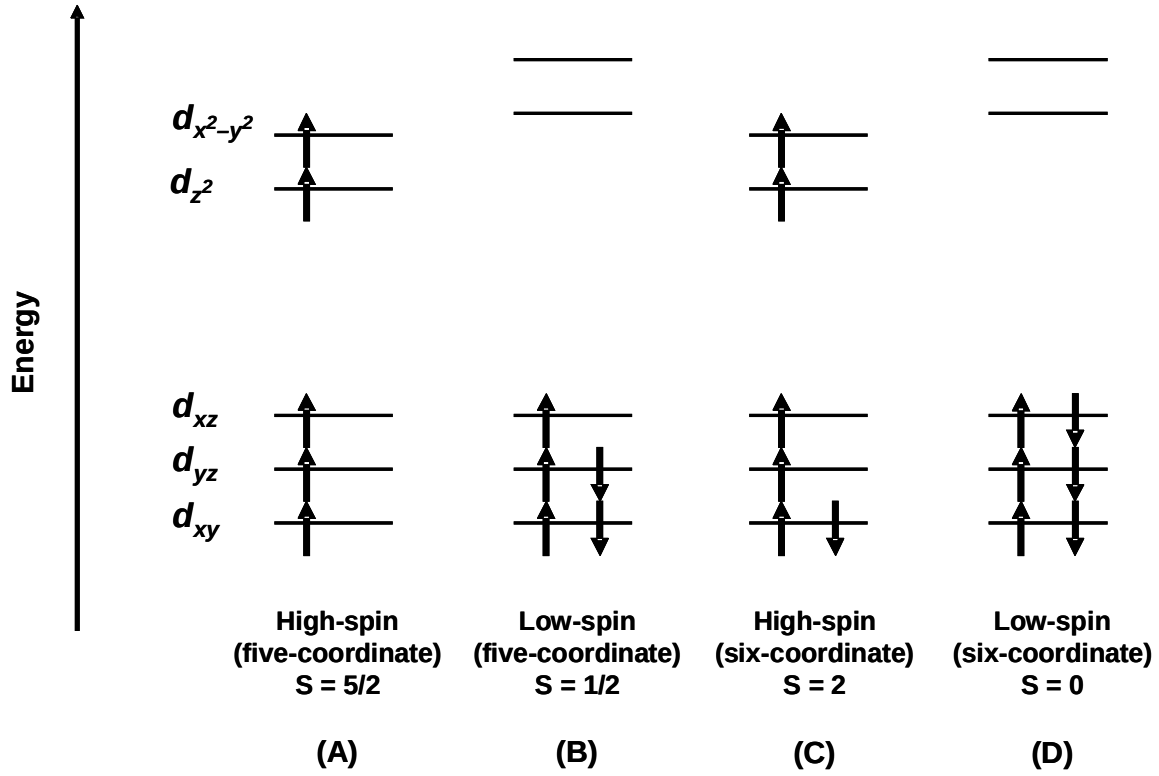

Figure 13. The *d* orbital electron configurations for five-coordinate and six-coordinate heme in the high-spin and low-spin states.[64] The absence of a distal ligand or the presence of a weak-field ligand reduces splitting of the *d* orbitals, enabling the promotion of electrons to the higher energy orbitals, unpairing the electrons (high-spin). The presence of a strong-field distal ligand increases the splitting of the *d* orbitals, making it unfavorable for electrons to move into the higher energy orbitals, causing electron pairing (low-spin). As unpaired electrons have a spin of 1/2, the number of 1/2's indicates the number of unpaired electrons (e.g. 5/2 implies that there are 5 unpaired *d* electrons).

field, such as covalent interactions with CO, result in a large separation between the two energy groups. This large difference will require energy larger than the spin pairing energy to promote electrons into the d_{z^2} and $d_{x^2-y^2}$ orbitals, which will favour the low-spin state.[63]

When no distal ligand is present, the ferric heme iron is five-coordinate. In the absence of H_4B, L-arginine, and any endogenous ligands, the heme iron is in the ferric state, with water assuming the position of the distal ligand. In this state, the Soret band is located at approximately 420 nm.[65] When either the substrate or H_4B are present, the water ligand is displaced, and the iron begins to convert to a five-coordinate and high-spin state, shifting the Soret band to approximately 400 nm. When both H_4B and L-arginine are present, the Soret band will shift to 396-399 nm, indicating that the heme iron has completely converted to the five-coordinate state.[65]

NOS protein that has been reduced to the ferrous state is naturally five-coordinate and high-spin in the absence of an oxygen molecule. In this state, binding of L-arginine and H_4B have no effect on the position of the Soret band, which is located at approximately 412 nm. Carbon monoxide will only bond to heme that is in the ferrous state, and this causes a conversion to the six-coordinate low-spin state, shifting the Soret band to 445 nm.[65] This shift in the Soret band is used as a diagnostic for coordination by a thiolate, although a shift may be observed to 420 nm, indicating that the iron has become five-coordinate having lost its thiolate ligation. NO can bind to either ferric or ferrous heme, and the binding of NO to these states will shift the Soret band to approximately 439 and 437 nm, respectively, corresponding to the formation of six-coordinate low-spin complexes.[65] The positions of the Soret band for the Fe(III)NO and Fe(II)NO complexes are unaltered by the addition of L-arginine or H_4B.[65]

Another diagnostic for heme proteins that is obtained from UV/visible spectroscopy is the charge transfer band. The charge transfer band is indicative of the high energy transition of an electron from a filled ligand π orbital being promoted to a *d* orbital of the metal.[66] This type of charge transfer thus occurs from the ligand to the metal, although the reverse transition is also possible. The ligand-to-metal charge transfer band is used within heme proteins as a diagnostic for high-spin state, and as such may be used to observe specific changes in molecular structure. This charge transfer band for all mammalian NOS isoforms occurs near 650 nm.[67] This diagnostic is very sensitive to changes in the heme binding pocket, with mutations in the nNOS and cytochrome P450 active sites resulting in shifts to the charge transfer band.[68; 69]

1.6. Resonance Raman Spectroscopy

When a beam of light is passed through a sample, the light may be absorbed, scattered, or pass through the sample unchanged. The light that is scattered may, in turn, be scattered elastically, meaning that it is of the same frequency as the original beam of light – termed Rayleigh scattering – or the light may be scattered inelastically, meaning that it is of a different frequency as the original beam – this is termed Raman scattering.[70] Raman scattering is divided into either Stokes or anti-Stokes scattering, with Stokes scattering corresponding to wavenumber shifts that are of lower energy than the Rayleigh scattering, and anti-Stokes scattering corresponding to wavenumber shifts that are of higher energy than the Rayleigh scattering. The magnitude of the shift corresponds to the energy absorbed by the molecules within the sample, and while the light source may be of any wavelength, the Raman scattered light always falls within the infrared region (see below), where vibrational modes of a molecule are detected.

Rayleigh scattering is stronger than either Stokes or anti-Stokes scattering, and Stokes scattering is more intense than anti-Stokes scattering.[70]

For smaller molecules, Raman spectroscopy is an effective technique, however for the study of proteins it requires enhancement, thus the use of resonance Raman spectroscopy. Resonance Raman spectroscopy intensifies the spectrum of a molecule by exciting the sample with light that has a wavelength corresponding to a frequency where the sample is known to possess an electronic absorption band.[66] This enhances the Raman effect of infrared modes associated with the electronic transition, simplifying the spectrum, as it highlights only the region of the molecule associated with generating the electronic absorption band (e.g. the heme iron), which is particularly useful for coloured metalloproteins, such as NOS. Resonance Raman also allows the use of small concentrations of protein, approximately 10 μM.[71]

There are several methods that can be employed to obtain structural information through resonance Raman spectroscopy. In heme-containing proteins, such as the NOS proteins, the iron-ligand bending and stretching modes can be obtained, providing information regarding the strength and geometry of bonds throughout the coordination complex, and the environment surrounding the ligand.[71] It is possible to record spectra under anaerobic conditions, enabling the reduction of the sample or acquisition in NO, CO, and O_2 environments.[71] Also, stable isotopes can be used to shift signals from labeled atoms, providing data for the environment surrounding those specific atoms.[71]

1.6.1. Resonance Raman Spectroscopy of Heme Proteins

Resonance Raman spectroscopy, specifically a Soret-enhanced refinement of this technique, is employed in the examination of the structural and functional

relationships within the active site of NOS. The theory of Raman spectroscopy involves changes in the vibrational states of the molecules within a sample. This energy change corresponds to 1.2-60 kJ mol^{-1}, which is the energy of light within the 100-5000 cm^{-1} range of the infrared (IR) region.[66] The application of a light source, typically a laser of monochromatic radiation, to the sample results in the excitation of the molecules from their lowest energy state, or ground state, to higher energy states.[70] At room temperature, most molecules within a sample will return to their ground state, although a very few molecules will be found at an excited vibrational state.

The high-frequency region of the resonance Raman spectrum of NOS is found between 1300-1700 cm^{-1}.[72] This region provides information regarding the oxidation, coordination and spin state of the porphyrin iron.[72] Although there are several modes identified in this region that correspond to porphyrin vibrations, of particular interest are the ν_4 and ν_3 modes for the heme. The oxidation state of the iron can be identified through the ν_4 vibrational mode that is found between 1340 and 1380 cm^{-1}, which corresponds to the electron density of the porphyrin ring. The coordination and spin state of the iron can be identified by the ν_3 vibrational mode that is found within the 1475 to 1520 cm^{-1} region.[65]

The low-frequency region of the Raman spectrum of NOS, found within the 200 to 800 cm^{-1} region, is used to observe iron-ligand stretching (ν) and bending (δ) modes, which are dependent on the length and angle of the bond between the iron and the proximal ligand. This can be observed in NOS, by comparing the heme when it is in the five-coordinate and six-coordinate states (Figure 14). When the heme iron binds CO, the iron is pulled towards CO, lengthening its bond to the cysteine ligand. The iron-

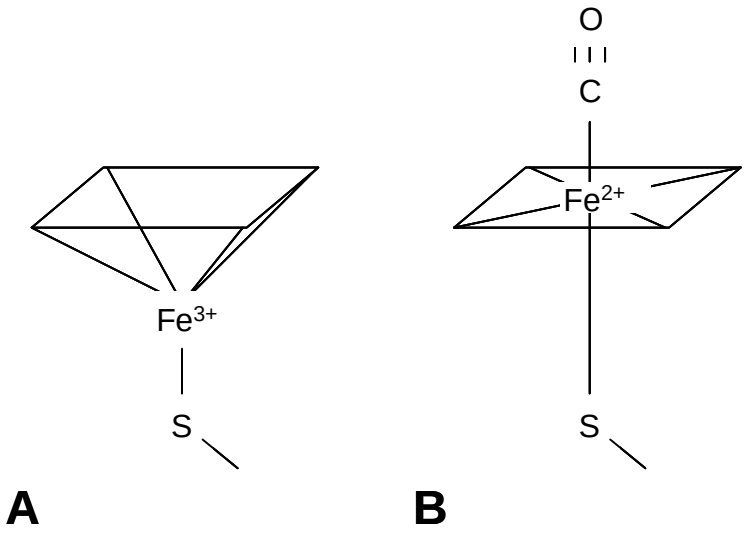

Figure 14. Stretching and bending modes can be detected for iron-ligand bonds. When the heme iron binds to a sixth ligand, such as CO (B), the iron is pulled towards the CO ligand, resulting in a longer bond between the iron and the cysteine ligand.

ligand stretching and bending modes refer to the length and angle of the Fe-CO bond, which can change depending on the coordination environment of the iron. When the heme iron binds NO, a similar phenomenon occurs in regards to the length of the Fe-S bond. What is unique about NO-binding, aside from its ability to bind to both ferric and ferrous iron, is that the angle of the Fe-NO bond depends upon the oxidation state of the iron, with Fe(III)NO complexes being typically straight, and Fe(II)NO complexes being bent.[73]

The low-frequency region also provides information regarding the shape of the porphyrin ring through the identification of modes that correspond to heme in-plane and out-of-plane modes. The appearance or increased intensity of these modes suggest that the heme is being distorted from a planar structure (D_{4h} symmetry) due to tertiary interactions.[74; 75] Several distortions have been identified, including ruffling (B_{1u}), saddling (B_{2u}), doming (A_{2u}), pyrrole propellering (A_{1u}), and waving (E_g) (Figure 15).[75] The resonance Raman bands for these deformations show little variation between distal ligands and NOS isoforms, and generally can be found near the frequencies listed in Table 1.

1.7. Enzyme Kinetics

The NOS reaction requires NADPH or H_4B, and molecular oxygen for both steps, from L-arginine to L-NHA, and from L-NHA to L-citrulline. H_2O_2 can be used as a substitute for both electron donors and O_2 in the catalytic cycle of cytochrome P450s and also NOS. L-arginine does not appear to be a viable substrate for this reaction involving H_2O_2, although it has been used for the bacterial NOSs, with some success, and will regulate the oxidation of L-NHA to NO_2^- and NO_3^-.[76; 77] The H_2O_2-dependent reaction is

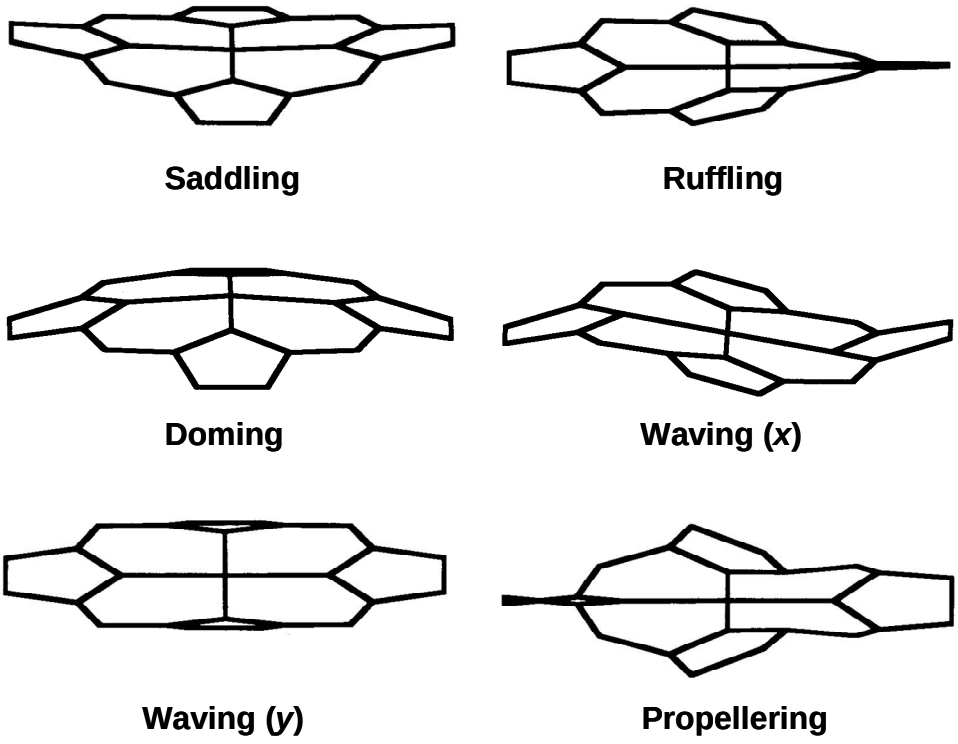

Figure 15. Out-of-plane heme distortions, as determined by Dr. John Shelnutt and colleagues.[75] This figure is available at http://www.sandia.gov/media/images/heme.gif.

Table 1. Approximate resonance Raman bands corresponding to heme distortions in NOSs.[65; 72; 78; 79]

Deformation Mode	Raman Bands (cm^{-1})
In-plane (D_{4h})	344, 676, 752
Saddling (B_{2u})	685, 693
Ruffling (B_{1u})	708-710, 718-722, 801
Doming (A_{2u})	352, 728-730
Pyrrole propellering (A_{1u})	744-746

reported to be enhanced in the presence of H_4B, although no enhancement was reported for saNOS and the NHS from *Deinococcus radiodurans*.[46; 76; 80]

The use of H_2O_2 to oxidize L-NHA bypasses the formation of the reduced ferrous-oxy complex in the second step of NO catalysis, progressing from ferric heme directly to the heme-peroxy complex. The heme-peroxy complex is protonated by L-NHA, generating an iron-oxo species and the L-NHA radical.[81] The iron-oxo species then reacts with the L-NHA radical to produce L-citrulline and NO^-, and also N^--cyanoornithine.[76; 81] NO^- becomes oxidized to either NO_2^- or NO_3^-, which are stable products that can be monitored.

The Griess reaction is used to estimate NOS activity, by quantifying the rate of NO_2^- production (Figure 17). The Griess reaction is a two-step process. Sulfanilamide becomes protonated in solution, enabling it to bind nitrite. This intermediate then reacts with N-(1-naphthyl)ethylenediamine to generate a purple azochromaphore which absorbs light at 540-550 nm.[82] Thus it is possible to correlate the intensity of absorbance of the reaction mixture to that of known nitrite standards, providing an estimate of nitrite production. The Griess reaction does not detect nitrate, but this product can be converted to nitrite using nitrate reductase to enable quantification.

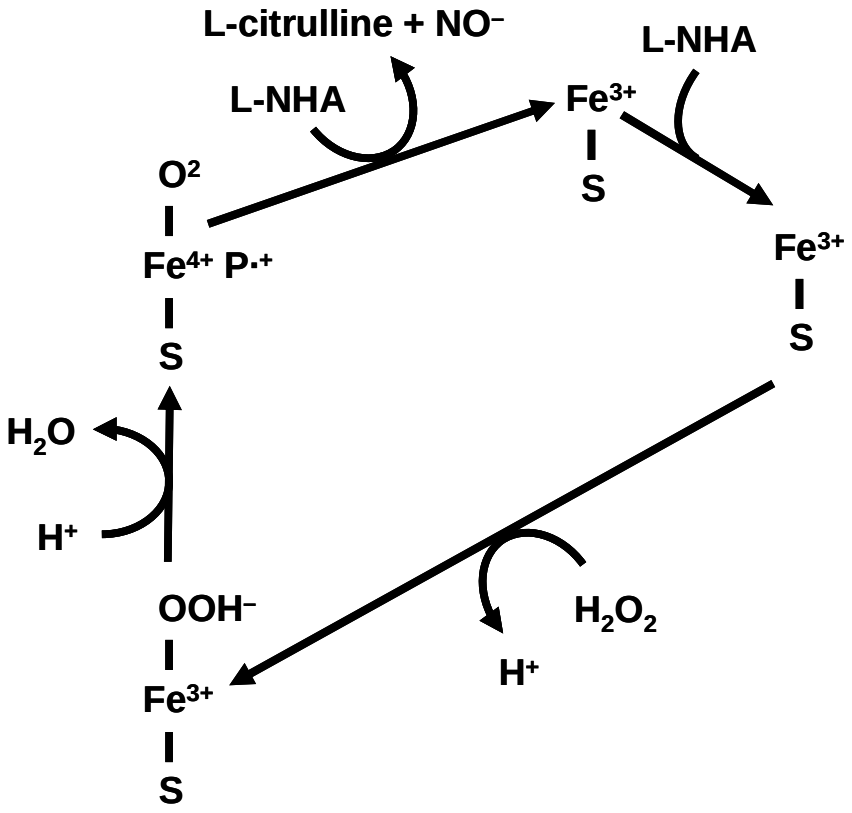

Figure 16. The proposed scheme for the H_2O_2-oxidation of L-NHA.[4] Ferric heme reacts with hydrogen peroxide to generate a heme-peroxy complex. This complex is protonated by L-NHA to produce a ferryl-oxy species and an L-NHA radical that then react with each other to produce L-citrulline and $NO^{\cdot}$, although $N^{\cdot}$-cyanoornithine may also be produced.

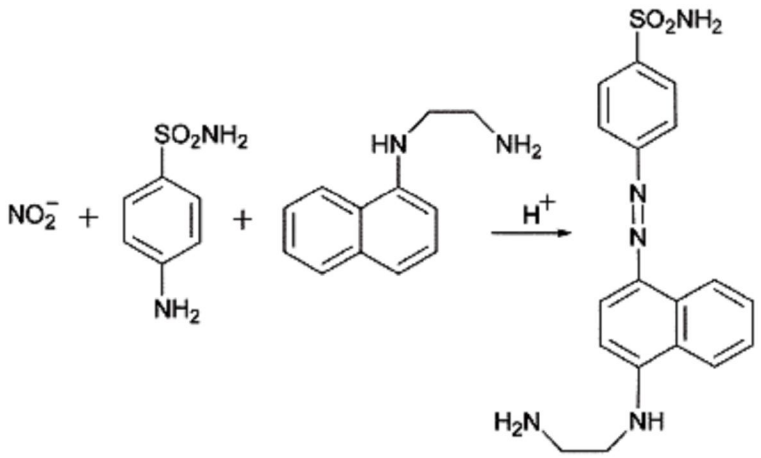

Figure 17. The Griess reaction scheme.[83] Nitrite reacts with protonated sulfanilamide. The intermediate then reacts with N-(1-naphthyl)ethylenediamine to produce an azo product which can be detected using UV/visible spectroscopy.

Chapter 2. Objectives of this Work

The expression and characterization of the eNOS variants in which a conserved tryptophan residue, W180 which hydrogen bonds to the proximal thiolate ligand, was replaced by phenylalanine or tyrosine are described in this work. The effects of the mutation of W180 in the eNOS oxygenase domain ($eNOS_{oxy}$), and of the analogous W56 residue in *Staphylococcus aureus* NOS (saNOS) to either phenylalanine or tyrosine are described within. Previous studies with nNOS have shown that the analogous mutations increase electron density on the thiolate due to loss of the hydrogen bond between the mutated residue ($eNOS_{oxy}$ W180F/Y, saNOS W56F/Y) and the cysteine ligand (C186, C62).

The saNOS W56F/Y homodimers are currently being characterized through resonance Raman spectroscopy by the lab of our collaborator Dr. Manon Couture; thus my project is focused on characterization of the mixed dimers of these proteins, where only one subunit carried the mutation. Thus the objectives of this thesis are to examine the homodimeric $eNOS_{oxy}$ W180F and W180Y proteins, as well as the saNOS W56/W56F and W56/W56Y heterodimers, utilizing UV-visible and resonance Raman spectroscopic methods to observe any changes in the electronegativity of the heme proximal thiolate ligand caused by the mutations.

In addition, the peroxide-dependent oxidation of N^G-hydroxy-L-arginine (L-NHA) was also used to determine the rates of nitrite production, which will be used to estimate nitric oxide production. This will identify if the mutants exhibit hyperactivity as has been reported previously.

Chapter 3. Materials and Methods

3.1. Vector Construction

The pET23a $eNOS_{oxy}$ wild-type, W180F, and W180Y, and pET9h saNOS vectors (Appendix A) were generated previously in Dr. Rafferty's laboratory.

The pET30b saNOS W56F and W56Y vectors were obtained from Dr. Manon Couture (Université Laval). The saNOS coding region for each vector was excised with Nde1 and Xho1, and ligated to the pET23a expression vector (Novagen, Madison, WI), which was linearized using the same restriction enzymes. The resulting vector was transformed into DH5α cells, and Ampicillin-resistant colonies were screened via PCR using the following oligonucleotides:

Sense: pCATATGTTATTTAAAGAGGCTCAAGC

Antisense: pCTCGAGSTGSTGGAAAGGGCACTGGTTAGC

Miniprep DNA was prepared from successfully amplified clones, which was then used to transform cells.

3.2. Bacterial Growth Conditions

Unless otherwise indicated, reagents and media were obtained from Sigma-Aldrich (Oakville, ON) or BioShop Canada (Burlington, ON). BL21(DE3) cells (Novagen, Madison, WI) were transformed with 5-10 ng of plasmid vector by either electroporation or heat shock. For double transformations, i.e. for the saNOS mixed dimers, an equal amount of each vector was used and the cells were transformed by electroporation. The pET23a vector possessed a His_6 tag and conferred ampicillin and carbenicillin resistance and the pET9h vector possessed a Glu_7 tag and conferred kanamycin resistance. 100

μL of transformed cells was spread onto LB-agar plates carrying the appropriate antibiotic, or antibiotics for double transformants, and incubated at 37 ˚C overnight. One colony from the plate was then used to inoculate 2 mL of Terrific Broth (TB) containing the appropriate antibiotic. The culture was then incubated at 37 ˚C in a New Brunswick Series 25 Incubator-Shaker at approximately 200 rpm until turbid. Frozen cell stocks could be made at this time, by adding an equal volume of 50% glycerol and dispensing 100 μL aliquots that were then stored at -80 ˚C.

Alternatively, the culture was divided into two equal volumes and centrifuged at 13 000 rpm for 1 minute in a Beckman Microfuge 12. The pellets were re-suspended in 1 mL of fresh TB which was then added to 500 mL of selective TB, and the culture was incubated in the Incubator-Shaker at 28-30 ˚C, 200 rpm, for 40 hours. The cells were harvested by centrifugation in a Sorvall RC-5C Plus centrifuge at 9700 x g and 4 ˚C for 10 minutes. The supernatant was discarded and the pellet was either frozen at -80 ˚C or used immediately for protein purification.

3.3. Purification of eNOS and saNOS Proteins

The bacterial pellet was re-suspended in 20 mL of the appropriate chilled Lysis Buffer (see Appendix A), and the protease inhibitor AEBSF was added, equal to 0.001% of the total mass of the pellet and Lysis Buffer, assuming that the density of the buffer is approximately 1 g/mL. The proteins were typically purified without H_4B, which was added to the purified protein solution when required. Cells were lysed using a Bead Beater (BioSpec, Bartlesville, OK), containing 0.1 mm glass beads (BioSpec) within the homogenizing chamber. Lysis buffer was used to moisten the beads and to prevent any air bubbles within the chamber. The cells then underwent four cycles of 30 seconds of

homogenization followed by 1 minute cooling periods. The mixture was centrifuged at 9700 x g and 4 ˚C for 10 minutes to remove the beads. Alternatively, the resuspended cell pellet was lysed using a Model 100 Sonic Dismembrator (Fisher Scientific), set to 60% output for 30 second pulses followed by 30 seconds of cooling on ice, repeated for six cycles. Following lysis, the cell solution was centrifuged for 25 minutes at 17 000 x g and 4 ˚C to isolate the protein-containing supernatant from the cell debris.

Purification involved nickel affinity chromatography, with a second anion exchange step used for the saNOS mixed dimer proteins. Nickel-nitrilotriacetic acid (Ni-NTA) Superflow resin (Qiagen, Mississauga, ON) was added to a Poly-Prep column (Bio-Rad, Hercules, CA). The volumes of resin used were 5-7 mL. The column was rinsed with two column volumes of the appropriate Lysis Buffer (see Appendix A) prior to loading.

The supernatant was loaded onto the Ni-NTA column and allowed to pass through the column. The column was then washed with two volumes of the appropriate Wash Buffer, and the protein was eluted with the corresponding Elution Buffer (see Appendix B). The homodimeric proteins were exchanged into their Lysis Buffer utilizing an Amicon Ultra 30 kDa cutoff centrifugal filtration device (Millipore, Billerica, MA), whereas the mixed dimer proteins were passed through a 10 mL P6-DG resin desalting column (Bio-Rad) containing saNOS AEC Starting Buffer (see Appendix A). Mixed dimer proteins then underwent anion exchange chromatography on a 10 mL Mono Q 10/100 GL column (Amersham Biosciences, Piscataway, NJ), with a salt gradient increasing from 0.1 M to 1 M NaCl, before undergoing buffer exchange into Lysis Buffer. The protein was flash frozen in liquid nitrogen, and stored at -80 ˚C, unless it was to be used immediately.

3.4. UV/Visible Spectroscopy

Optical spectroscopy was performed on purified proteins to observe the position of the protein peak, Soret peak, and the charge transfer band. Optical spectra were also obtained before and after resonance Raman acquisition to determine if photodissociation of the sample had occurred. A Cary 400 spectrophotometer (Varian, Palo Alto, CA) was used to record measurements between 250 and 700 nm, with samples placed in a cuvette with a 1 cm path length (Hellma, Müllheim, Germany). The spectra were baseline corrected with 1 mL of buffer corresponding to that which contained the sample. The data was analyzed using Cary Win UV software (Varian, Palo Alto, CA).

3.5. Resonance Raman Spectroscopy

Resonance Raman spectroscopy was performed in the laboratory of our collaborator Dr. Manon Couture at Université Laval. The samples were prepared for spectroscopy by passing the sample through a 2 mL P6-DG resin (Bio-Rad) desalting column, containing glycerol-free Lysis Buffer. The protein was loaded and collected such that the concentration was approximately 50 μM. A Cary 3 spectrophotometer was used to record optical spectra, which were baseline corrected with glycerol-free Lysis Buffer. The desalted protein was transferred to a custom-made glass cell that was then sealed with a septum. The optical spectrum was obtained, paying particular attention to the Soret band, as this provided information regarding the state of the protein. The cell was then flushed with Argon gas (Praxair, Mississauga, ON) for five minutes to remove oxygen.

The sample then underwent UV/visible and resonance Raman spectroscopy to observe the ferric state of the protein. Following this, 1.5 μL of 10 mM anaerobic sodium

dithionite was injected into the cell to reduce the protein to its ferrous state. The UV/visible spectrum was then obtained to determine if the heme iron had been reduced. This should have been observed by a shift in the Soret band from approximately 400 nm to between 412 and 417 nm. The reduced sample then underwent resonance Raman acquisition to observe the ferrous state. Next, the sample was injected with 200 μL of CO (Praxair), thoroughly mixed, and the optical spectrum obtained to determine if CO had bound to the heme iron. This is characterized as a shift in the Soret band between 445 and 450 nm.

Once the samples were prepared in their appropriate state, resonance Raman acquisitions were obtained. All acquisitions were obtained at room temperature for 30 minutes, with one spectrum being obtained every minute. Once the acquisition period ended, the spectra were averaged together to produce a composite image and baseline corrected, using Grams/AI v8.0 software (ThermoGalactic, Salem, NH). To excite the sample, the ferric and ferrous samples were exposed to a krypton ion laser (Coherent, Santa Clara CA), with an output of 413.1 nm, at a power of 3 to 6 mW (Figure 18). The CO-bound samples were exposed to a helium/cadmium laser (Liconix, Melles-Griot, Albuquerque, NM), with an output of 441.6 nm, at a power of 6 mW. The cell was rotated at approximately 3000 rpm to prevent photodissociation of the sample by the laser. The scattered laser light was collected at 90˚ using an F#1 lens, and then refocused using an F#9.8 lens onto the entrance slit of a 0.75 m SpectraPro 750 spectrometer (Acton Research, Acton, MA). Rayleigh scattering was prevented by the positioning of a notch filter, set to block light at either 441.6 nm (MK Photonics, Albuquerque, NM) or at 406 and 413 nm (Kaiser Optical, Ann Arbor, MI), in front of the entrance slit of the spectrometer, which was set to a width of 100 μm. The diffracted

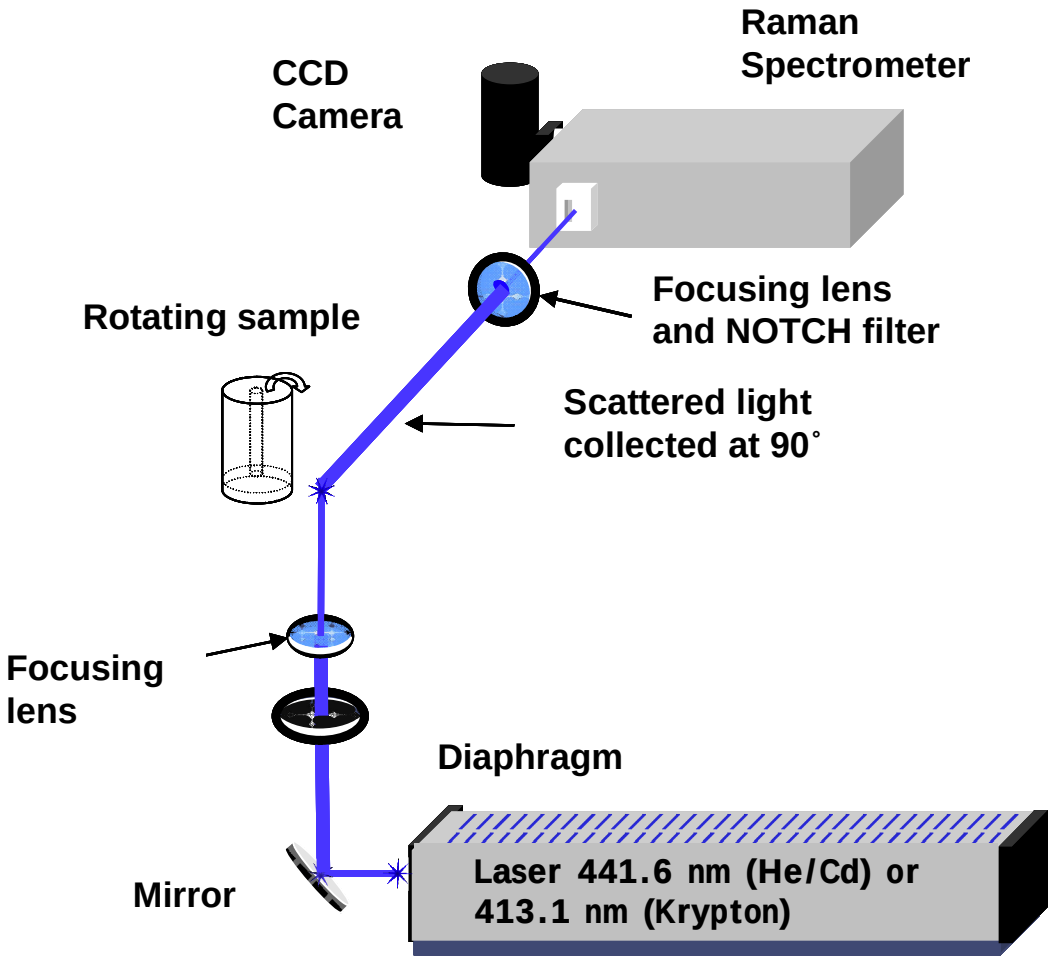

Figure 18. Schematic representation of the instrument used for resonance Raman spectroscopy. The Kr laser was used to excite the natural and reduced protein samples. The He/Cd laser was used to excite the CO- and NO-bound protein samples. (Courtesy of Dr. Manon Couture).

light was then detected by a liquid nitrogen-cooled CCD camera (Roper Scientific, Trenton, NJ). The instrument was calibrated in the high- and low-frequency regions using indene, and ferrocyanide and acetone were used to calibrate the instrument in the very high-frequency region.

3.6. Enzyme Activity Assays

To estimate the amount of nitric oxide generated, the production of nitrite through the peroxide-dependent oxidation of L-NHA was performed and measured using the Griess reaction. Sodium nitrite standards were prepared from 0 to 11 μM nitrite, in 1 μM increments. These standards were stored at 4 ˚C protected from light when not in use. Samples were prepared such that the reaction mixture contained 5 μM NOS suspended in L-arginine-free Lysis Buffer (see Appendix A), 1 mM L-NHA (Alexis Biochemicals), 100 mM HEPES, pH 7.5, and 100 μM H_4B if required. Aliquots of 70 μL of reaction mixture were injected into the appropriate wells of a 96-well plate. 200 μL of 100 mM HEPES, pH 7.5, were injected into the appropriate wells as blank controls. 100 μL of the nitrite standards were injected into the appropriate wells. The plate was then incubated on a hot block at 37 ˚C for five minutes. Following incubation, without removing the plate from the hot block, the reaction was initiated by adding 30 μL of 83 mM H_2O_2 (BioShop). The reaction was quenched at the appropriate time by adding 100 μL of Working Griess Reagent (equal parts of Griess Reagent A and B, see Appendix A). The Griess Reagents A and B were stored at 4 ˚C protected from light when not in use. The quenched reaction was incubated for an additional 15 minutes at 37 ˚C for optimum colour development. The plate was then read in a Bio-Rad Model 680 Microplate

Reader (Bio-Rad) at 550 nm, and the nitrite concentration of the samples was then determined from the absorbance of the sodium nitrite standards.

Chapter 4. Results

4.1. Purification and Identification of Homodimeric and Mixed Dimer Proteins

As NOS is a heme-containing protein, its presence of NOS can be monitored throughout the purification process by observing a reddish-brown hue to the cell lysates and eluants. During purification of homodimeric NOS, the Ni-NTA resin binds to all of the His_6-tagged protein, resulting in a considerable loss of colour, and protein, in the flow-through from the initial lysate provided the resin is not saturated. This is not observed during purification of the NOS heterodimer, as the Glu_7-tagged homodimer is found in the flow-through. The eluant contains both the His_6-tagged homodimer and the His_6/Glu_7-tagged heterodimer, which are then separated using anion exchange chromatography.

The cell and protein yields from *E. coli* BL21(DE3) are summarized in Table 2. Although the saNOS mixed dimers resulted in low protein yields, the yields for the homodimeric $eNOS_{oxy}$ proteins were consistently lower than those obtained for homodimeric saNOS. As NOS possesses a distinctive UV/visible spectrum, it is possible to use the intensity of the peaks corresponding to the aromatic residues (280 nm) and the heme (~400 nm), to determine protein purity and concentration. It has been reported that an A_{400}/A_{280} ratio of ~0.6 is considered to be 95% pure through SDS-PAGE analysis, and an A_{400}/A_{280} ratio greater than 0.55 is considered acceptable.[84] The saNOS W56/W56F and W56/W56Y heterodimers exhibited very high A_{400}/A_{280} ratios (0.75-0.85), in comparison to those obtained for homodimeric saNOS (0.50-0.65), due in part to the additional anion exchange purification step. The increased ratios are

Table 2. Average cell and protein yields obtained during the purification of $eNOS_{oxy}$ and saNOS proteins.

Protein	Cell Yield (g/L)	Protein Yield (mg/L)
$eNOS_{oxy}$ W180	18.8	5.1
$eNOS_{oxy}$ W180F	16.7	1.8
$eNOS_{oxy}$ W180Y	21.3	2.4
saNOS W56	15.2	8.9
saNOS W56F	13.8	6.5
saNOS W56/W56F	14.5	5.5
saNOS W56Y	18.0	11.4
saNOS W56/W56Y	16.2	3.8

primarily due to the decrease in A_{280} caused by the loss of the tryptophan residue.

The purification procedure for the saNOS heterodimers was monitored at each step for the presence of heme-containing proteins. The protein yields recovered at each step of purification are displayed in Table 3, for a preparation of W56/W56F heterodimer. This purification began with a pellet mass of 43.56 g. If the homodimers were expressed at similar levels and the monomers were associating independently, it would be expected that there would be a 1:2:1 ratio of Glu_7-tagged homodimer: His_6/Glu_7-tagged heterodimer: His_6-tagged homodimer. The results in Table 3 indicates that this is occurring; however, during the purification of the W56/W56Y heterodimer it was observed that the Glu_7-tagged homodimer was more highly expressed than the proteins containing His_6 tags, a finding that was also noted by McDonald, who reported a 2.5:1:1 ratio of Glu_7-tagged homodimer: His_6/Glu_7-tagged heterodimer: His_6-tagged homodimer.[84]

4.2. Anion Exchange Chromatography

Anion exchange chromatography was performed to separate the heterodimer from His6-tagged homodimeric protein. The Glu7 tag confers a slightly more negative charge to the protein subunit, and thus the use of an anion exchange resin enabled separation of the proteins based on the overall charge of the protein, with the heterodimer eluting after the His6-tagged homodimer (Figure 19). The injection of the Ni-NTA eluant onto a Mono Q column did not result in significant separation between the His6-tagged homodimer and the His6/Glu7-tagged heterodimers (Figure 20, trace a). The fractions corresponding to the latter retention time were pooled and reinjected onto the Mono Q column, which resulted in separation that was approximately 40:60

Table 3. Mass of heme protein identified during each step of W56/W56F heterodimer purification.

Step	Concentration of Heme-containing Protein (mg/mL)	Volume (mL)	Mass of Heme-containing Protein (mg)	Relative Mass
Ni-NTA Flow-through	0.92	28	26.6	1
Ni-NTA Eluant	9.36	5	46.8	2
His_6-tagged Homodimer from Mono Q	7.89	3	23.7	1
His_6/Glu_7-tagged Heterodimer from Mono Q	6.30	4	25.2	1

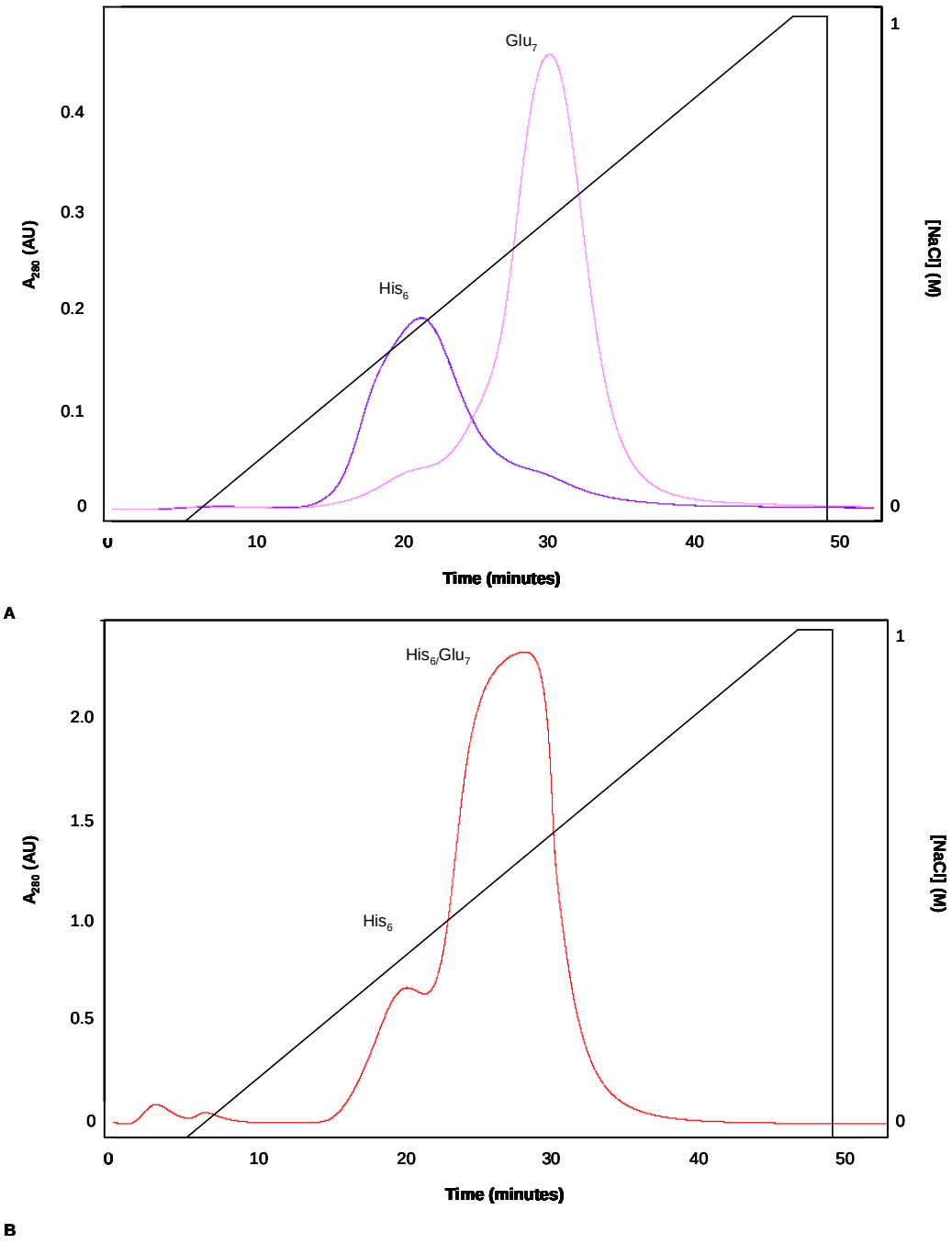

Figure 19. Anion exchange chromatography profiles for heterodimeric saNOS using a Mono Q column on an HPLC. As the Glu_7 tag increases the negative charge of the protein, on the Mono Q column, proteins can be separated based on the number of subunits carrying Glu_7 tags. As any Glu_7-tagged homodimeric proteins were eliminated during Ni-NTA chromatography, it may be assumed that any protein corresponding to the second peak is heterodimer.

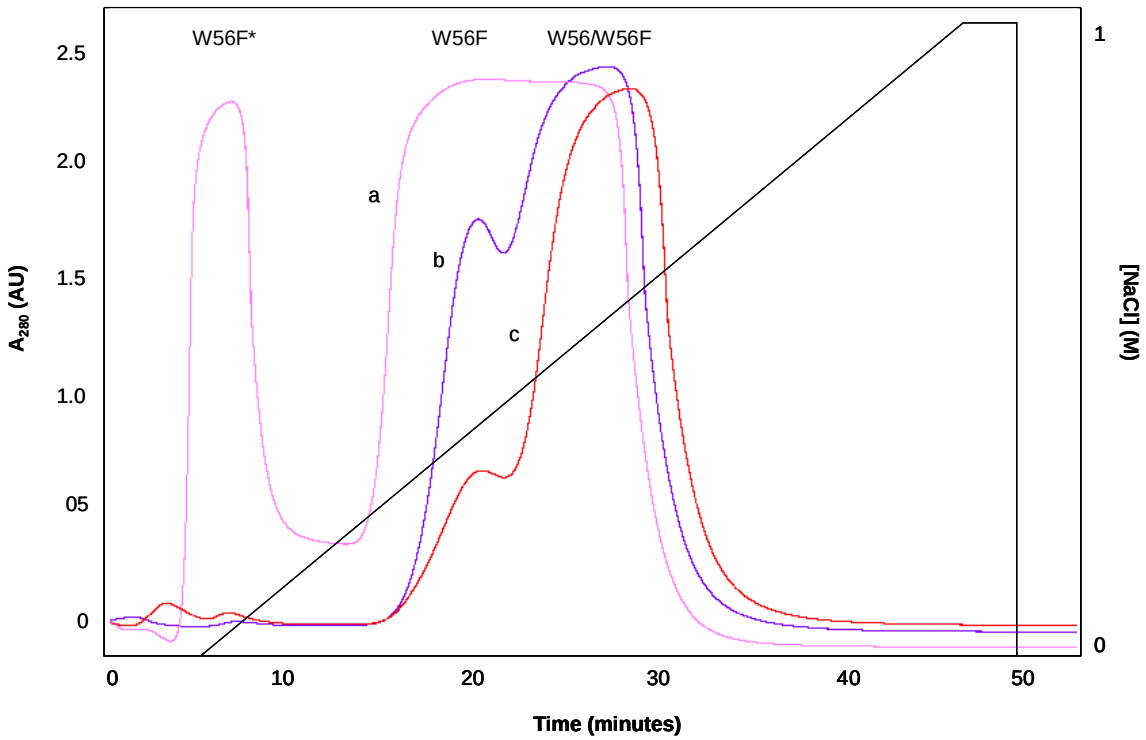

Figure 20. The separation of His_6-tagged W56F homodimer and His_6/Glu_7-tagged W56/W56F heterodimer by anion exchange chromatography on an HPLC. Ni-NTA eluant was exchanged into saNOS AEC Starting Buffer and injected onto a Mono Q column and eluted over a linear NaCl gradient from 0-1 M. (a) The initial injection yielded two peaks, the latter peak corresponding to an approximately equal mixture of His-tagged W56F homodimer and His_6/Glu_7-tagged W56/W56F heterodimer. (b) Fractions corresponding to this peak were pooled and injected onto a second Mono Q column. (c) The fractions corresponding to the heterodimer from the second column were applied to a third column, which resulted in optimal separation.

Homodimer: mixed dimer (Figure 20, trace b). Once again the fractions corresponding to the mixed dimer were pooled and injected onto a third, and final, anion exchange column. This final separation yielded 25:75 His_6-tagged homodimer: mixed dimer (Figure 20, trace c).

4.3. Spectroscopy

The UV/visible and resonance Raman spectroscopy experiments performed on the eNOSoxy proteins are summarized in Table 4, and those for the saNOS proteins are summarized in Table 5.

The difficulties with eNOS expression levels led to the decision to pursue mixed dimer studies with saNOS instead of eNOS. The resonance Raman spectra of homodimeric wild-type and the homodimeric W56F and W56Y mutant saNOS proteins have already been characterized by Jérôme Lang at Université Laval, which led the way for similar experiments involving mixed dimers of saNOS, where one subunit was wild-type and the other subunit possessed either the phenylalanine or tyrosine mutation at the W56 site. (For comparison purposes, the resonance Raman data, including spectra, for homodimeric saNOS proteins are originally from Jérôme Lang's research project; these are being used with his permission).

4.3.1. Ferric Forms of the $eNOS_{oxy}$ W180 Proteins

The UV/visible spectra obtained for the wild-type, W180F, and W180Y proteins all exhibit the characteristic spectrum for NOS, with increases in absorbance at approximately 400 nm, corresponding to the Soret band, and also between 600 and 800 nm, corresponding to the charge transfer band (Figure 21). In the presence of 5 mM L-arginine, the Soret band of the wild-type spectrum was located at 399 nm, and was

Table 4. Summary of spectroscopic experiments performed on $eNOS_{oxy}$ wild-type and W180 mutants. N/D – not determined

Protein	State	Substrate/ Cofactor	Discussed in Text
$eNOS_{oxy}$ W180	Ferric	+L-Arg/-H_4B	Figure 21; Figure 22
$eNOS_{oxy}$ W180	Ferric	+L-Arg/+H_4B	Figure 23
$eNOS_{oxy}$ W180	Ferrous	+L-Arg/-H_4B	Figure 24
$eNOS_{oxy}$ W180	Ferrous	+L-Arg/+H_4B	-N/D-
$eNOS_{oxy}$ W180	Fe(II)CO	+L-Arg/-H_4B	Figure 25; Figure 26; Figure 27
$eNOS_{oxy}$ W180	Fe(II)CO	+L-Arg/+H_4B	Figure 28; Figure 29
$eNOS_{oxy}$ W180	Fe(III)NO	-L-Arg/-H_4B	Figure 30
$eNOS_{oxy}$ W180	Fe(III)NO	+L-Arg/-H_4B	Figure 31
$eNOS_{oxy}$ W180	Fe(III)NO	+L-Arg/+H_4B	Figure 32
$eNOS_{oxy}$ W180F	Ferric	+L-Arg/-H_4B	Figure 21; Figure 22
$eNOS_{oxy}$ W180F	Ferric	+L-Arg/+H_4B	Figure 23
$eNOS_{oxy}$ W180F	Ferrous	+L-Arg/-H_4B	Figure 24
$eNOS_{oxy}$ W180F	Ferrous	+L-Arg/+H_4B	-N/D-
$eNOS_{oxy}$ W180F	Fe(II)CO	+L-Arg/-H_4B	Figure 25; Figure 26; Figure 27
$eNOS_{oxy}$ W180F	Fe(II)CO	+L-Arg/+H_4B	Figure 28; Figure 29
$eNOS_{oxy}$ W180F	Fe(III)NO	-L-Arg/-H_4B	Figure 30
$eNOS_{oxy}$ W180F	Fe(III)NO	+L-Arg/-H_4B	Figure 31
$eNOS_{oxy}$ W180F	Fe(III)NO	+L-Arg/+H_4B	Figure 32
$eNOS_{oxy}$ W180Y	Ferric	+L-Arg/-H_4B	Figure 21; Figure 22
$eNOS_{oxy}$ W180Y	Ferric	+L-Arg/+H_4B	Figure 23
$eNOS_{oxy}$ W180Y	Ferrous	+L-Arg/-H_4B	Figure 24
$eNOS_{oxy}$ W180Y	Ferrous	+L-Arg/+H_4B	-N/D-
$eNOS_{oxy}$ W180Y	Fe(II)CO	+L-Arg/-H_4B	Figure 25; Figure 27
$eNOS_{oxy}$ W180Y	Fe(II)CO	+L-Arg/+H_4B	Figure 28; Figure 29
$eNOS_{oxy}$ W180Y	Fe(III)NO	-L-Arg/-H_4B	Figure 30
$eNOS_{oxy}$ W180Y	Fe(III)NO	+L-Arg/-H_4B	Figure 31
$eNOS_{oxy}$ W180Y	Fe(III)NO	+L-Arg/+H_4B	Figure 32

Table 5. Summary of spectroscopic experiments performed on saNOS wild-type, homodimeric W56F mutants, and heterodimeric W56 mutants. Spectra shown for homodimeric saNOS proteins not listed here are from Jérôme Lang's research (unpublished). N/D – not determined

Protein	State	Substrate	Discussed in Text
saNOS W56	Ferric	+L-Arg	Figure 33; Figure 34
saNOS W56	Ferrous	+L-Arg	Figure 35
saNOS W56	Fe(II)CO	+L-Arg	Figure 37
saNOS W56	Fe(III)NO	+L-Arg	Figure 40
saNOS W56	Fe(III)NO	-L-Arg	Figure 41
saNOS W56F	Ferric	+L-Arg	Figure 33
saNOS W56/W56F	Ferric	+L-Arg	Figure 33
saNOS W56/W56F	Ferrous	+L-Arg	-N/D-
saNOS W56/W56F	Fe(II)CO	+L-Arg	Figure 37; Figure 38
saNOS W56/W56F	Fe(III)NO	+L-Arg	Figure 40
saNOS W56/W56F	Fe(III)NO	-L-Arg	Figure 41
saNOS W56Y	Ferric	+L-Arg	Figure 34
saNOS W56/W56Y	Ferric	+L-Arg	Figure 34
saNOS W56/W56Y	Ferrous	+L-Arg	Figure 35
saNOS W56/W56Y	Fe(II)CO	+L-Arg	Figure 36; Figure 37; Figure 39
saNOS W56/W56Y	Fe(III)NO	+L-Arg	Figure 40
saNOS W56/W56Y	Fe(III)NO	-L-Arg	Figure 41

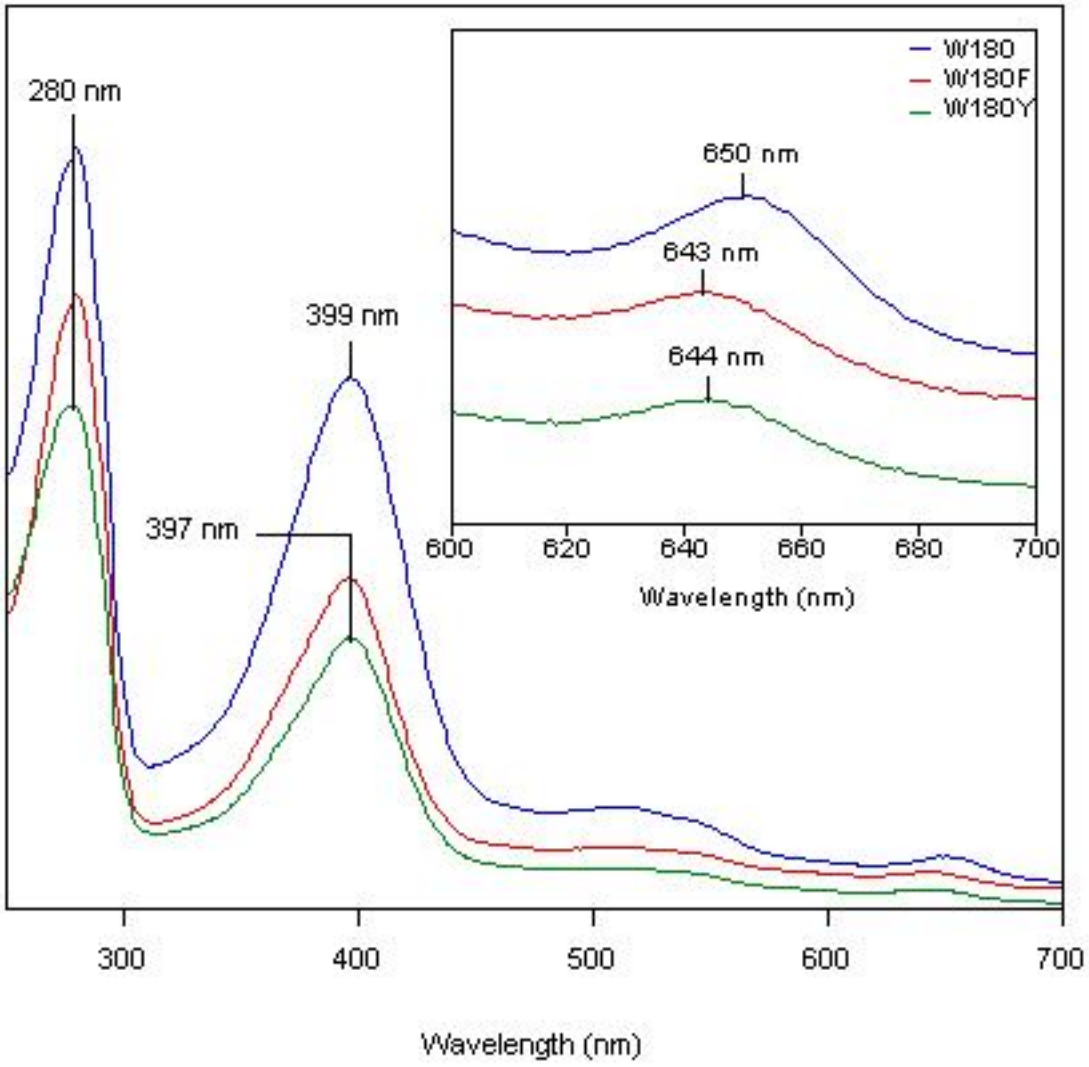

Figure 21. The UV/visible spectra of ferric $eNOS_{oxy}$ proteins in the presence of 5 mM L-arginine. Wild-type $eNOS_{oxy}$ (blue) displays characteristic Soret (399 nm) and charge transfer bands (650 nm). These bands are shifted for the W180F (red) and W180Y (green) $eNOS_{oxy}$ proteins.

found at 397 nm for both the W180F and W180Y mutants, corresponding to a five-coordinate high-spin state. The resonance Raman spectra also indicate that the $eNOS_{oxy}$ proteins were five-coordinate and high-spin based on two modes. The ν_3 mode, which is sensitive to the coordination and spin state of the heme iron, was identified at 1487 cm^{-1} (Figure 22), indicating that the heme iron is in the high-spin state. The ν_4 stretching mode, which is sensitive to the electron density on the heme and the oxidation state of the heme iron, was found at 1369 cm^{-1} for the wild-type protein, and at 1370 cm^{-1} for the mutant proteins (Figure 22), suggesting that the heme iron was five-coordinate in all cases.

Wild-type eNOS typically exhibits a small peak in the UV/visible spectrum at 650 nm corresponding to the charge transfer band (Figure 21). This band was shifted to 643 nm upon the mutation of W180 to either phenylalanine or tyrosine, indicating an increase in electron density towards the thiolate ligand from the iron.

When H_4B was present in addition to arginine, the Soret bands of the $eNOS_{oxy}$ proteins blue-shifted to 395 nm for wild-type, and 396 nm for W180F and W180Y, indicating that the proteins are also five-coordinate high-spin when H_4B is present (Figure 23). There was no observed effect of H_4B on the position of the charge transfer band for any of the $eNOS_{oxy}$ proteins.

4.3.2. Ferrous Forms of the $eNOS_{oxy}$ W180 Proteins

The ferrous species of the $eNOS_{oxy}$ proteins were generated by adding sodium dithionite to the protein sample. The ferrous spectra were obtained in the high-frequency region of the resonance Raman spectrum for the wild-type, W180F, and W180Y proteins (Figure 24). The presence of ν_3 at 1466 cm^{-1} suggests that in their

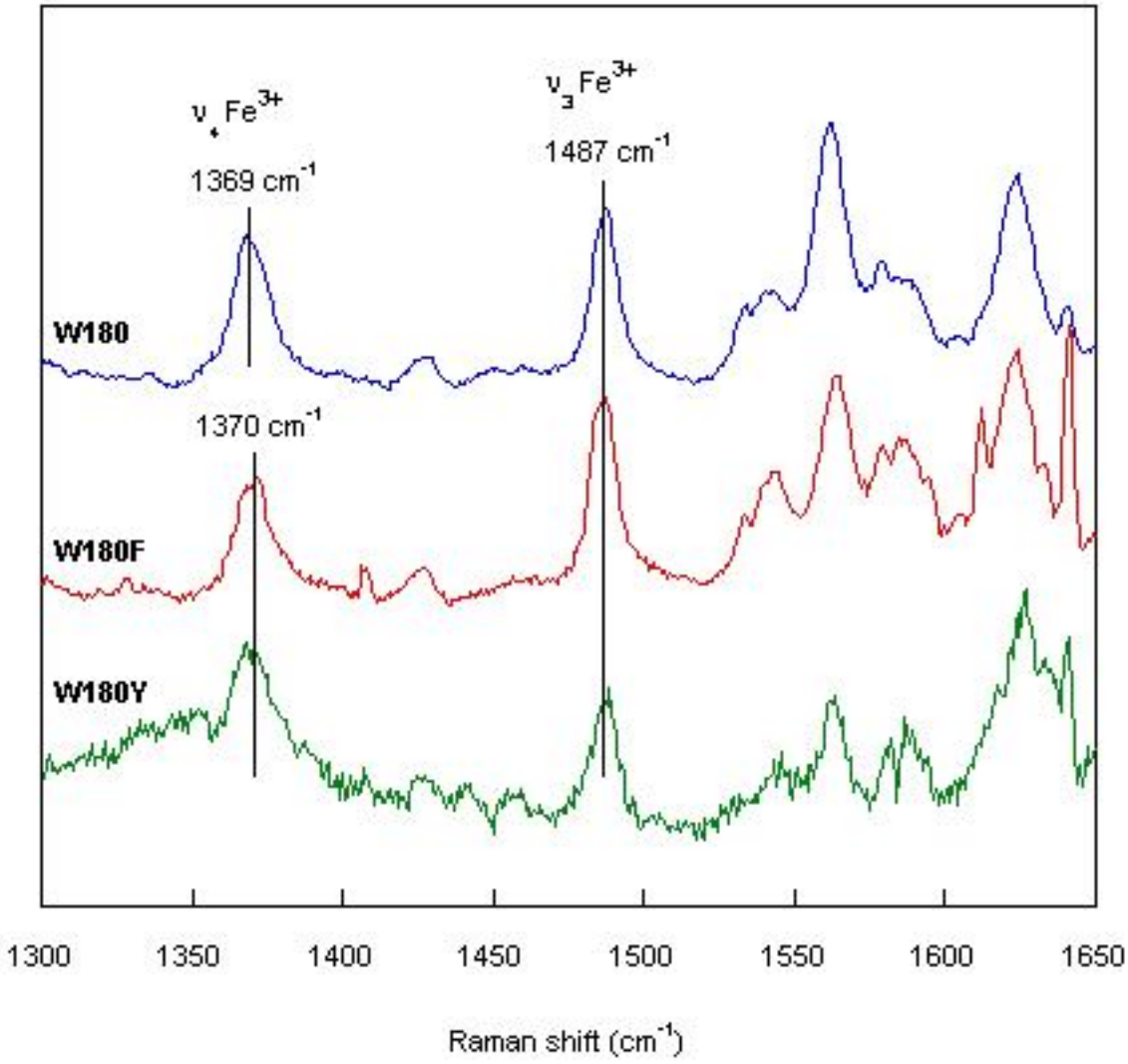

Figure 22. The high-frequency region of the resonance Raman spectrum of ferric $eNOS_{oxy}$ proteins in the presence of 5 mM L-arginine. The samples were excited at 413.1 nm with a laser power less than 6 mW. The positions of the ν_4 mode indicate that the proteins were present in the five-coordinate high-spin state.

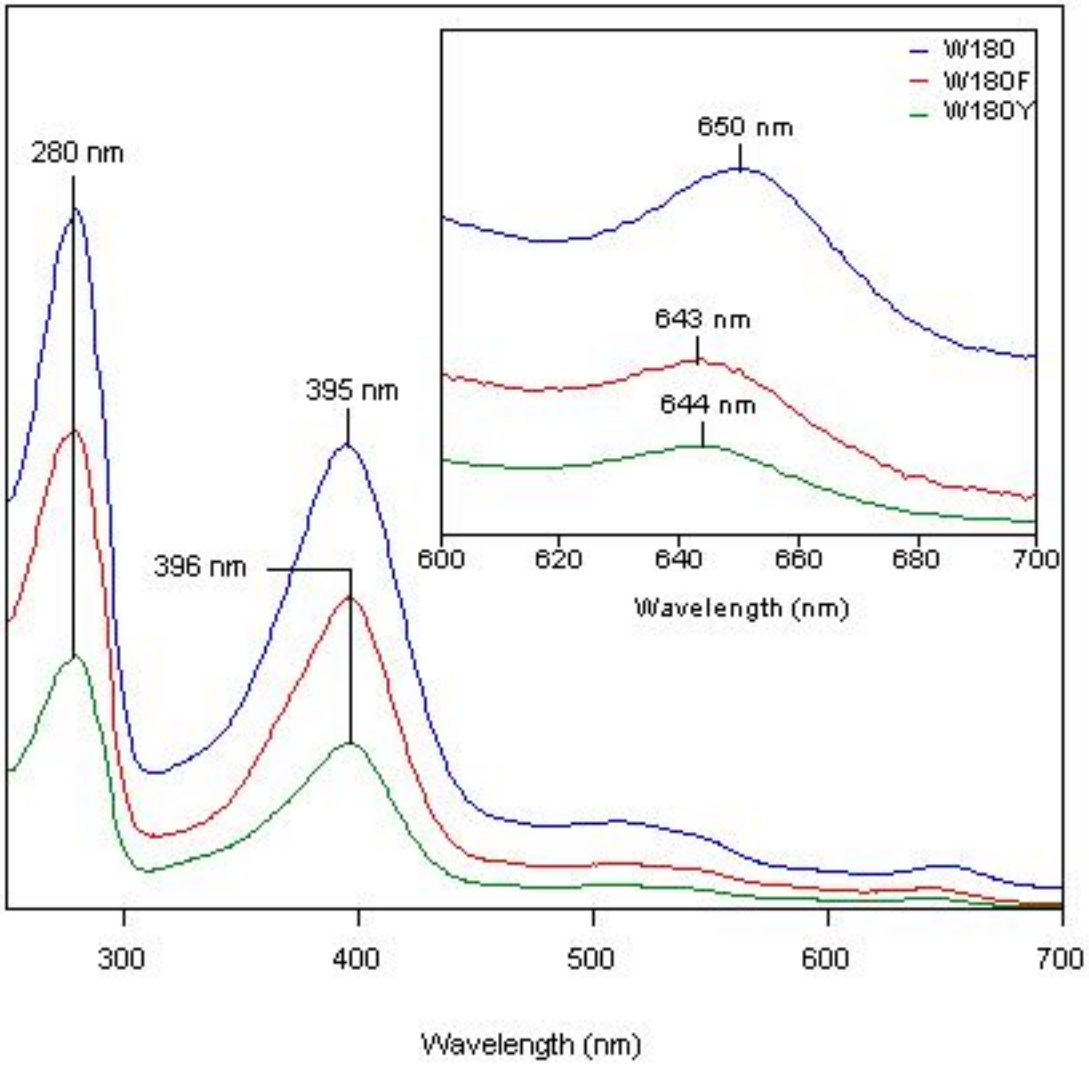

Figure 23. The UV/visible spectra of $eNOS_{oxy}$ proteins in the presence of 5 mM L-arginine and 2 mM H_4B. The Soret band for wild-type $eNOS_{oxy}$ (blue), W180F (red), and W180Y (green) are blue shifted in the presence of H_4B.

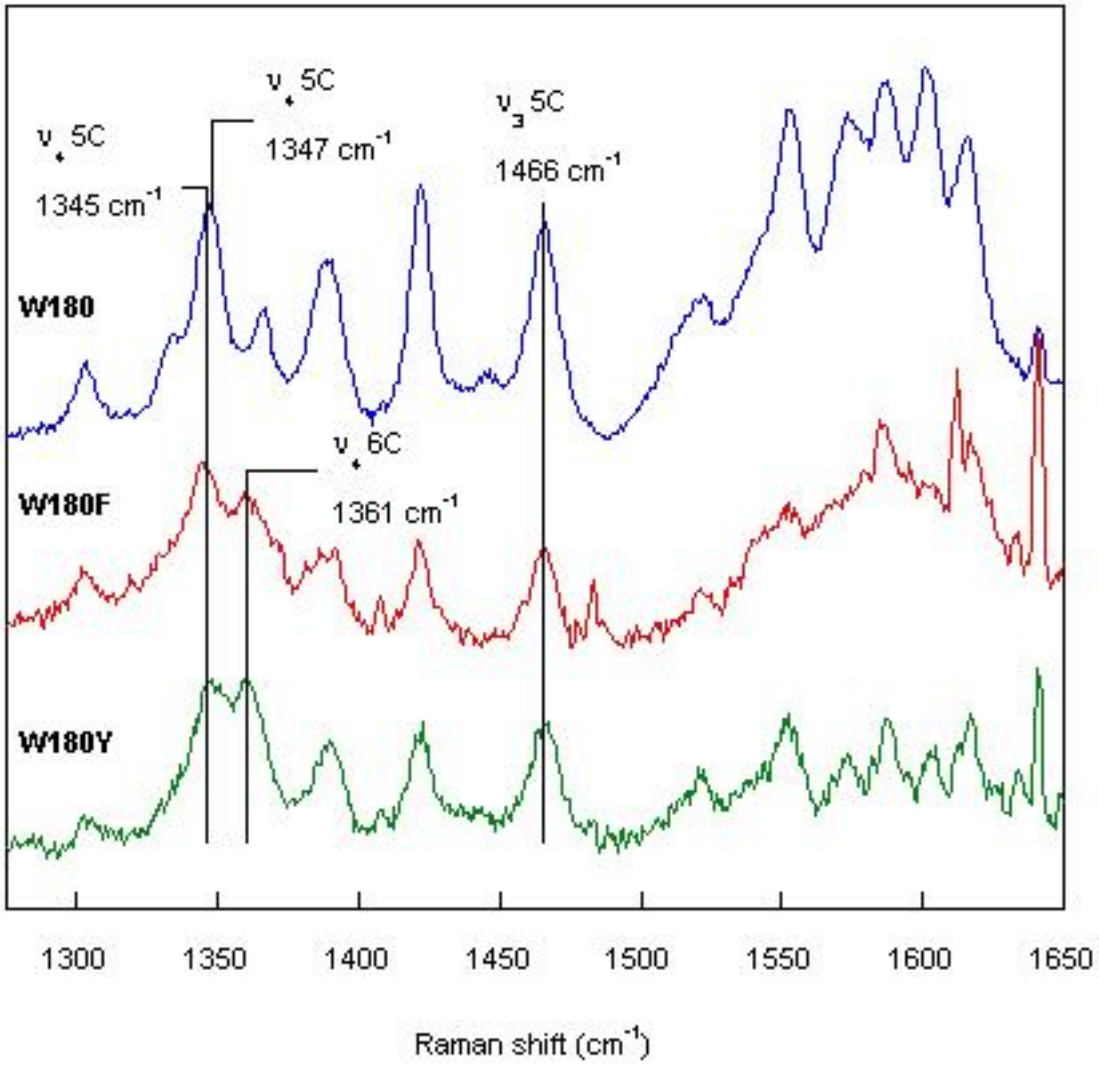

Figure 24. The high-frequency region of the resonance Raman spectrum of ferrous $eNOS_{oxy}$ proteins in the presence of 5 mM L-arginine. The samples were excited at 413.1 nm with a laser power less than 6 mW. The positions of ν_3 and ν_4 indicate that both proteins were present in the five-coordinate high-spin state. The presence of an additional ν_4 signal in the spectrum for W180F and W180Y suggests that some protein was present in the six-coordinate low-spin state.

ferrous forms, the heme iron of the wild--type and mutant $eNOS_{oxy}$ proteins is present in the five-coordinate high-spin state. The ν_4 mode was identified at 1347 cm^{-1} for wild-type, and was shifted to 1345 cm^{-1} for the mutants, indicating an increased basicity of the thiolate ligand for the mutants. An additional ν_4 mode for the W180F and W180Y proteins, detected at 1361cm^{-1}, indicates that some of the protein was present in the six-coordinate low-spin state.

4.3.3. Ferrous-CO Complexes of the $eNOS_{oxy}$ W180 Proteins

When the sodium dithionite-reduced sample was treated with CO, the Soret band of the UV/visible spectra shifted to 441 nm for wild-type, 444 nm for W180F, and 443 nm for W180Y, indicating that the Fe(II)CO complexes were in the six-coordinate low-spin state (Figure 25). Also, there was a large second Soret band located at 421 nm for W180Y, which was not significantly present for wild-type or W180F, which corresponds to an inactive form of cytochrome P450 enzymes.

The Fe(II)CO complexes of the $eNOS_{oxy}$ proteins were also examined to observe the coordination and oxidation states of the heme iron in the presence of a distal ligand, in the high-frequency region of the Raman spectrum. The presence of ν_4 at 1368 cm^{-1} in the wild-type and W180F proteins indicates that the heme iron of the Fe-CO complex for both of these proteins is six-coordinate (Figure 26). The presence of a ν3 mode at 1494 cm^{-1} indicates that the heme iron is in the low-spin state. Additional vibrational modes in both spectra corresponding to ν_3 and ν_4 at 1466 cm^{-1} and at approximately 1345 cm^{-1}, respectively, indicate that some of the protein was present in the five-coordinate high-spin state, for which CO was not bound to the heme iron (Figure 26). Spectra were not obtained for the Fe(II)CO complex of W180Y in the high-frequency region, due to

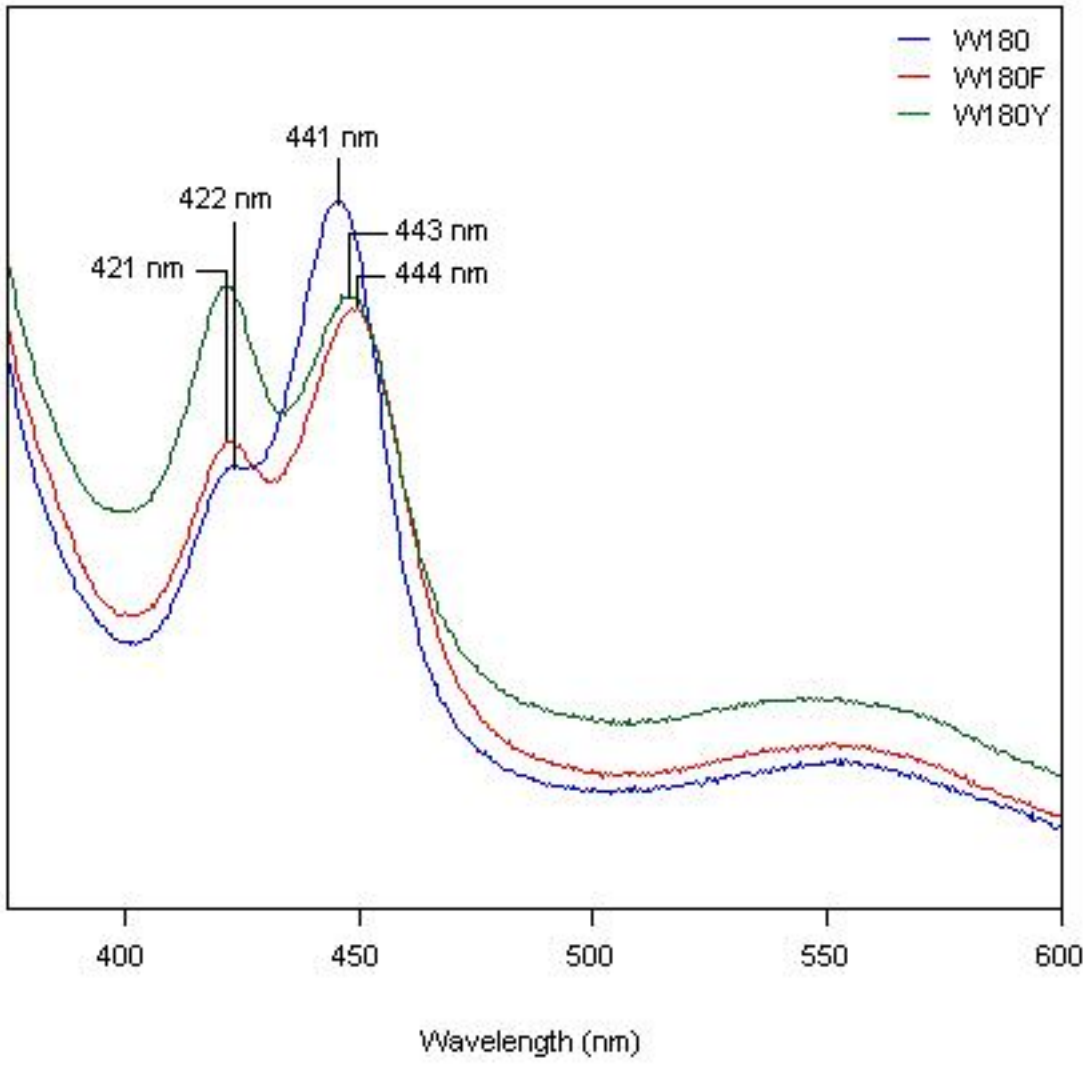

Figure 25. The UV/visible spectra of the Fe(II)CO complexes of $eNOS_{oxy}$ proteins in the presence of 5 mM L-arginine. A Soret band near 450 nm is typical of ferrous-CO complexes in NOS. The presence of a second Soret band at 420 nm suggests some protein is in an inactive state having lost thiolate ligation.

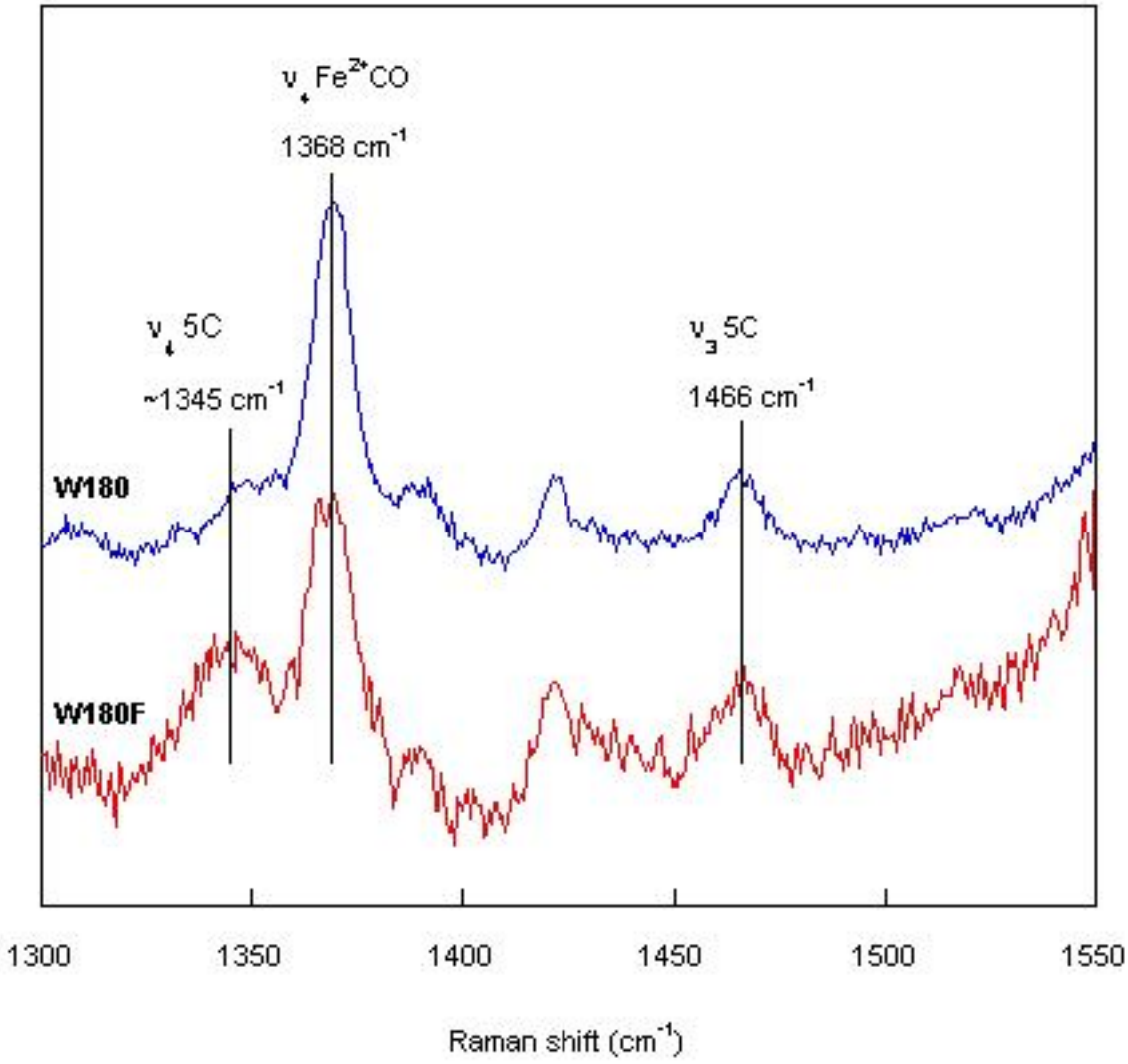

Figure 26. The high-frequency region of the resonance Raman spectrum of the Fe(II)CO complexes of wild-type and W180F $eNOS_{oxy}$ in the presence of 5 mM L-arginine. The samples were excited at 441.6 nm with a laser power of 3 mW for wild-type and 6 mW for W180F. The presence of ν_4 in both proteins indicates that the proteins were present in the six-coordinate low-spin state. The presence of additional ν_3 and ν_4 signals in both spectra are indicative of five-coordinate high-spin protein being present.

persistent precipitation of the sample during this experiment.

Examining the low-frequency region of the resonance Raman spectrum provided information regarding the Fe-CO stretching (ν_{Fe-CO}) and bending (δ_{Fe-C-O}) modes. The spectra were obtained for the wild-type, W180F, and W180Y proteins purified in the presence of 5 mM L-arginine, both with and without H_4B. The ν_{Fe-CO} mode for wild-type eNOS purified without the addition of H_4B was found at 509 cm^{-1}, which is at a higher frequency than the 507 cm^{-1} signals obtained for both the W180F and W180Y mutants, indicating that the -2 cm^{-1} shifts were the result of the mutation (Figure 27). This again indicates increased electron density from the iron to the thiolate ligand. The δ_{Fe-C-O} mode was found at 568 cm^{-1} in all three eNOS proteins, suggesting that the Fe(II)CO complex remains linear (Figure 27). Heme deformation modes were present at 678, 684, 710, 744, 752, and 803 cm^{-1} in all three proteins. Increases in the 752 and 803 cm^{-1} modes have been previously observed for $iNOS_{oxy}$ in the presence of L-arginine.[79] The largest out-of-plane mode observed for the $eNOS_{oxy}$ proteins was the mode at 684 cm^{-1}, corresponding to a saddled heme. The 710 and 744 cm^{-1} modes were enhanced for the W180F and W180Y mutants, indicating an increase in ruffling and pyrrole propeller distortions for these proteins.

The addition of 2 mM H_4B reduced the appearance of this second band significantly, and also resulted in a slight red shift of the main Soret band for the proteins, to 448 nm for the W180F protein (Figure 28). The Soret band was found at 446 nm for both wild-type and W180Y $eNOS_{oxy}$, suggesting that the heme environments of the Fe(II)CO complexes were the same for these two proteins. The Fe(II)CO complexes were stable for at least 30 minutes (Figure 28).

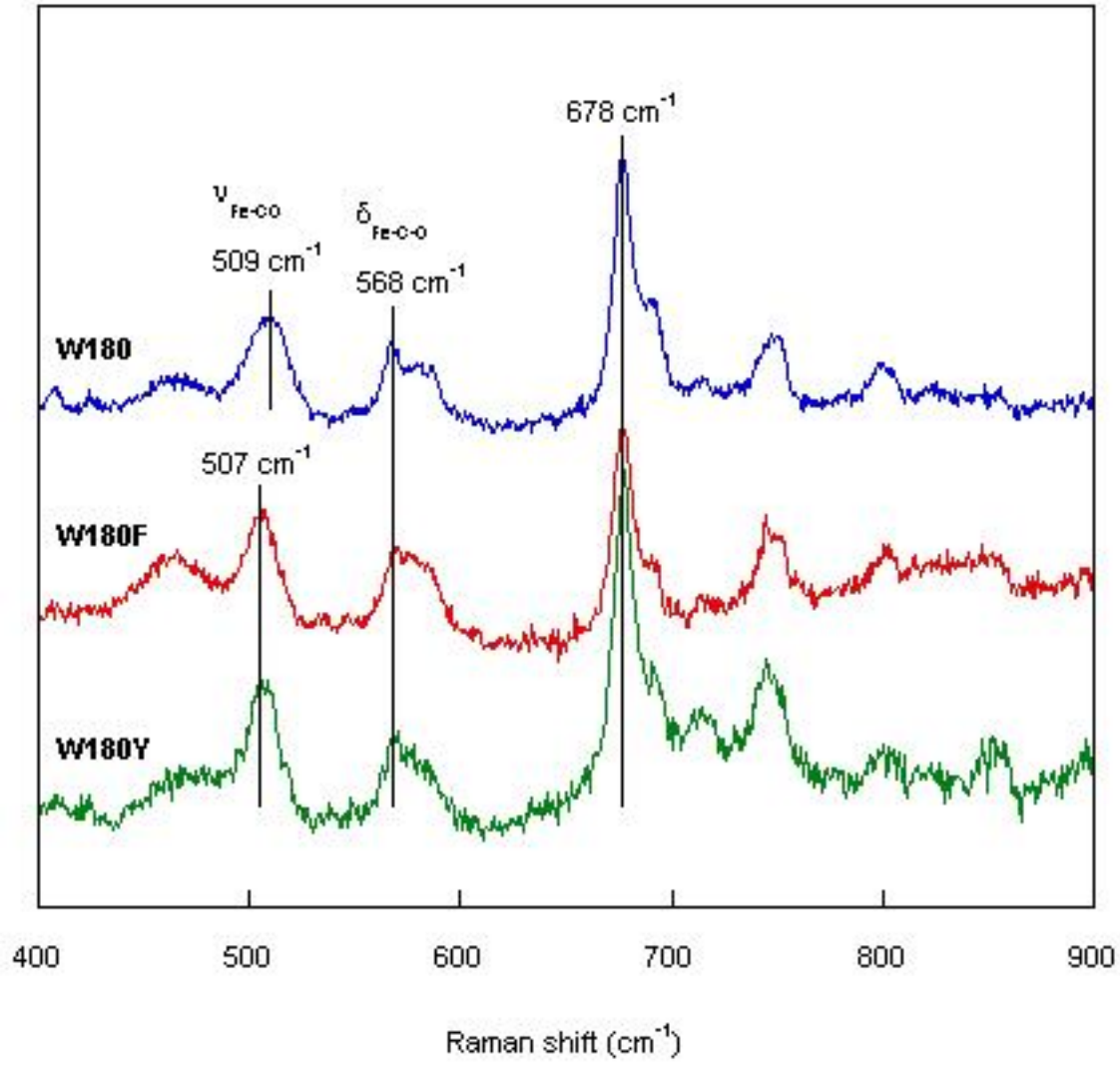

Figure 27. The low-frequency region of the resonance Raman spectrum of the Fe(II)CO complexes of $eNOS_{oxy}$ proteins in the presence of 5 mM L-arginine. The samples were excited at 441.6 nm with a laser power of 4 mW. The Fe-C-O bending mode ($\delta_{Fe\text{-}C\text{-}O}$) did not shift from 568 cm^{-1} with the introduction of the mutations. The Fe-CO stretching mode ($\nu_{Fe\text{-}CO}$) shifted from 509cm^{-1} in the wild-type to 507 cm^{-1} for W180F and W180Y.

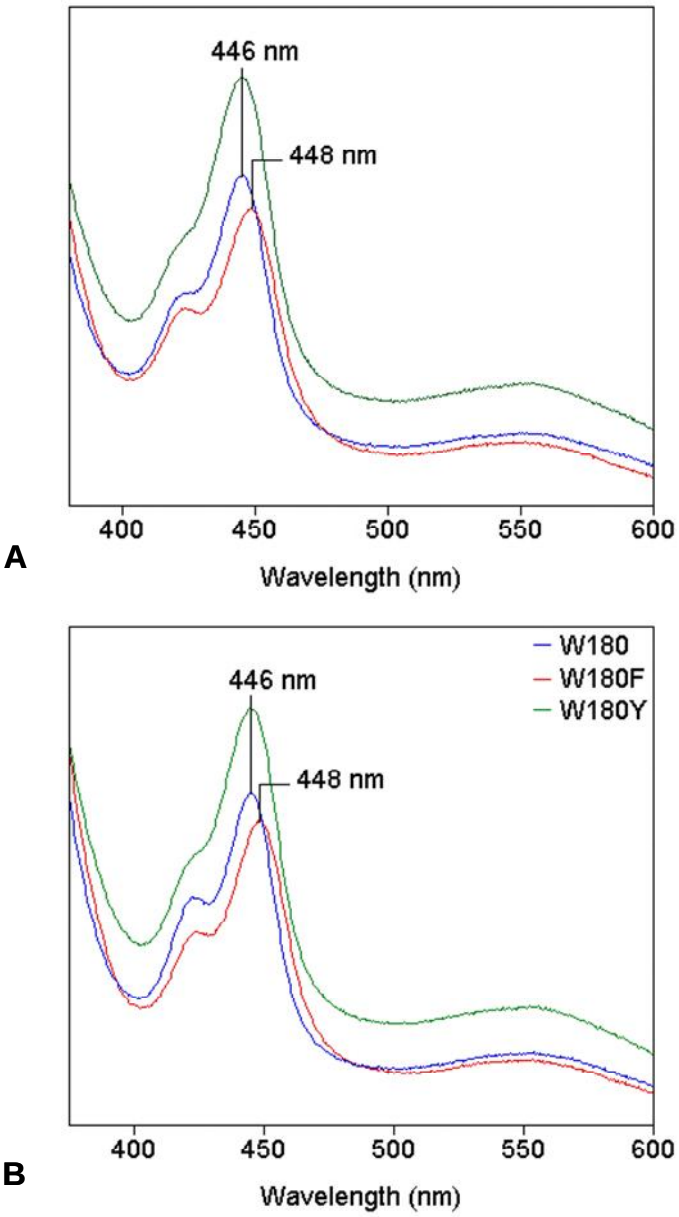

Figure 28. The UV/visible spectra of the Fe(II)CO complexes of $eNOS_{oxy}$ proteins in the presence of 5 mM L-arginine and 2 mM H_4B. In the presence of H_4B, there was very little formation of the P420 form of the proteins immediately after the addition of CO (A). The $eNOS_{oxy}$ proteins in the P450 state remained stable for at least 30 minutes (B).

Resonance Raman spectroscopy on the $eNOS_{oxy}$ proteins in the presence of 2 mM H_4B identified the ν_{Fe-CO} mode at 508 cm^{-1} for W180F (Figure 29). This mode was found at 512 cm^{-1} for both the wild-type and W180Y $eNOS_{oxy}$ proteins, indicating that in the presence of H_4B there is no change in thiolate basicity upon the mutation of W180 to W180Y. A lower-frequency shoulder was observed for the ν_{Fe-CO} modes for wild-type and W180Y, suggesting the presence of a second CO-bound species in these proteins. Thus, there was a -4 cm^{-1} shift due to the W180F mutation. The overall effect of H_4B was to increase the Raman shift by 3 cm^{-1} for wild-type, 1 cm^{-1} for W180F, and 5 cm^{-1} for W180Y. Once again, there is no change in the δ_{Fe-C-O} mode from 568 cm^{-1} upon introduction of either mutation, indicating that the Fe(II)CO complex is linear. Heme in-plane modes were identified at 678 and 752 cm^{-1}. Heme out-of-plane modes are present at 684, 710, 744, and the 803 cm^{-1} mode is shifted more towards 798 cm^{-1}. The 752 and possibly 798 cm^{-1} modes are enhanced in the presence of H_4B, which have been observed for the other mammalian NOSs, although the increase at 752 cm^{-1} may be due to a decrease in intensity of the 744 cm^{-1} mode.[85; 86] The mode identified at 684 cm^{-1} was again the strongest out-of-plane mode, suggesting saddling of the heme. The modes observed for W180Y at 710 cm^{-1} and 746 cm^{-1} were decreased with the addition of H_4B, suggesting less ruffling and propellering of the heme.

4.3.4. Ferric-NO Complexes of the $eNOS_{oxy}$ W180 Proteins

The ferric NO-bound complexes also display two modes, the Fe(III)NO stretching (ν_{Fe-NO}) and bending (δ_{Fe-N-O}) modes in the low-frequency region. When the Fe(III)NO complexes of the wild-type and W180F proteins were explored in the absence of L-arginine and H_4B, the ν_{Fe-NO} mode was detected at 538 cm^{-1} for wild-type eNOS, 530 cm^{-}

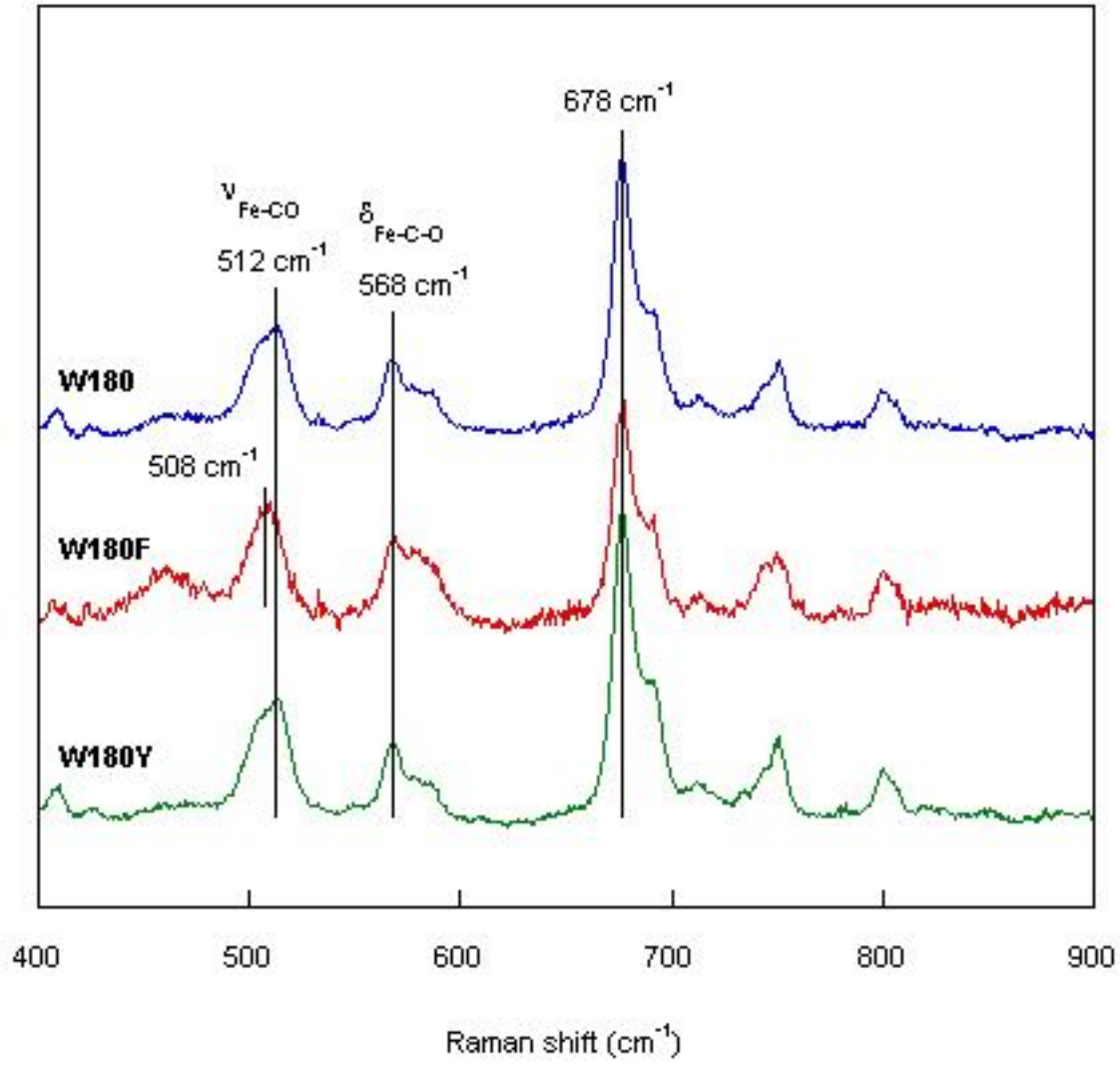

Figure 29. The low-frequency region of the resonance Raman spectrum of the Fe(II)CO complexes of $eNOS_{oxy}$ proteins in the presence of 5 mM L-arginine and 2 mM H4B. The samples were excited at 441.6 nm with a laser power of 4 mW. The Fe-C-O bending mode ($\delta_{Fe\text{-}C\text{-}O}$) did not shift from 568 cm^{-1} with the introduction of the mutations. The Fe-CO stretching mode ($\nu_{Fe\text{-}CO}$) shifted from 512cm^{-1} in the wild-type and W180Y proteins to 508 cm^{-1} for W180F.

[1] for W180F, and 533 cm^{-1} for W180Y (Figure 30). This indicates a -8 cm^{-1} shift induced by the phenylalanine mutation and a -5 cm^{-1} shift induced by tyrosine (Figure 30). Heme deformation modes were identified at 674, 684, 707, 729, 744, 752, and 803 cm^{-1}, indicating distortion of the heme along several coordinates.

When the Fe(III)NO complexes of the wild-type and W180F proteins were explored in the presence of 5 mM L-arginine, the $\delta_{Fe\text{-}N\text{-}O}$ mode was detected at 542 cm^{-1} for wild-type eNOS and 539 cm^{-1} for W180F and W180Y, indicating a -3 cm^{-1} shift induced by the mutation (Figure 31). The $\nu_{Fe\text{-}NO}$ mode was obscured by the $\delta_{Fe\text{-}NO}$ signal. Heme deformation modes were identified at 676, 684, 707, 729, 744, 752, and 803 cm^{-1}, indicating distortion of the heme along several coordinates.

When the NO complexes were formed in the presence of 1 mM L-arginine and 1 mM H_4B, the Fe-NO bending mode ($\delta_{Fe\text{-}N\text{-}O}$) was observed. Unlike with the Fe(II)CO complexes, the signal for this mode is the same for W180F and W180Y (540 cm^{-1}), whereas the $\delta_{Fe\text{-}N\text{-}O}$ mode for the wild-type protein was detected at 546 cm^{-1}, indicating a -6 cm^{-1} shift due to the mutation (Figure 32). The shifts corresponding to H_4B were 4 cm^{-1} for wild-type and 1 cm^{-1} for W180F and W180Y. The same heme distortion modes that were found in the absence of H_4B were also detected, although the relative intensity of the out-of-plane 684, 707, 729, and 803 cm^{-1} modes were increased in the presence of H_4B, suggesting increased saddling, doming, and possibly ruffling of the heme. The 744 cm^{-1} mode was enhanced for wild-type $eNOS_{oxy}$, but not for the mutant proteins, suggesting that there may be more propellering of the heme in the wild-type protein.

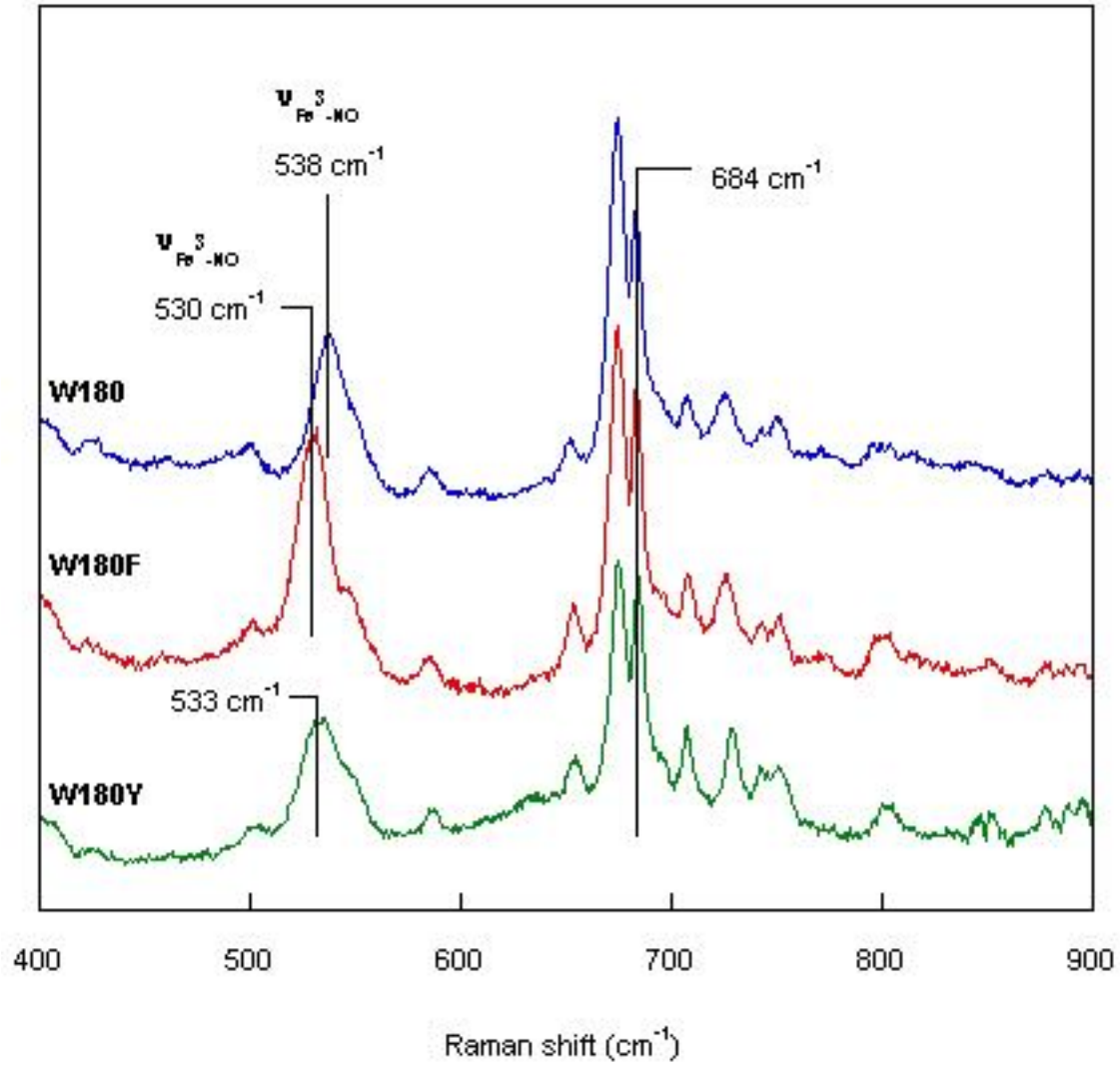

Figure 30. The low-frequency region of the resonance Raman spectrum of the Fe(III)NO complexes of $eNOS_{oxy}$ proteins when L-arginine and H_4B are absent. The samples were excited at 441.6 nm with a laser power of 6 mW. The Fe-NO stretching mode ($\nu_{Fe\text{-}N\text{-}O}$) shifted from 538 cm^{-1} in the wild-type protein to 530 cm^{-1} in W180F and 533 cm^{-1} in the W180Y mutant.

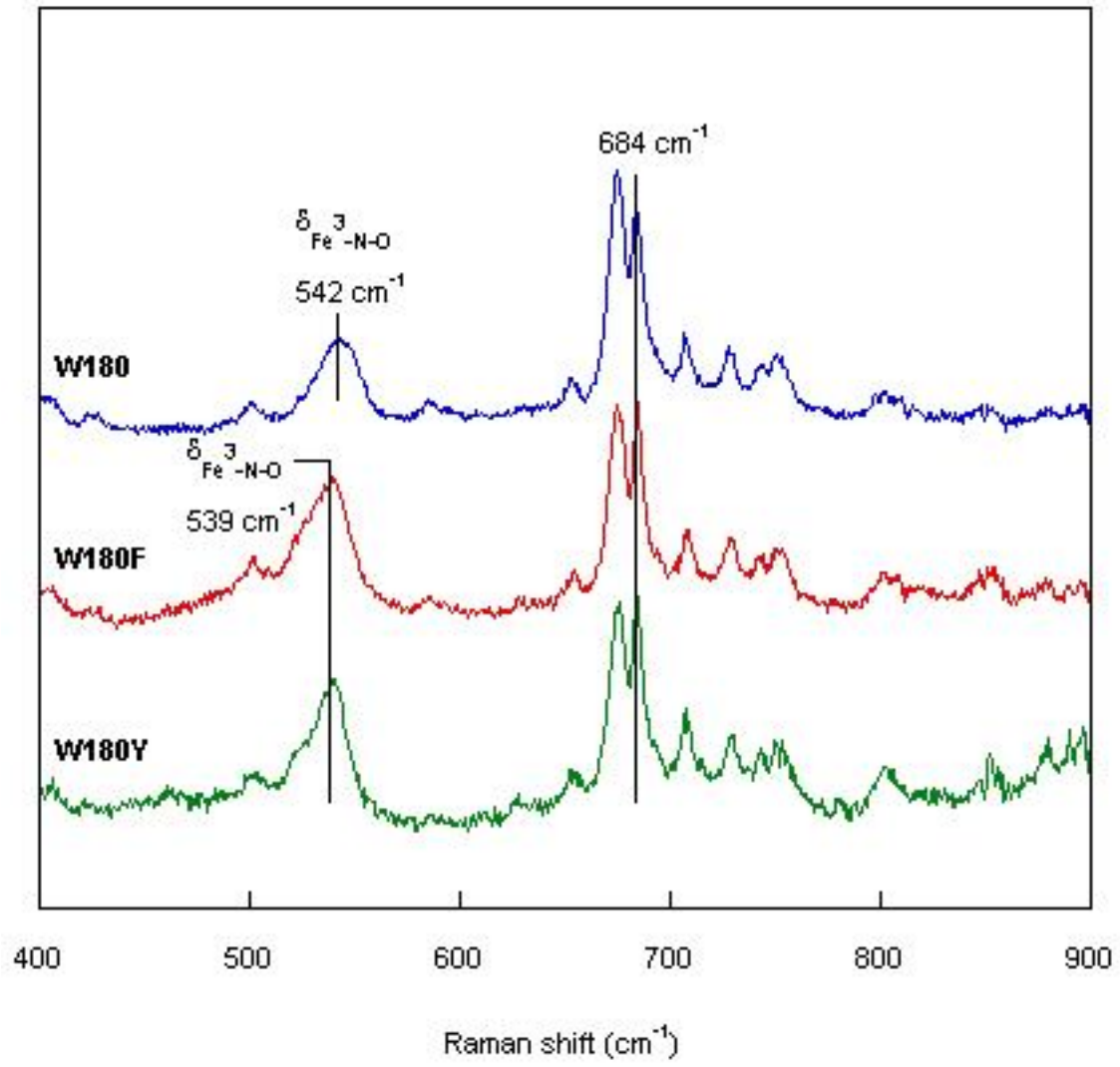

Figure 31. The low-frequency region of the resonance Raman spectrum of the Fe(III)NO complexes of $eNOS_{oxy}$ proteins in the presence of 5 mM L-arginine. The samples were excited at 441.6 nm with a laser power of 6 mW. The Fe-NO bending mode ($\delta_{Fe\text{-}N\text{-}O}$) shifted from 542 cm^{-1} in the wild-type protein to 539 cm^{-1} in the W180F and W180Y mutants.

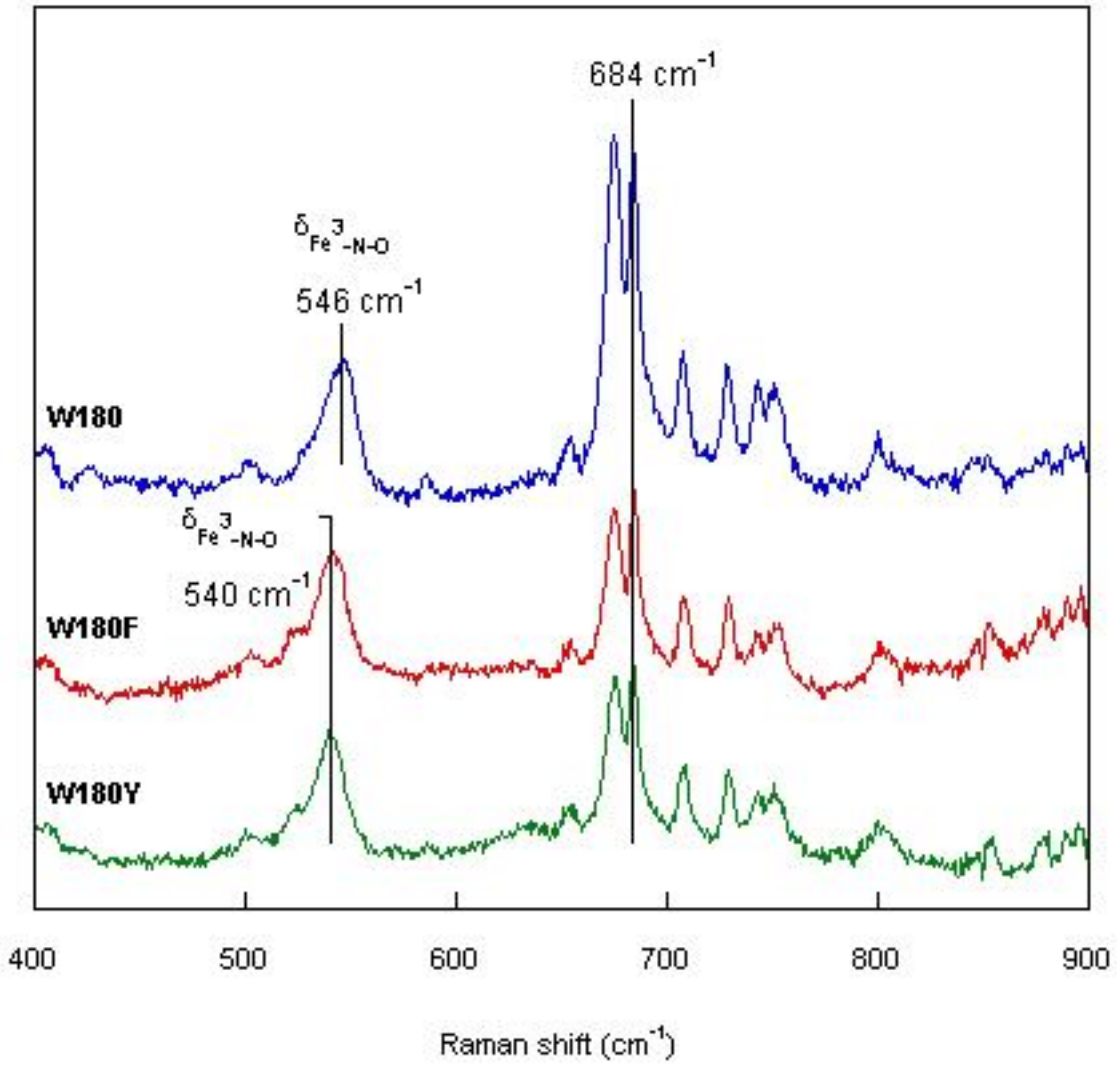

Figure 32. The low-frequency region of the resonance Raman spectrum of the Fe(III)NO complexes of $eNOS_{oxy}$ proteins in the presence of 5 mM L-arginine and 1 mM H_4B. The samples were excited at 441.6 nm with a laser power of 6 mW. The Fe-NO bending mode (δ_{Fe-N-O}) shifted from 546 cm^{-1} in the wild-type protein to 540 cm^{-1} in the W180F and W180Y mutants.

4.3.5. Ferric Forms of the saNOS W56 Heterodimers

The spectra obtained for the wild-type, W56F, W56Y, and heterodimeric proteins also exhibit the characteristic UV/visible spectrum for NOS, with a Soret band at approximately 400 nm and a charge transfer band between 600 and 800 nm (Figure 33 and Figure 34). In the presence of 5 mM L-arginine, the Soret band was located at 395 nm for wild-type saNOS and at 397 nm for W56F and W56Y, indicative of the five-coordinate high-spin state (Figure 33 and Figure 34, respectively). The Soret bands for the W56/W56F and W56/W56Y heterodimers in the ferric state were also found at 397 nm.

The charge transfer band was found at 646 nm for wild-type saNOS (Figure 33and Figure 34), and was shifted to 639 nm for W56F (Figure 33) and 641 nm for W56Y (Figure 34). The W56/W56F heterodimer exhibited a charge transfer band at 641 nm, between the signals for the wild-type and W56 homodimer, which could be indicative of the shared effects of both subunits (Figure 33). The charge transfer band was shifted to 643 nm for W56/W56Y (Figure 34), again indicating a combined effect.

4.3.6. Ferrous Forms of the saNOS W56 Heterodimers

The sodium dithionite-reduced W56/W56Y mixed dimer was examined in the high-frequency region to observe the coordination and oxidation states of the protein in comparison to wild-type and homodimeric W56Y proteins (Figure 35). These proteins displayed signals for ν_4 at 1347 cm^{-1} for the wild-type proteins, and at 1346 cm^{-1} for the proteins containing W56Y subunits, indicating that these proteins were present in the five-coordinate high-spin state. Also observed for the W56Y-containing proteins was an additional ν_4 signal at 1360 cm^{-1}, which corresponds to some of the proteins being in the

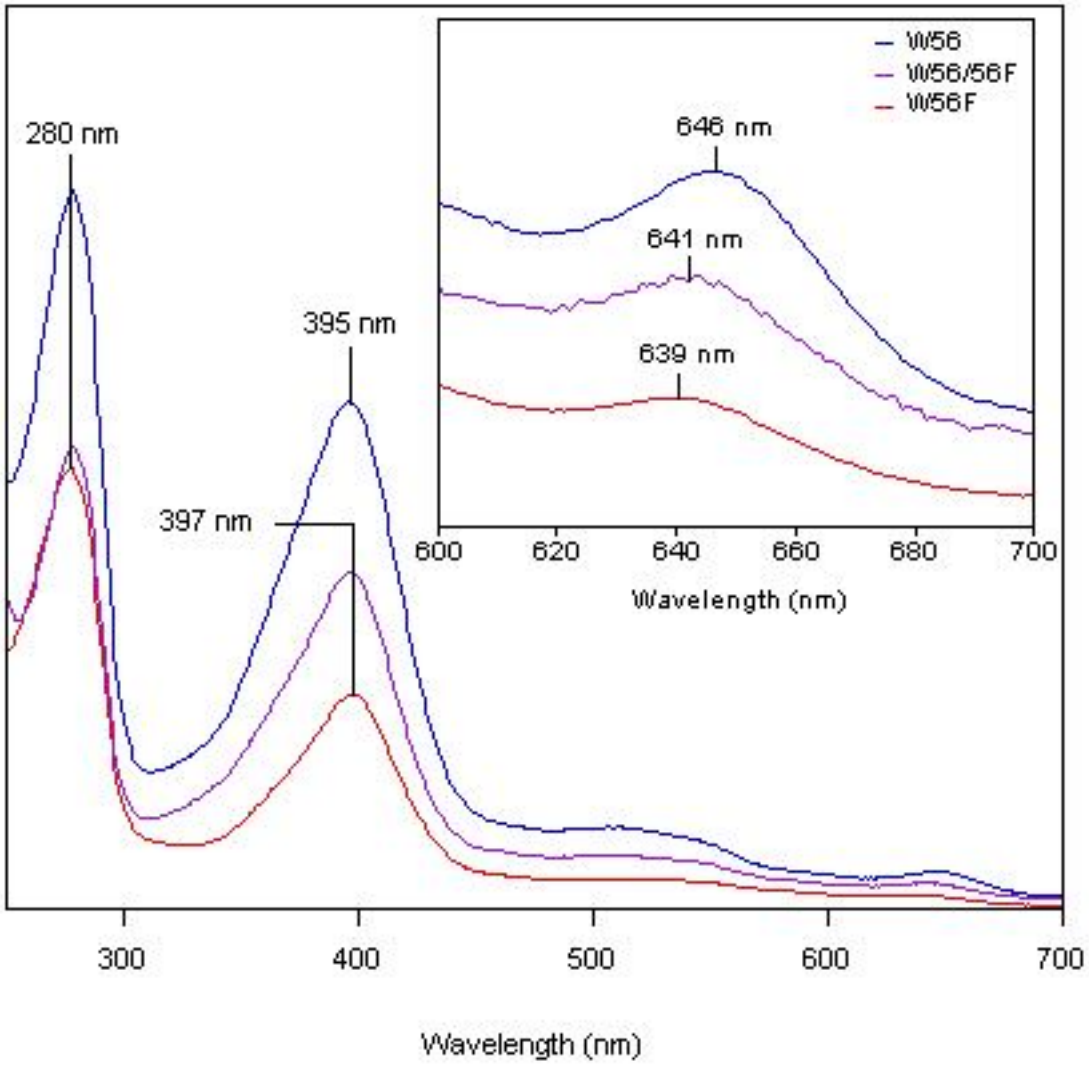

Figure 33. The UV/visible spectra of ferric wild-type, W56F, and W56/W56F saNOS in the presence of 5 mM L-arginine. Wild-type saNOS (blue) displays characteristic Soret (395 nm) and charge transfer bands (646 nm). These bands are shifted for the W56F (red) and W56/W56F (purple) saNOS proteins.

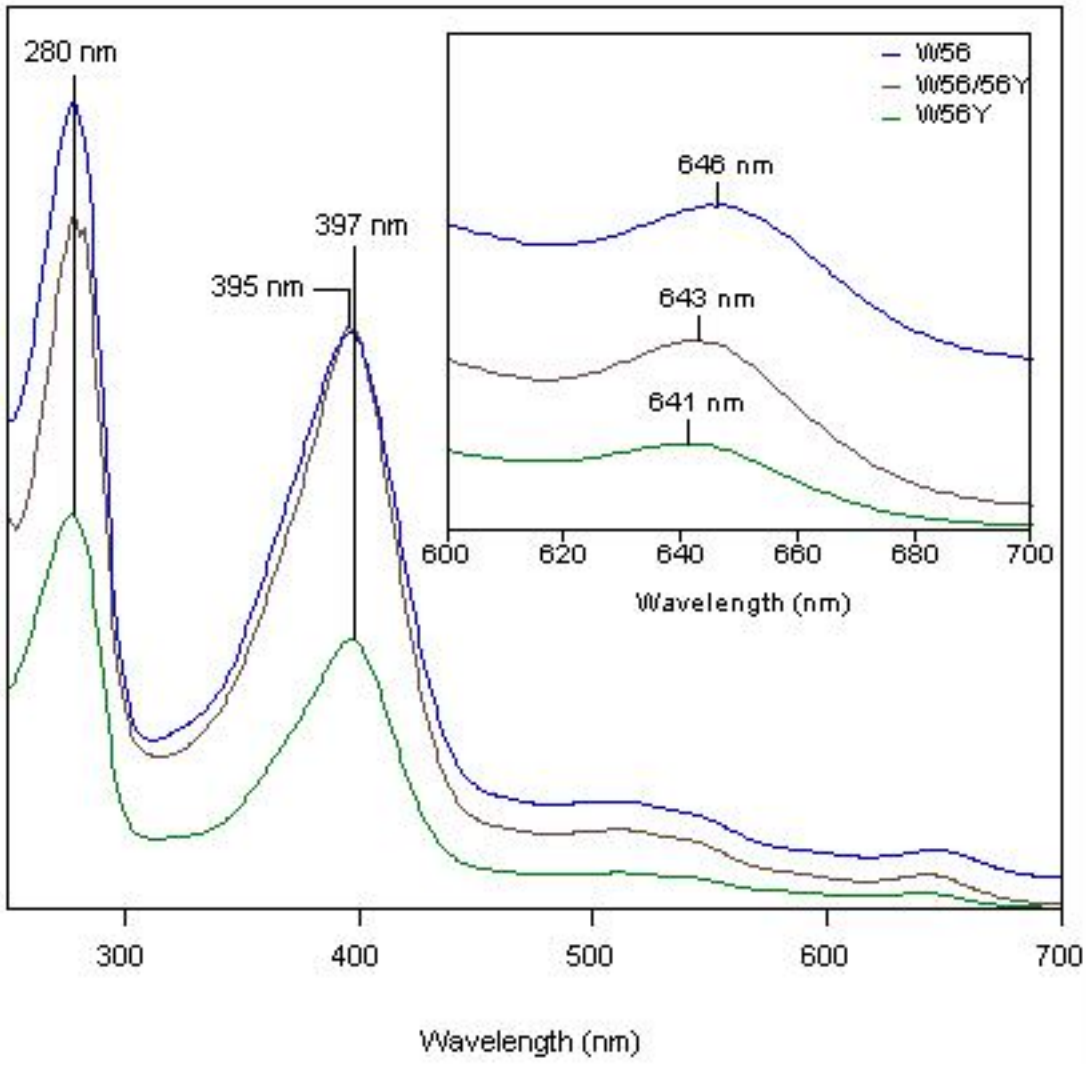

Figure 34. The UV/visible spectra of ferric wild-type, W56Y, and W56/W56Y saNOS in the presence of 5 mM L-arginine. Wild-type saNOS (blue) displays characteristic Soret (395 nm) and charge transfer bands (646 nm). These bands are shifted for the W56Y (green) and W56/W56Y (brown).

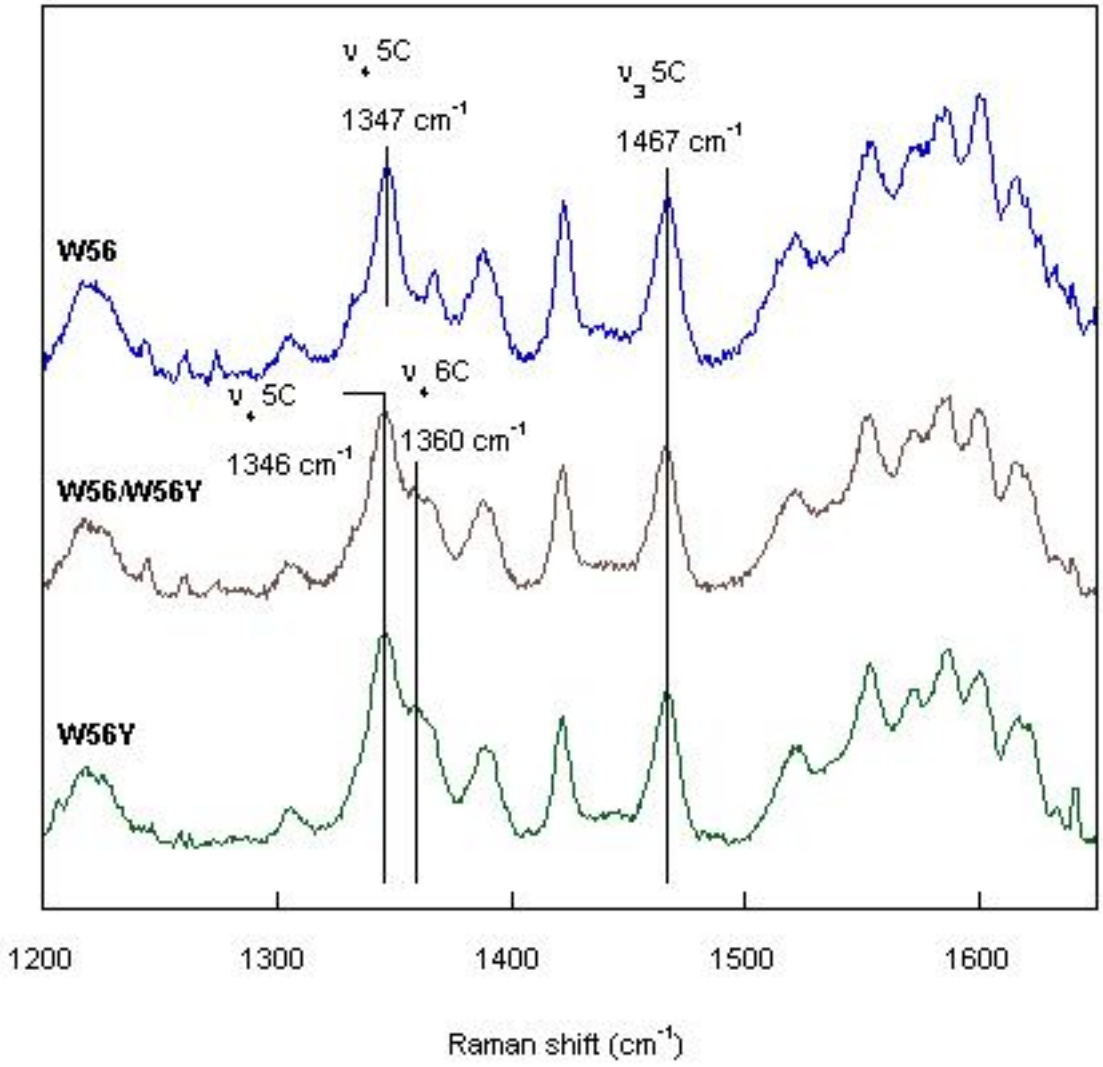

Figure 35. The high-frequency region of the resonance Raman spectrum of ferrous wild-type (blue), W56Y (green), and W56/W56Y (brown) saNOS in the presence of 1 mM L-arginine. The samples were excited at 413.1 nm with a laser power of 6 mW. The presence of ν_4 at 1346 and 1347 cm^{-1} and ν_3 at 1467 cm^{-1} indicate that all proteins were present in the five-coordinate high-spin state. The presence of an additional ν_4 signal at 1360 cm^{-1} in the spectra for the W56Y and W56/W56Y suggests that some protein was present in the six-coordinate low-spin state.

six-coordinate low- spin state.

4.3.7. Ferrous-CO Complexes of the saNOS W56 Heterodimers

The Fe(II)CO complexes of the heterodimers exhibited two Soret bands at 422 and 445 nm (Figure 36). These bands are thought to correspond to the iron centers of the wild-type and mutant subunit individually, as the Soret band for the Fe(II)CO complexes of homodimeric saNOS proteins has been reported at 449 nm for wild-type and at 422 nm W56F and W56Y (Lang and Couture, unpublished). Unlike the two bands observed for the Fe(II)CO complex of the $eNOS_{oxy}$ W180Y and W180F variants, which corresponded to protein in both the P420 and P450 states, wild-type saNOS is exclusively P450, and the W56F and W56Y proteins are entirely P420. The formation of the P420 state indicates loss of thiolate ligation. This could arise from protonation of the thiolate, and as W56/W56Y slowly converted to the P420 state, the protein was exchanged into a pH 10 buffer. This did not reduce the formation of the P420 form of the Fe(II)CO complex of W56/W56Y, suggesting that the conversion to this form does not arise from thiolate protonation.

The optical spectra of the saNOS W56/W56F and W56/W56Y proteins suggest that both the P420 and P450 hemes are present within the mixed dimers. Therefore, excitation of the mixed dimers near 420 nm will probe the mutant subunit and excitation near 450 nm will probe the wild-type subunit of the same heterodimer. Thus it is possible to observe the effects of the mutation on both the mutated and wild-type subunits of the heterodimer, such that any differences reflect the influence of the partner subunit, which cannot be determined by examining a homodimeric mutant.

Excitation of the saNOS mixed dimers at 442 nm enabled the examination of the

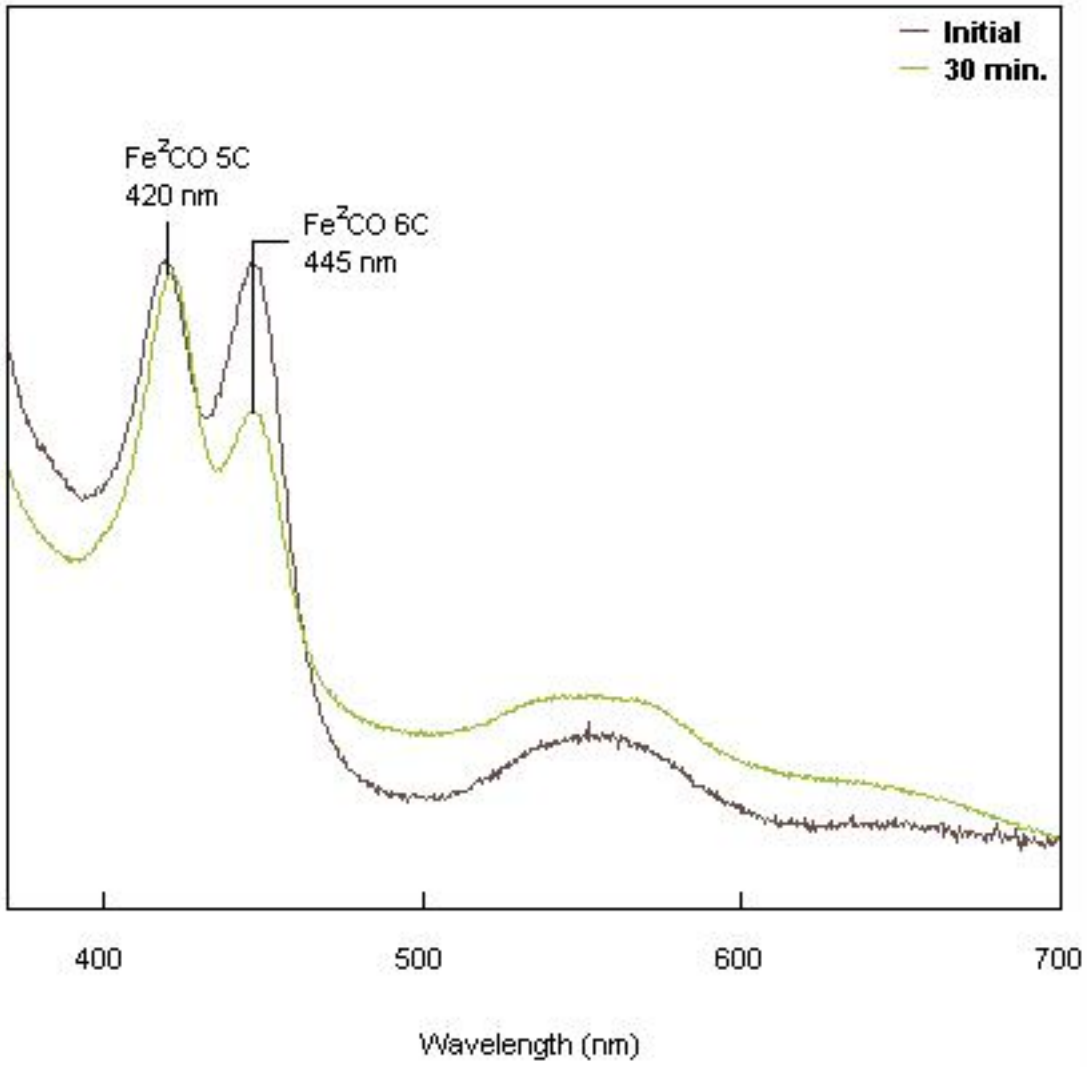

Figure 36. The UV/visible spectra of the Fe(II)CO complex of W56/W56Y saNOS immediately after the addition of CO (brown) and 30 minutes after the addition of CO (straw).

heme within the wild-type subunit of the mutant heterodimers (Figure 37). Upon examination of the low-frequency region of the resonance Raman spectra, it was observed that the spectra for the W56/W56F and W56/W56Y proteins were identical to that of the wild-type homodimeric saNOS, with the $\nu_{Fe\text{-}CO}$ modes present at 503 cm^{-1} and $\delta_{Fe\text{-}C\text{-}O}$ modes at 566 cm^{-1}. This indicates that the heme environment of the wild-type subunit of the mixed dimers is the same as that for wild-type homodimeric saNOS. The heme deformation modes are also consistent between the proteins, with enhancements at 676 (an in-plane mode), 692, 751, and a broad peak between 798 and 801 cm^{-1}, all of which correspond to saddling, although the mode at 801 cm^{-1} may also be indicative of heme ruffling.

When the mixed dimers were excited at 413 nm, the heme within the mutated subunit of the heterodimers was probed. Similar to the wild-type subunits, the W56F (Figure 38) and W56Y (Figure 39) subunits do not exhibit any difference from their homodimeric counterparts, nor do they differ from each other. Both proteins possessed $\nu_{Fe\text{-}CO}$ modes at 494 cm^{-1} and $\delta_{Fe\text{-}C\text{-}O}$ modes at 586 cm^{-1}. The heme deformation modes are also consistent between the proteins, with a ruffling mode at 719 cm^{-1} and a saddling mode at 753 cm^{-1}. There was also a small sharp peak located at 729 cm^{-1}, which may correspond to doming of the heme, although it is more likely that this is a laser line. This suggests that the heme environment of the mutated subunits is the same as that for the mutant homodimers in their Fe(II)CO complexes.

4.3.8. Ferric-NO Complexes of saNOS W56 Heterodimers

The ferric Fe-NO complexes were observed in the low-frequency region for the W56/W56 and W56/W56Y mixed dimer proteins. In the presence of 5 mM L-arginine,

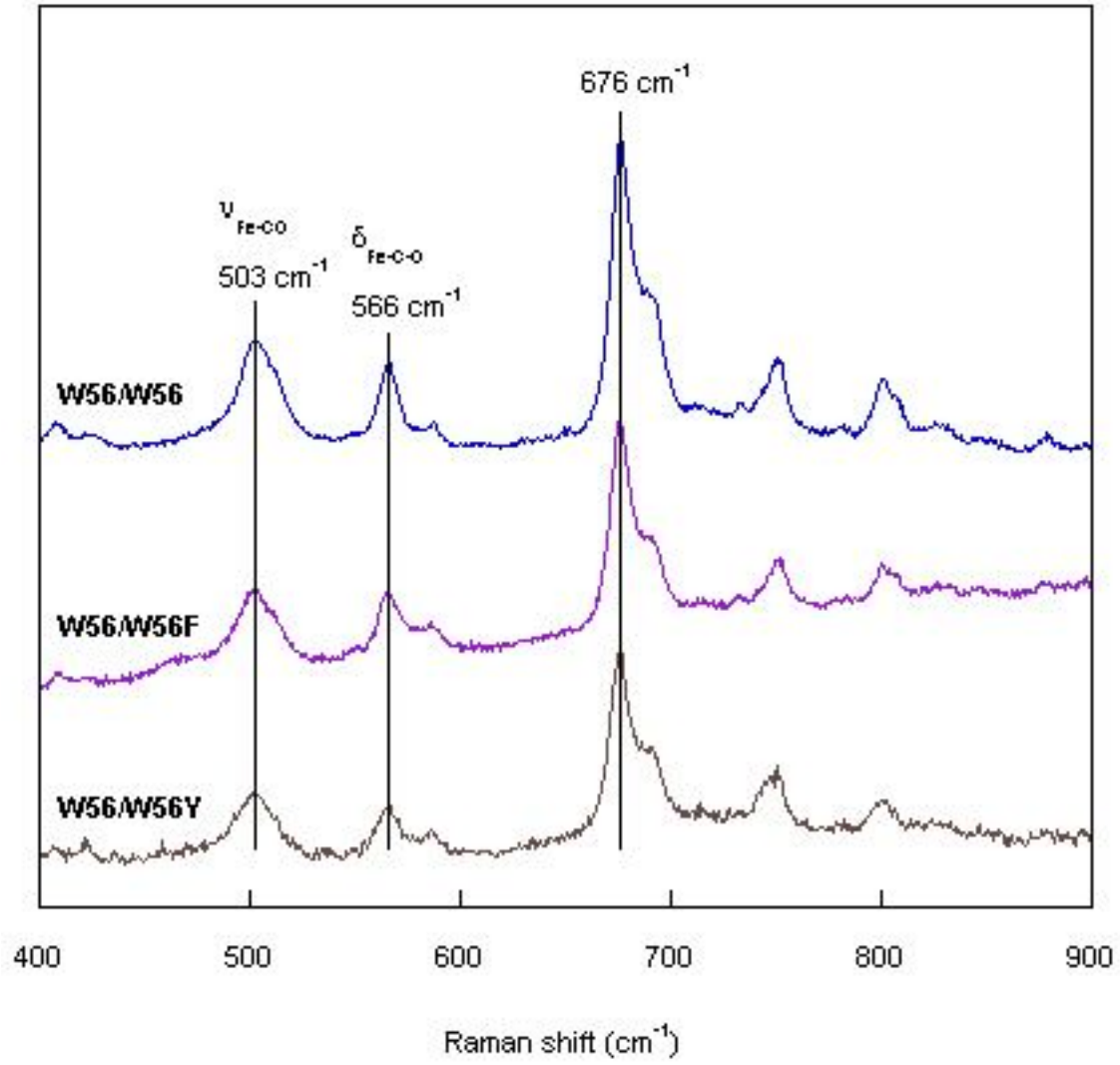

Figure 37. The low-frequency region of the resonance Raman spectrum of the Fe(II)CO complexes of wild-type, and W56/W56F and W56/W56Y heterodimeric saNOS in the presence of 1 mM L-arginine. The samples were excited at 441.6 nm with a laser power of 3 mW. The unshifted positions of $\nu_{Fe\text{-}CO}$ and $\delta_{Fe\text{-}C\text{-}O}$ indicate that the heme environment of the wild-type subunit of the heterodimer is identical to that of the wild-type homodimer.

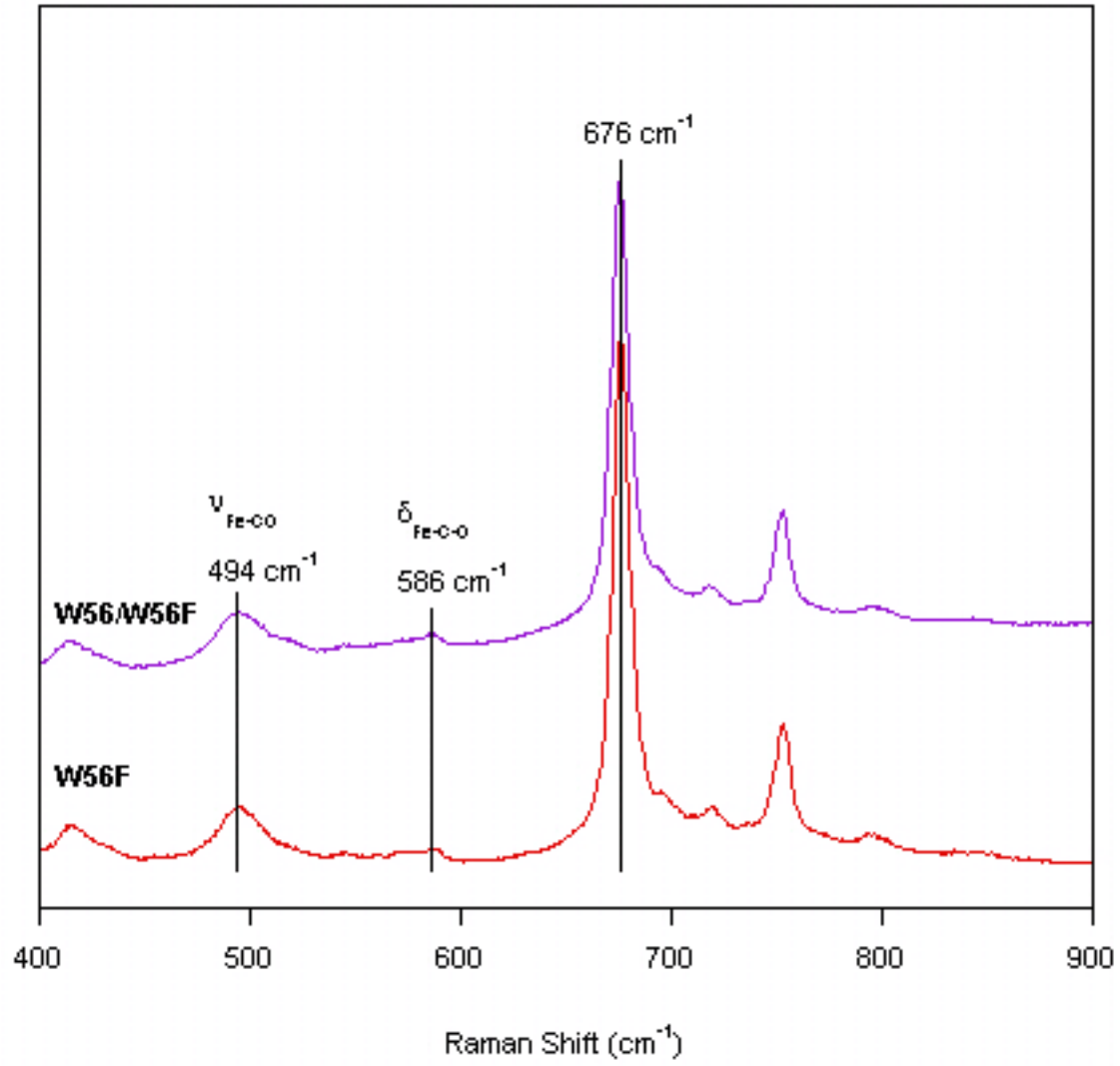

Figure 38. The low-frequency region of the resonance Raman spectrum of the Fe(II)CO complexes of W56/W56F and W56F saNOS in the presence of 1 mM L-arginine. The samples were excited at 413.1 nm with a laser power of 3 mW. The unshifted positions of $\nu_{Fe\text{-}CO}$ and $\delta_{Fe\text{-}C\text{-}O}$ indicate that the heme environment of the wild-type subunit of the heterodimer is identical to that of the wild-type homodimer.

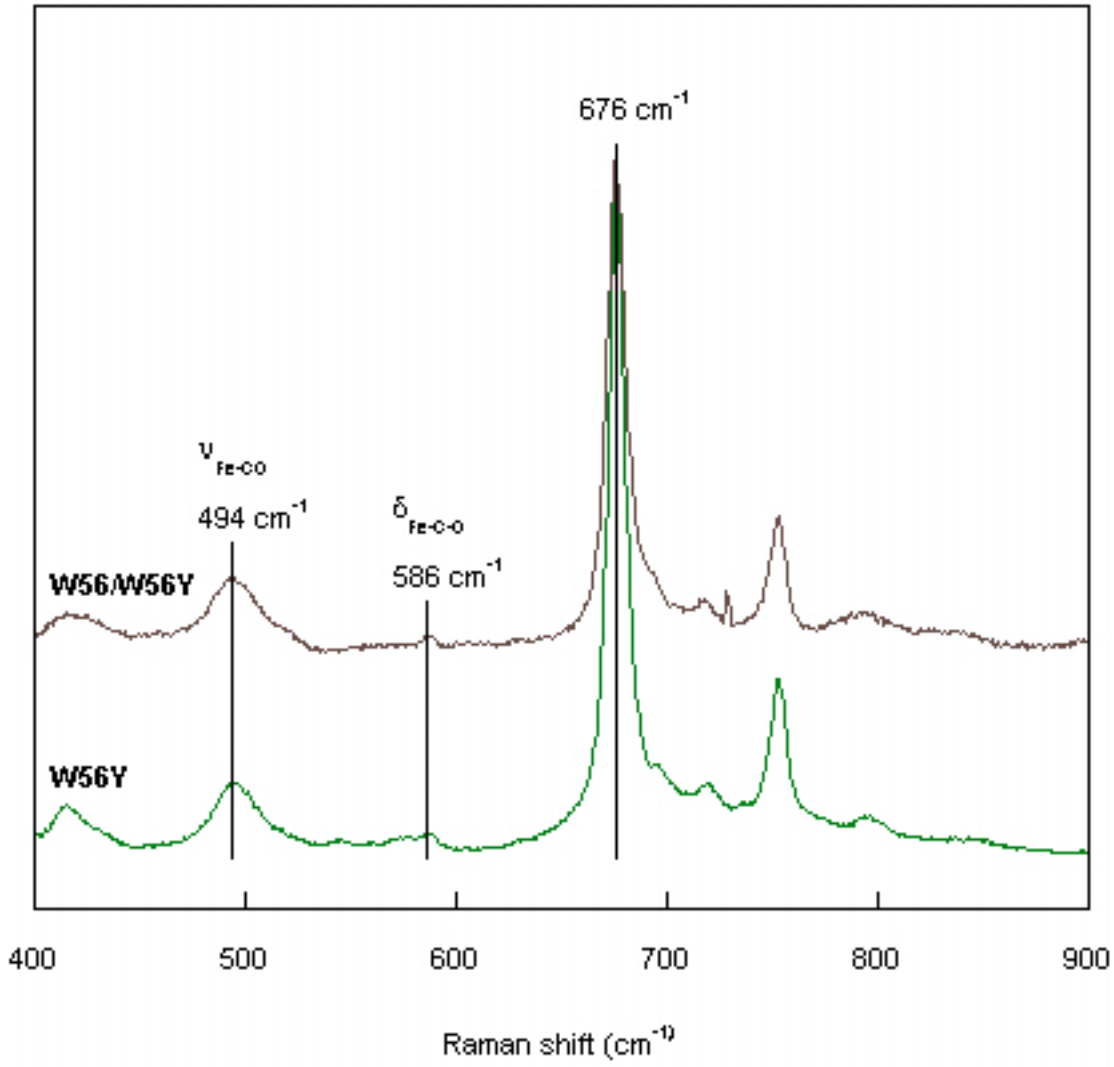

Figure 39. The low-frequency region of the resonance Raman spectrum of the Fe(II)CO complexes of W56/W56Y and W56Y saNOS in the presence of 1 mM L-arginine. The samples were excited at 413.1 nm with a laser power of 3 mW. The unshifted positions of $\nu_{Fe\text{-}CO}$ and $\delta_{Fe\text{-}C\text{-}O}$ indicate that the heme environment of the W56Y subunit of the heterodimer is identical to that of the W56Y homodimer.

the $\delta_{Fe\text{-}NO}$ mode is visible at 541 cm^{-1} for the wild-type saNOS, and at 537 cm^{-1} for the W56F and W56Y homodimers, and W56/W56F and W56/W56Y heterodimers (Figure 40). This suggests that the angle of the Fe-N-O complex for the mutants is more linear than it is for wild-type saNOS. In plane heme modes were identified at 675 and 752 cm^{-1}. Out-of-plane heme deformation modes were identified at 684, 708, 728, 744, and 801 cm^{-1}, corresponding to saddling, ruffling, doming, and propellering of the heme.

In the absence of L-arginine, the $\nu_{Fe\text{-}NO}$ mode is visible. This mode was found at 539 cm^{-1} for wild-type saNOS, but was shifted to a lower frequency for the mutants (Figure 41). The W56/W56F and W56/W56Y heterodimers possessed $\nu_{Fe\text{-}NO}$ modes at 537 and 536 cm^{-1}, respectively, which indicate longer Fe-NO bonds for the mutants, due to increased basicity to the thiolate. The $\nu_{Fe\text{-}NO}$ mode was shifted to a lower frequency, 532 cm^{-1}, for both W56F and W56Y homodimeric proteins (Lang and Couture, unpublished), which may indicate that the shifts observed for the heterodimers arose from contribution by both subunits equally. The signals for the out-of-plane deformation modes appeared decreased in the presence of L-arginine, suggesting that the heme may be more planar when L-arginine is bound in the distal pocket.

4.4. Nitrite Production

The rate of H_2O_2-dependent oxidation of L-NHA by the NOS proteins was monitored by the colorimetric Griess Assay. The results of the fixed-time 10 minute assay performed in the absence of H_4B, and in the presence of 100 μM H_4B for the $eNOS_{oxy}$ proteins, are summarized in Table 6.

For the $eNOS_{oxy}$ proteins in the absence of H_4B, hyperactivity was observed for both W180F and W180Y over wild-type, 7.9- and 1.7-fold, respectively. In the presence

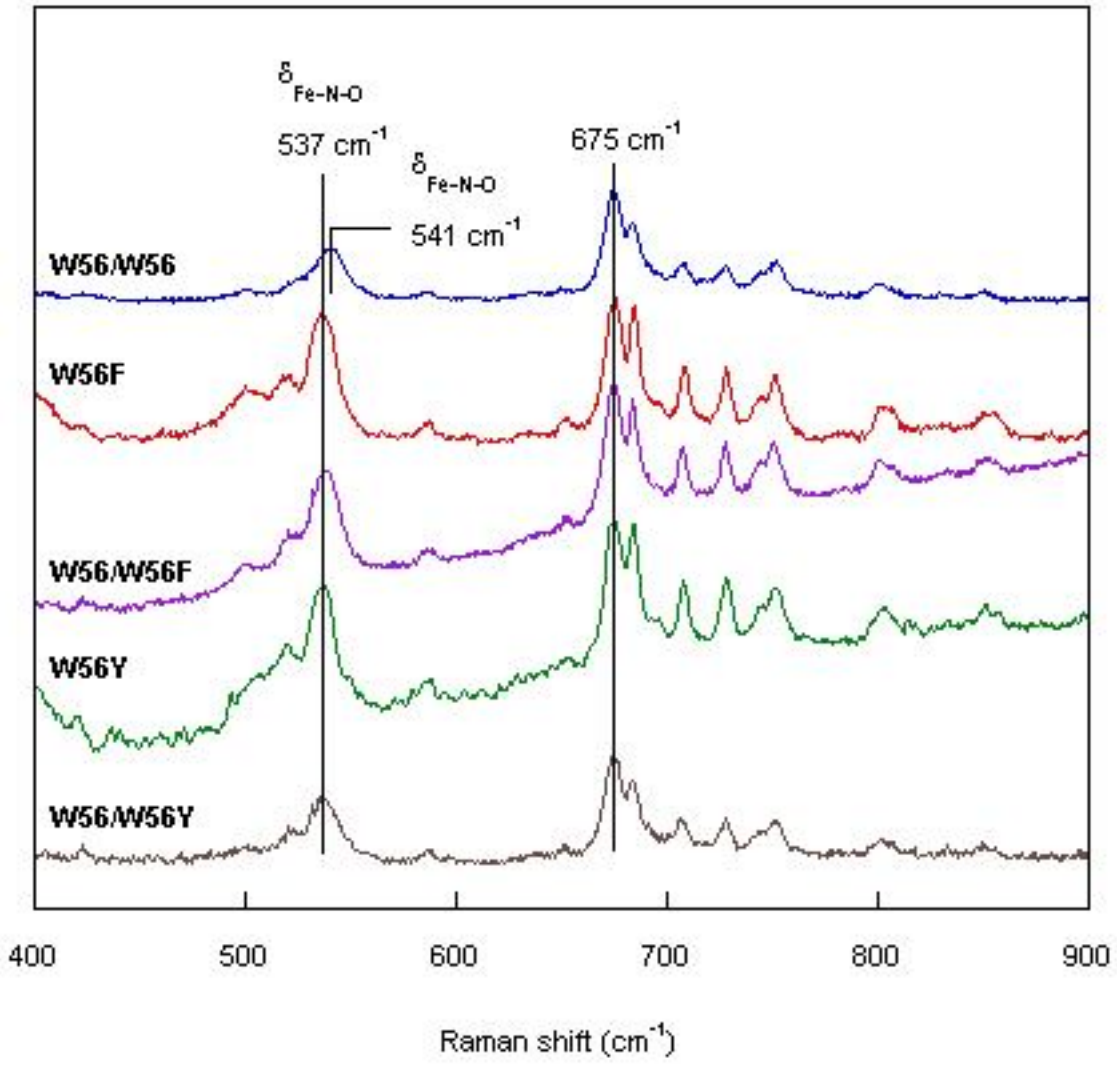

Figure 40. The low-frequency region of the resonance Raman spectrum of the Fe(III)NO complexes of wild-type and W56F/Y homodimeric and heterodimeric saNOS in the presence of 1 mM L-arginine. The samples were excited at 441.6 nm with a laser power of 3 mW. In the presence of L-arginine the $\delta_{Fe\text{-}N\text{-}O}$ was indentified at 541 cm^{-1} for wild-type, and 537 cm^{-1} for the other proteins, indicating that the Fe-N-O complex remained linear with the introduction of the mutations.

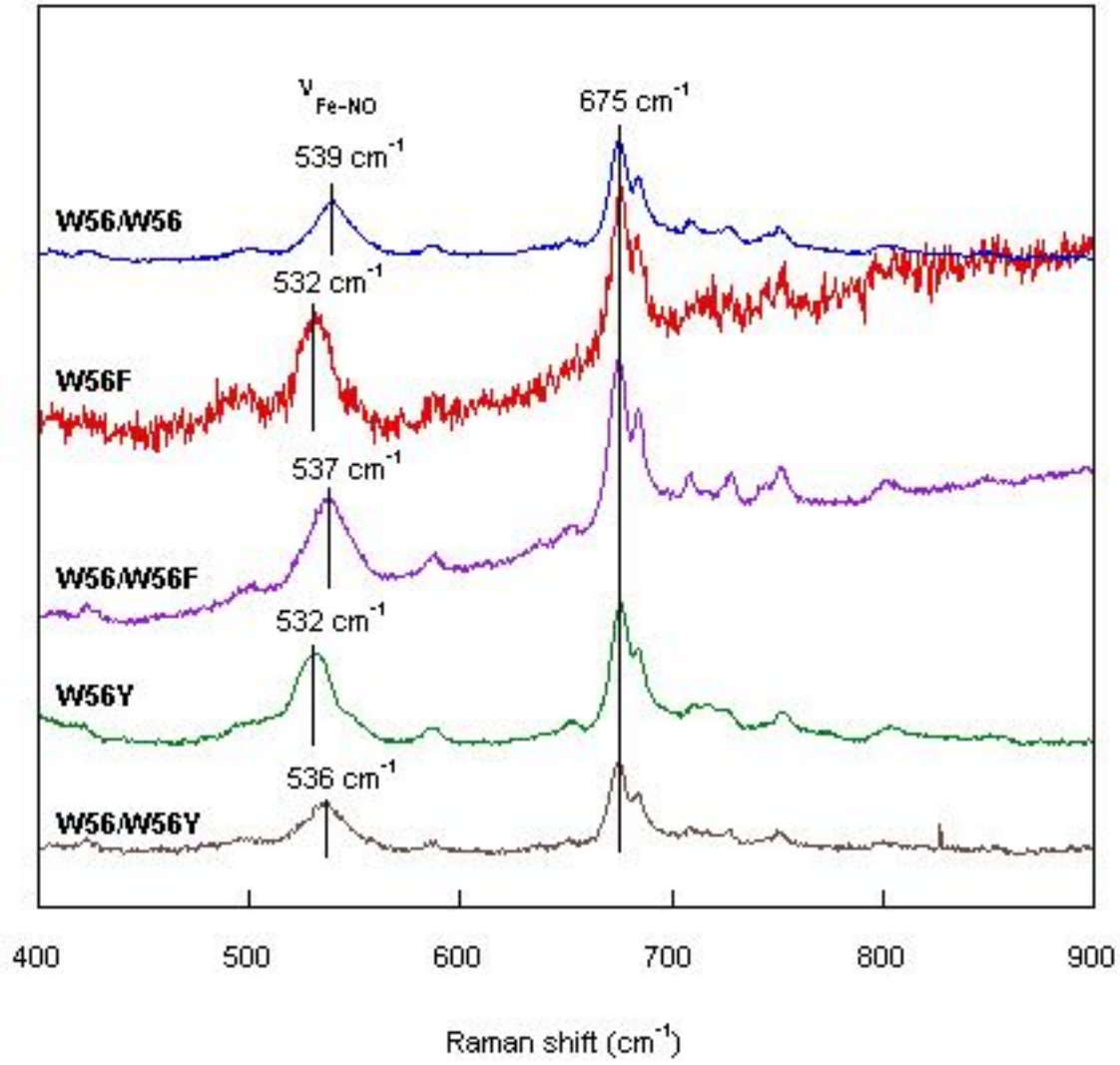

Figure 41. The low-frequency region of the resonance Raman spectrum of the Fe(III)NO complexes of wild-type and W56F/Y homodimeric and heterodimeric saNOS in the absence of L-arginine. The samples were excited at 441.6 nm with a laser power of 3 mW. When L-arginine is not present the $\nu_{Fe\text{-}NO}$ was identified at different frequencies for all of the proteins.

of H_4B, the rates for the $eNOS_{oxy}$ proteins decreased, but the activities of the mutants were still greater than wild-type, such that W180F was 3.2-fold faster than wild-type and W180Y was 2.1-fold faster than wild-type.

For the saNOS assays performed in the absence of H_4B, the rate of wild-type saNOS was determined to be approximately 0.13 mol NO_2^-/mol protein/min (Table 6). Rates were also obtained for the homodimeric W56F and W56Y, and heterodimeric W56/W56F and W56/W56Y proteins, which did not vary significantly from the rate obtained for wild-type saNOS.

Table 6. Nitrite production of $eNOS_{oxy}$ W180 and saNOS W56 proteins. Nitrite production was measured through the H_2O_2-dependent oxidation of L-NHA and quantified using the Griess reaction. All units are mol NO_2^-/mol protein/min.

Protein	**Mean +/- SD (-H_4B)**	**Mean +/- SD (+ 100 μM H_4B)**
$eNOS_{oxy}$ W180	0.12 +/- 0.02	0.08 +/- 0.02
$eNOS_{oxy}$ W180F	0.92 +/- 0.19	0.26 +/- 0.07
$eNOS_{oxy}$ W180Y	0.20 +/- 0.01	0.17 +/- 0.01
saNOS W56	0.13 +/- 0.03	-N/D-
saNOS W56F	0.17 +/- 0.03	-N/D-
saNOS W56/W56F	0.13 +/- 0.03	-N/D-
saNOS W56Y	0.15 +/- 0.03	-N/D-
saNOS W56/W56Y	0.12 +/- 0.04	-N/D-

Chapter 5. Discussion

5.1. Summary of Findings

From the wealth of (sometimes bewildering) spectroscopic data certain trends could be identified. The coordinations and spin-states of the heme iron were consistent between $eNOS_{oxy}$ and saNOS wild-type proteins in the ferric and ferrous states. In the ferric state, the heme iron of the $eNOS_{oxy}$ and saNOS proteins was five-coordinate and high-spin. In the ferrous state, these proteins also contained five-coordinate high-spin hemes; however, the mutants presented a combination of five-coordinate high-spin and six-coordinate low-spin hemes. The mutant proteins also displayed evidence of increased electron donation from the thiolate to the iron. One exception to this is the Fe(II)CO complex of $eNOS_{oxy}$ W180Y, in which the strength of the thiolate-iron ligation appeared to be the same as that for wild-type $eNOS_{oxy}$. Heme deformations were also very consistent, with saddling and ruffling distortions being predominant, although other distortions were observed. There were also similarities between wild-type $eNOS_{oxy}$ and saNOS in their rates of nitrite production, which differed significantly between the various mutants.

5.2. The Effect of Aromatic Substitution on the Electron Density of the Proximal Thiolate

The conserved tryptophan residue that is the focus of this study has been associated with lowering the electronegativity of the cysteine ligand in NOS proteins through hydrogen bonding between the indole nitrogen and thiolate. Comparison with cytochrome P450, which lacks appropriate residues to create this hydrogen bond, indicate that in the absence of this bond there is a greater electron density on the

thiolate.[87] In cytochrome c peroxidase, it was shown that the mutation of a tryptophan, engaged in hydrogen bonding with an axial ligand, to phenylalanine increased the electronegativity of the ligand, strengthening its interaction with the heme iron.[88; 89] It was thus proposed that this tryptophan residue influences heme chemistry through its hydrogen bonding with iron-bound ligands and through $\pi-\pi^*$ interactions with the porphyrin.[88; 89]

The influence of tryptophan interaction with the thiolate ligand has also been reported for W409 and $W409_{oxy}$ in nNOS, and is one of the studies that formed the basis for this thesis. The W409 residue, which is analogous to W180 in eNOS and W56 in saNOS, was mutated to either phenylalanine or tyrosine. The charge transfer band of the $nNOS_{oxy}$ mutants was shifted from 646.5 nm for wild-type, to 640.0 and 640.5 nm for W409F and W409Y, respectively.[68] These shifts of approximately -6 nm are consistent with the -7 and -6 nm shifts observed for W180F and W180Y of $eNOS_{oxy}$, indicating that the W180F/Y mutants of $eNOS_{oxy}$ also caused an increase in thiolate basicity.

5.2.1. The Fe(II)CO Complexes of the $eNOS_{oxy}$ Proteins

The use of CO as a distal ligand to probe the properties of the proximal ligand is common. CO is both a σ-donor and a π-acceptor, as it will donate its lone electron pair to the iron d_{z^2} orbital, forming a σ bond with the iron, and will also accept electrons through back-donation from the iron d_π orbitals to its empty π^* orbital, forming a π bond. CO thus engages in σ competition with the proximal ligand, and the presence of an electron-rich proximal ligand, such as thiolate, increases σ competition, weakening the Fe-CO bond, which is indicated by a decrease in the $\nu_{Fe\text{-}CO}$ mode. An electron-rich ligand could induce changes to the extent of π back-bonding. An increase in back-

bonding, which would decrease the $\nu_{Fe\text{-}CO}$ mode and increase the $\nu_{C\text{-}O}$ mode. Thus, back-bonding is modulated by changes in the distal environment, while σ bonding is affected by changes in the proximal environment.[65]

The Fe(II)CO complexes of the W409F/Y mutants have not been examined in the absence of H_4B, and have not been characterized at all by resonance Raman spectroscopy, perhaps because these complexes are unstable.[54] Thus, no direct comparison can be made regarding the basicity of the thiolate in the Fe(II)CO complexes of the nNOS and $eNOS_{oxy}$ proteins when L-arginine is present and H_4B is absent.

The Fe(II)CO complex of the W180Y mutant was observed to be unstable in comparison with wild-type and W180F, as was evident by the high ratio of P420:P450 Fe(II)CO complexes for W180Y. As the P420 state denotes loss of the proximal thiolate ligation to the heme, the presence of this form in W180Y suggests destabilization of the proximal heme environment. The P420 form has also been observed for the W56F and W56Y mutants of saNOS, and is the only Fe(II)CO complex formed by these mutants, while wild-type saNOS forms the P450 state exclusively (Lang and Couture, unpublished). Three explanations for the loss of thiolate ligation are discussed below. It has been reported that in the absence of H_4B there is destabilization of the heme domain in iNOS and nNOS, which relaxes thiolate coordination.[90] The absence of H_4B, and its stabilizing effects on the heme environment, may provide an explanation for the observed instability of the Fe(II)CO complexes of W180Y and the nNOS W409 mutants.

Changes in the frequencies of the $\nu_{Fe\text{-}CO}$ modes for the $eNOS_{oxy}$ proteins were detected in the presence of L-arginine. These modes were decreased by 2 cm^{-1} for the W180F and W180Y proteins, indicating an increased basicity of the thiolate. This could

be indicative of increased σ competition between the thiolate and CO, as described above. It is also possible that some of the increased electron density on the thiolate was transferred to the iron d_π orbital, which would lead to increased back-bonding to the π^* orbital of CO,. This would be detected as an increase in the frequency of the $\nu_{Fe\text{-}CO}$ mode and a decrease in the frequency of the $\nu_{C\text{-}O}$ mode, which could be apparently reducing the σ bonding effect observed for the W180 mutants.[91] The $\nu_{C\text{-}O}$ mode has been elusive, due to poor signal quality, and thus it cannot be determined if back-bonding is a factor in the observed shift in frequency of the $\nu_{Fe\text{-}CO}$ mode of W180F and W180Y.

The frequencies of the $\delta_{Fe\text{-}C\text{-}O}$ modes for $eNOS_{oxy}$ proteins in the presence of L-arginine did not change with the introduction of the mutations. The position of this mode is comparable to that for the Fe(II)CO complex of nNOS, indicating that the $eNOS_{oxy}$ proteins were thiolate-heme coordinated.[79; 85; 92] It was reported that the presence of a hydrogen bond between L-arginine and CO restricts the movement of Fe-C-O bonds, which is also indicated by the insensitivity of $\delta_{Fe\text{-}C\text{-}O}$ modes to changes in the heme environment that can induce large changes in $\nu_{Fe\text{-}CO}$ modes.[65; 92]

5.2.2. The Fe(III)NO Complexes of the $eNOS_{oxy}$ Proteins

The Fe(II)CO and Fe(III)NO heme irons are isoelectronic, with each complex sharing six electrons between the metal *d* and π orbitals, and both species binding as linear complexes (i.e. Fe-C-O, Fe-N-O) perpendicular to the heme iron.[93] As in the case of the Fe(II)CO complexes, an electronegative proximal ligand increases σ and π competition between the ligand and NO, resulting in a weaker Fe-NO bond which is

indicated by a lower frequency of the $\nu_{Fe\text{-}NO}$ mode.[94] The Fe(II)CO and Fe(III)NO complexes differ in terms of C-O and N-O bond lengths to this response, as a weaker Fe-CO bond results in a stronger C-O bond, whereas a weaker Fe-NO bond also weakens the N-O bond.[95]

In the absence of L-arginine and H_4B, the decreased frequencies of the $\nu_{Fe\text{-}NO}$ modes for the $eNOS_{oxy}$ mutants from that of wild-type was consistent with those observed for the W409F mutant of $nNOS_{oxy}$, which was also shifted -8 cm^{-1} from wild-type, and the W409Y mutant was shifted -6 cm^{-1} from wild-type.[94] That the frequencies of the $\nu_{Fe\text{-}NO}$ modes for $eNOS_{oxy}$ 180F and $nNOS_{oxy}$ 409F were identified at 8 cm^{-1} lower than their respective wild-type proteins is significant, as it suggests that the hydrogen bond between tryptophan and the thiolate ligand were of similar strengths in both isoforms in the absence of substrate and pterin. The $\nu_{Fe\text{-}NO}$ modes for $eNOS_{oxy}$ W180Y and $nNOS_{oxy}$ W409Y were shifted less than for the phenylalanine mutants, suggesting that the tyrosine residue is mediating thiolate basicity, although not to the same extent as tryptophan.

The decreased frequencies of the $\nu_{Fe\text{-}NO}$ modes for the $nNOS_{oxy}$ W409 mutants were associated directly with increased electronegativity to the thiolate caused by the loss of the hydrogen bond between the thiolate and the mutated residue thereby increasing the strength of the σ bond between the iron and thiolate and weakening the σ bond between the heme iron and NO.[94] The shift in the $\nu_{Fe\text{-}NO}$ mode observed for W180F is consistent with this conclusion, as the aromatic ring is incapable of forming a hydrogen bond with the thiolate.

The presence of L-arginine increased the intensity of the $\delta_{Fe\text{-}N\text{-}O}$ mode in the $eNOS_{oxy}$ species, preventing the detection of the $\nu_{Fe\text{-}NO}$ mode in these proteins. There have been no reports of detectable $\delta_{Fe\text{-}N\text{-}O}$ modes when the Fe(III)NO complex is linear, suggesting that detection of the $\delta_{Fe\text{-}N\text{-}O}$ mode corresponds to a bent structure.[65] Thus, the Fe(III)NO complexes of the $eNOS_{oxy}$ proteins may be bent, which suggests an interaction between NO and L-arginine.[65] The frequencies of the $\delta_{Fe\text{-}N\text{-}O}$ modes for the W180F and W180Y mutants were both shifted -3 cm^{-1} from wild-type $eNOS_{oxy}$, which indicates less bending of Fe-N-O for the mutants. This may correspond to a shorter bond between the heme iron and NO, reducing the potential for interaction between NO and L-arginine. The $nNOS_{oxy}$ proteins did not possess $\delta_{Fe\text{-}N\text{-}O}$ modes in the presence of L-arginine, thus indicating that the complexes were linear and the distal pocket of $nNOS_{oxy}$ did not present the same steric constraints as were observed for $eNOS_{oxy}$.[94; 96]

Bending is a result of an electronic effect introduced by heme distortion, particularly the enhancement of out-of-plane modes.[79] In the absence of H_4B, several out-of-plane heme deformation modes were identified for the Fe(III)NO complexes of the $eNOS_{oxy}$ proteins, although the saddling deformation was the most prominent. The increase in non-planarity of the heme has been correlated to a decrease in the reduction potential of the heme, and the saddling deformation specifically has been connected with an increase in the σ donating ability of the heme iron.[97]

5.2.3. saNOS Heterodimers

Lang and Couture (unpublished) have observed that the thiolate ligation in saNOS W56F and W56Y mutants is extremely unstable in the Fe(II)CO state. The presence of a 420 nm Soret band, which was not present in wild-type saNOS, was

attributed to loss of thiolate ligation to the heme. The P420 form has been identified in cytochrome P450 enzymes, and corresponds to protonation of the cysteine to a thiol ligand.[57] If the thiolate is being protonated, then increasing the pH of the protein environment should deprotonate the tyrosine residue, causing it to strip a proton from the thiol, rescuing thiolate ligation. As increasing the pH of W56/W56Y did not prevent the formation of the P420 form, the possibility of thiolate protonation was considered to be unlikely. Lang and Couture have suggested two additional possible rationalizations for the presence of the P420 state in the saNOS mutants. The first of these, which appears to be the most common loss of thiolate ligation, suggests that the thiolate ligation is being replaced by a histidine residue.[98] Examination of the crystal structure of saNOS indicated that there were no histidine residues in the heme environment, which makes this explanation unlikely without a large conformational change.[46] The second rationalization provided was that in the absence of the tryptophan residue, the thiolate forms very strong hydrogen bonds with nearby amide groups of the protein backbone or with water molecules.

The Fe(II)CO complexes of the saNOS W56/W56F and W56/W56Y heterodimers exhibited the P420 and P450 forms of the enzyme, which is consistent with one subunit bearing the mutation and one subunit being wild-type. The resonance Raman shifts for these complexes indicated that the environments of each particular subunit, mutant or wild-type, are identical to their respective homodimers. Thus, mutation does not appear to be affecting the strength of the thiolate ligation in the wild-type subunit, as the $\nu_{Fe\text{-}CO}$ mode for the wild-type subunit of the mutant heterodimers is found at the same frequency as that for wild-type homodimer.

Over time, the P450 state of the Fe(II)CO complexes of the saNOS heterodimers decays to a P420 state. This decay has not been observed in wild-type saNOS, but has been detected for the W56F and W56Y homodimers, indicating that this is a mutation specific effect. Despite the resonance Raman spectroscopic evidence that the heterodimers appear to be structurally similar to their homodimeric subunits, the decay to P420 suggests that the mutated subunit is causing destabilization in the wild-type subunit. Other NOS proteins decay to the P420 state over time in the absence of H_4B, including the W180Y mutant of $eNOS_{oxy}$, and so it is possible that the presence of an appropriate cofactor in the pterin binding site may stabilize the saNOS subunits through electrostatic interactions with the porphyrin ring.[90]

In the presence of L-arginine, the $\delta_{Fe\text{-}N\text{-}O}$ modes of the Fe(III)NO complexes of the heterodimers were identified. This mode was located at the same frequency for the homodimeric and heterodimeric mutants, 537 cm^{-1}, which was 4 cm^{-1} lower from the frequency of $\delta_{Fe\text{-}N\text{-}O}$ in wild-type saNOS (Lang and Couture, unpublished). This indicates that the Fe-N-O complex in the mutated proteins, heterodimers included, may experience a greater steric effect through interaction with L-arginine.

In the absence of L-arginine, the $\nu_{Fe\text{-}NO}$ modes for the saNOS proteins were detected. The frequencies of the $\nu_{Fe\text{-}NO}$ mode observed for the heterodimers were lower than those for wild-type, but higher than those for their respective homodimeric mutant. This indicates an increase in the basicity of the proximal thiolate with respect to wild-type saNOS, and a decreased basicity in respect to the homodimeric mutants. That the frequencies of the $\nu_{Fe\text{-}NO}$ modes in the heterodimers were approximately halfway between those for wild-type and homodimeric mutant suggests that the individual

subunits of the mixed dimers are contributing to the overall mode in a 1:1 ratio, reducing the effect of the increased basicity of the thiolate.

5.3. The Distal Effect of H_4B Binding in the Presence of Heme Ligands

5.3.1. The Fe(II)CO Complexes of the $eNOS_{oxy}$ Proteins

The presence of H_4B in the $eNOS_{oxy}$ proteins strengthened the Fe-CO complex for all three proteins, as was indicated by a perceived decrease in the P420:P450 ratio and an increase in $\nu_{Fe\text{-}CO}$, indicating that the presence of H_4B had an indirect electronic effect on the heme. It has been reported that for $nNOS_{oxy}$ and $iNOS_{oxy}$, that the frequency of $\nu_{Fe\text{-}CO}$ in the presence of L-arginine does not shift when H_4B is added, which suggests that eNOS has a stronger tryptophan-thiolate hydrogen bond, when either H_4B is present or absent, than the other mammalian isoforms.[65; 79; 85] The evidence provided below supports this hypothesis; however, it cannot be confirmed without obtaining the $\nu_{C\text{-}O}$ modes for the $eNOS_{oxy}$ proteins to compare the distal environments of eNOS and nNOS.

The presence of a shoulder in the $\nu_{Fe\text{-}CO}$ modes for wild-type and W180Y $eNOS_{oxy}$ in the presence of H_4B should also be discussed. The similarity between the frequencies of the $\nu_{Fe\text{-}CO}$ modes in the absence of H_4B and the shoulder observed in the presence of H_4B for these proteins could indicate incomplete binding of H_4B, although H_4B was present in excess and should have saturated the enzyme.

The presence of two $\nu_{Fe\text{-}CO}$ modes has also been observed in nNOS, when L-arginine is not present.[87] These modes have been assigned as corresponding to α and β conformations, where the β conformation (the lower frequency) has a less constrained

distal environment. When L-arginine is present; however, only the α form was observed in nNOS, consistent with the polar and steric effects induced by L-arginine on the bound CO.[87] Conversion between the α and β forms can occur through the dissociation of CO, which first requires that L-arginine either detaches or swings away from the binding pocket.[87; 99] The rebinding of CO occurs more quickly than the rebinding of L-arginine, thus generating a short-lived β conformation when CO rebinds.[99] Thus, the presence of two $\nu_{Fe\text{-}CO}$ modes for wild-type and W180Y $eNOS_{oxy}$ may suggest the temporary dissociation of L-arginine, which would weaken the Fe-CO bond possibly even resulting in CO dissociation. W180F only exhibits the β conformation of the $\nu_{Fe\text{-}CO}$ mode. The absence of the α conformation in W180F may arise from the Fe-CO bond being already weakened in this complex.

The power of the excitation laser is capable of converting the Fe(II)CO complex between the α and β forms, when L-arginine is either present or absent.[87] The sensitivity of the NOS proteins to laser power may explain why preliminary experiments on the Fe(II)CO complex of W180Y in the presence of H_4B involving different acquisition periods (30-60 s) and laser power (between 1.4 and 6 mW) were inconsistent (data not shown). At acquisition periods of 30 s and a laser power of 4 mW, the $\nu_{Fe\text{-}CO}$ mode for W180Y was identified at the same frequency as wild-type (Figure 29); however, a longer acquisition period (60 s) with a slightly decreased laser power (3.5 mW) resulted in the identification of the $\nu_{Fe\text{-}CO}$ mode at a frequency similar to that for W180F. It is thus possible that increased exposure to the laser weakened the Fe-CO bond, thereby increasing the strength of the Fe-S bond, as has been reported previously in nNOS.[87]

The two Fe(II)CO conformations do not arise from the presence of the P420 form of the heme, as the samples were excited at 441.6 nm, which is selective for heme in the P450 state and not for P420 heme. In addition, the UV/visible spectra of the $eNOS_{oxy}$ proteins in the presence of L-arginine and H_4B are primarily in the P450 state.

The UV/visible spectra of the wild-type, W409F, and W409Y $nNOS_{oxy}$ proteins reduced in the presence of CO, in the presence of L-arginine and H_4B, exhibited Soret bands at 443, 446.5, and 445.5 nm, respectively, indicating a change in the heme environment for these mutants.[68] These are comparable to the shifts observed for the $eNOS_{oxy}$ proteins in the absence of H_4B; however, the presence of H_4B shifted the Soret band of the wild-type and W180Y proteins to 446 nm, and the W180F protein to 448 nm. The increase in the frequency of the Soret band for wild-type $eNOS_{oxy}$ protein over $nNOS_{oxy}$ may imply that the hydrogen bond between the tryptophan and the thiolate ligand is inherently stronger in eNOS. This has been indicated previously for the full-length enzymes, as the $\nu_{Fe\text{-}CO}$ resonance Raman frequency for eNOS is 9 cm^{-1} higher for eNOS (512 cm^{-1}) than nNOS (503 cm^{-1}).[86; 87] Out-of-plane heme deformations were also increased in the presence of H_4B, particularly the 752 cm^{-1} mode, which were previously reported to not be connected to changes in the Fe-C-O modes for the mammalian NOSs, suggesting again that in the presence of H_4B, $eNOS_{oxy}$ behaves differently than nNOS.[65]

The phenylalanine mutants of both $eNOS_{oxy}$ and $nNOS_{oxy}$ exhibit Soret bands of longer wavelengths than wild-type, suggesting that the thiolate of these complexes is more electronegative than for the wild-type or tyrosine mutant proteins. This is consistent with the loss of the hydrogen bond between the thiolate and the mutated residue, as phenylalanine does not possess a side chain capable of hydrogen bonding.

The positions of the Soret band are very close to that of the aptly named cytochrome P450, which lacks an appropriate residue to generate this hydrogen bond.[100] The increased electron density of the thiolate in W180F was also observed in the resonance Raman spectrum, as the frequency of the $\nu_{Fe\text{-}CO}$ mode is 4 cm^{-1} lower than for wild-type.

The $nNOS_{oxy}$ W409Y protein also exhibits an increased frequency of the Soret band in comparison with wild-type, consistent with loss of the hydrogen bond. This was not observed for the W180Y mutant of $eNOS_{oxy}$, as the position of the Soret bands of W180Y and wild-type $eNOS_{oxy}$ were identical, as were the resonance Raman shifts. This indicates that the electronegativity of the thiolate was similar in both proteins, and suggests that in the presence of H_4B, W180Y is able to form a hydrogen bond with the thiolate ligand. A comparison of the structures of $eNOS_{oxy}$ (PDB: 2nse) and $nNOS_{oxy}$ (PDB: 1zvl) demonstrates that the tryptophan-thiolate bonds are identical (at 3.40 Å, as calculated using Protein Workshop), which should not affect the ability for tyrosine to hydrogen bond to the thiolate. The tryptophan (PDB: 1ccp) to phenylalanine mutation (PDB: 4ccp) in cytochrome c peroxidase increased the minimum distance between the residue and its hydrogen bonding partner by 0.7 Å (3.7 Å for W51F vs. 2.9 Å for W51). Increasing the distance between the thiolate and the hydroxyl of tyrosine by 0.7 Å, even though it is probable that this distance is less considering the OH^- group, still puts this group within hydrogen bonding distance with the thiolate. Unfortunately, the crystal structures for the $eNOS_{oxy}$ 180F/Y and nNOS W409F/Y mutants are not available to support this hypothesis.

5.3.2. The Fe(III)NO Complexes of the $eNOS_{oxy}$ Proteins

The Fe(III)NO complexes of the $eNOS_{oxy}$ proteins have yet to provide evidence that W180Y resembles wild-type. The $\nu_{Fe\text{-}NO}$ mode for the $eNOS_{oxy}$ proteins in the presence of H_4B have not yet been determined, but Dr. Rafferty's and Dr. Couture's laboratories are in the process of identifying these modes. This mode was identified at 546 cm^{-1} in wild-type $nNOS_{oxy}$ in the presence of L-arginine, shifting to 539 cm^{-1} for both W409F and W409Y.[94] In the absence of L-arginine, the frequency of the $\nu_{Fe\text{-}NO}$ mode decreased to 542 cm^{-1}, indicating weaker σ bonding between the iron and NO. Similar shifts are observed for the $eNOS_{oxy}$, but it is more likely that they correspond to $\delta_{Fe\text{-}N\text{-}O}$ modes, as this mode is enhanced in the presence of H_4B in nNOS due to an interaction between L-arginine and NO, restricting the detection of the $\nu_{Fe\text{-}NO}$ mode.[65]

Upon the addition of H_4B, the Fe(III)NO complex of wild-type $eNOS_{oxy}$, in the presence of L-arginine, experienced an increase in the frequency of the $\delta_{Fe\text{-}N\text{-}O}$ mode by 4 cm^{-1}, corresponding to an increase in the Fe-N-O angle. The Fe(II)NO complex also exhibits an increase in this angle, which has been attributed to an increase in the tilt between the iron and nitrogen atoms of approximately 2°.[101] This increase in tilt would likely arise from steric interactions or even hydrogen bonding between NO and L-arginine.[65] The frequency of the $\delta_{Fe\text{-}N\text{-}O}$ mode is also detected in both nNOS and $iNOS_{oxy}$, and it has been suggested that H_4B binding decreases the distance between L-arginine and the heme iron, which would enable interaction between NO and L-arginine, increasing the tilt or bending of the Fe-N-O bond.[65; 79]

As the $\delta_{Fe\text{-}N\text{-}O}$ mode is absent when the Fe(III)NO complex is linear, the presence of these modes for the $eNOS_{oxy}$ proteins when L-arginine and H_4B are bound, indicates

that the Fe-N-O bonds were bent. The presence of H_4B increased the frequency of the $\delta_{Fe\text{-}N\text{-}O}$ modes for the W180F and W180Y mutants by 3 cm^{-1}, indicating a slight increase in the tilt of these mutants in comparison to wild-type, which is attributable to H_4B. The lack of $\delta_{Fe\text{-}N\text{-}O}$ data for the $nNOS_{oxy}$ W409 mutants suggests that these complexes remained linear in the presence of H_4B.[94]

As bending is associated with the enhancement of out-of-plane modes, it was not surprising that in the presence of H_4B, the heme deformation modes of the $eNOS_{oxy}$ proteins were enhanced. The deformation modes corresponding to saddling were enhanced the most, but ruffling and doming deformations were also increased.[79] These increased distortions have also been reported previously for $iNOS_{oxy}$ in the presence of H_4B.[79]

5.4. Catalytic Implications

The tryptophan residue has been proposed to play a role in the modulation of autoinhibition by NO, by increasing the strength of the Fe-NO bond. Clearly, the substitution of this residue, eliminating its interaction with the thiolate ligand, introduces electronic shifts that strengthen the Fe-S ligation, as has been observed previously for nNOS and saNOS, and was identified in $eNOS_{oxy}$. A similar phenomenon was observed for a tryptophan to phenylalanine mutant in cytochrome c peroxidase, in which the increase in electronegativity to the axial ligand translated into higher enzyme activity, through an increase in k_{cat}.[88; 89]

It was reported that the hyperactivity observed for the nNOS mutants was due to slower reduction of the heme than reported for wild-type nNOS, which reduced the formation of the Fe(II)NO complex, leading to a faster reaction of these complexes with

O_2.[49; 50] Thus the mutants spent more time as active, ferric heme, whereas wild-type nNOS heme is mostly in the inactive Fe(II)NO complex.[49; 51] W409F was observed to be slightly more active than W409Y (3.7 vs. 1.5 x greater than wild-type), which was explained by a lower k_{cat} than wild-type and a lesser tendency to form an Fe(II)NO complex than W409Y.[49] This is consistent with the reported effect of a mutation to a conserved residue in the proximal heme pocket of cytochrome $P450_{cam}$ that is involved in modulating the electronegativity of the thiolate.[91] Cytochrome $P450_{cam}$ does not possess a tryptophan residue that hydrogen bonds with the thiolate; however, the thiolate does form three hydrogen bonds to the amide protons of the following three residues, similar to NOS.[100] The mutation removed one of these hydrogen bonds, and was associated with a lower heme reduction potential, increased thiolate basicity, and hyperactivity.[91]

As the synthesis of NO by eNOS is regulated differently from that of nNOS, it would be expected that the overall activity of eNOS would be lower than that of nNOS, which was observed above. Also, as reported for the nNOS W409 mutants, in the presence of H_4B, the W180F and W180Y mutants were hyperactive in comparison with wild-type $eNOS_{oxy}$ (Table 6). The mutants exhibited increases in activity that were similar to those reported for the nNOS mutants in the presence of H_4B, with the phenylalanine mutant being approximately 3.5 x faster than wild-type, and the tyrosine mutant being approximately twice as fast as wild-type.[53] As eNOS inherently forms very little of the Fe(II)NO complex, it is possible that the hyperactivity observed for the $eNOS_{oxy}$ mutants are a result of faster heme reduction and reaction with O_2, and not of reduced Fe(II)NO complex buildup. This could be determined through stopped-flow experiments examining the rates of formation and decay of the $Fe(II)O_2$ complexes, or

through mixed flow transient resonance Raman spectroscopy, as described by Takashi Ogura and colleagues.[102]

That wild-type activity increased when H_4B was absent is inconsistent with published results for the H_2O_2-dependent oxidation of L-NHA, which report that H_4B enhances catalysis in iNOS and nNOS.[76; 81] The much greater activity observed for W180F over wild-type and W180Y, and the increased rates over the proteins in the presence of H_4B, could be a result of the unique NO regulation by eNOS. The increase in catalysis could be due to an increase in reduction potential for the heme, which has been observed for nNOS and iNOS in the absence of H_4B.[103] Increasing the heme reduction rate in the $eNOS_{oxy}$ mutants would increase formation of the Fe(II)NO complex, but the rapid dissociation of NO would likely not result in build-up of this complex, thereby increasing catalysis.[51]

Unlike eNOS, the addition of H_4B was reported to not have any effect on nitrite production in saNOS.[46] Furthermore, as H_4B is not thought to be a physiological ligand, the experiments performed on saNOS in this project did not involve the inclusion of H_4B. The rate for wild-type nitrite production by saNOS (~0.13 +/- 0.03 mol NO_2^-/mol protein/min) was comparable to the reported rate of 0.15 +/- 0.01 mol NO_2^-/mol protein/min, indicating reproducibility of the modified assay.[46] The rates of wild-type $eNOS_{oxy}$ and saNOS were very similar (Table 6), which is consistent with the structural similarities between these proteins.[46]

Another difference between saNOS and $eNOS_{oxy}$ was that hyperactivity was not observed for the saNOS mutants (Table 6). As stated above, the $eNOS_{oxy}$ W180F and W180Y proteins exhibit hyperactivity, as was expected from the structural analysis

indicating weakening of the Fe-NO bond in these mutants. The saNOS proteins also exhibited signs of increased electron density to the thiolate, and yet this was not coupled to the activity of the proteins.

The slight increase in the angle of the dimer interface, coupled with the absence of pterin binding in saNOS, granted greater accessibility to solvent of the D ring propionate.[46] This could decrease the heme reduction potential, and if saNOS possessed a faster rate of Fe(II)NO formation, activity of the mutants would not be affected to the same extent as with eNOS or saNOS. It has also been suggested previously that bacterial NHS enzymes may have a lower affinity for H_2O_2, or that they form an iron-oxy species that is less reactive toward L-NHA than mammalian NOSs.[80]

There was also no significant variation in activity for the saNOS W56/W56F and W56/W56Y heterodimers in comparison to the nitrite production rates observed for the other saNOS proteins. It is not surprising that the activities of the saNOS heterodimers are not distinct, as there were no significant variations in homodimeric activity for comparison. It should be noted, that heterodimers of $iNOS_{oxy}$, demonstrated reduced activity from homodimeric wild-type, when one subunit contained an inactivating mutation.[59] Also, studies involving the oxygenase domain of iNOS have indicated that the two active sites of the NOS_{oxy} dimer functioned independently, as only one heme needed to be reduced for NO synthesis to occur.[15; 104] Interestingly, generating mixed dimers in $iNOS_{oxy}$ containing one wild-type and one W188F subunit, resulted in proteins that could not form stable dimers, leading to the conclusion that the presence of a wild-type subunit cannot repair the deleterious effects of the mutation.[59] These findings suggest that the effects of a structurally deleterious mutation near the dimer interface cannot be restricted to the mutated subunit only, but that if dimerization can occur then

some function may be retained. There have been few heterodimeric studies conducted to fully determine the extent of cooperativity between the subunits, which makes it all the more difficult to reach a conclusion regarding the catalytic fecundity of the saNOS W56 heterodimeric proteins.

It should be mentioned that the rates of nitrate production were not measured, primarily because it is customary to determine only the rates of nitrite production. This is due to the relatively consistent ratio of 0.7-0.85 for nitrite: nitrate production.[76] The reduction of nitrate to nitrite during the H_2O_2-dependent oxidation of L-NHA would enable quantification of total NO production, which may increase the sensitivity of this assay, particularly for saNOS.

Chapter 6. Conclusions

This project has provided evidence for the influence of proximal thiolate electronegativity on the distal heme environment in $eNOS_{oxy}$. The conserved tryptophan residue plays a key role in regulating the basicity of the thiolate through its hydrogen bonding to this group, which may have an indirect effect on the eNOS autoinhibitory mechanism. The presence of H_4B, in addition to L-arginine, enhances non-planarity of the porphyrin ring and increases the stability of the heme through electrostatic interactions, possibly enabling tyrosine to act as a functional replacement for tryptophan in $eNOS_{oxy}$.

The saNOS heterodimers demonstrated that the structural effects of altering the proximal thiolate ligation in one subunit influence the other subunit as well, thereby affecting dimer stability, despite the individual subunits retaining their unique heme environments.

References

1. (1998). Press Release: The 1998 Nobel Prize in Physiology or Medicine. The Nobel Assembly at Karolinska Institutet, Karolinska Institutet.
2. Boucher, J.-L., Moali, C. & Tenu, J. (1999). Nitric oxide biosynthesis, nitric oxide synthase inhibitors and arginase competition for L-arginine utilization. *Cellular and Molecular Life Sciences* **55**, 1015-1028.
3. Granik, V. & Grigor, N. (2002). Nitric oxide synthase inhibitors: biology and chemistry. *Russian Chemical Bulletin, International Edition* **51**, 1973-1995.
4. Alderton, W. K., Cooper, C. E. & Knowles, R. G. (2001). Nitric oxide synthases: structure, function and inhibition. *Biochemical Journal* **357**, 593-615.
5. Busconi, L. & Michel, T. (1993). Endothelial nitric oxide synthase. N-terminal myristoylation determines subcellular localization. **268**, 8410-8413.
6. Nathan, C. & Xie, Q. W. (1994). Regulation of biosynthesis of nitric oxide. **269**, 13725-13728.
7. Li, H., Raman, C., Martasek, P., Masters, B. S. S. & Poulos, T. L. (2001). Crystallographic studies on endothelial nitric oxide synthase complexed with nitric oxide and mechanism-based inhibitors. *Biochemistry* **40**, 5399-5406.
8. Venema, R. C., Sayegh, H. S., Kent, J. D. & Harrison, D. G. (1996). Identification, characterization, and comparison of the calmodulin-binding domains of the endothelial and inducible nitric oxide synthases. *Journal of Biological Chemistry* **271**, 6435-6440.
9. Marletta, M. A. (1994). Nitric-Oxide Synthase - Aspects Concerning Structure and Catalysis. *Cell* **78**, 927-930.
10. Cho, H. J., Xie, Q. W., Calaycay, J., Mumford, R. A., Swiderek, K. M., Lee, T. D. & Nathan, C. (1992). Calmodulin Is a Subunit of Nitric-Oxide Synthase from Macrophages. *Journal of Experimental Medicine* **176**, 599-604.
11. Zhang, J., Martasek, P., Paschke, R., Shea, T., Masters, B. S. S. & Kim, J. J. P. (2001). Crystal structure of the FAD/NADPH-binding domain of rat neuronal nitric-oxide synthase - Comparisons with NADPH-cytochrome P450 oxidoreductase. *Journal of Biological Chemistry* **276**, 37506-37513.
12. Ghosh, D. K., Abu-Soud, H. M. & Stuehr, D. J. (1996). Domains of macrophage NO synthase have divergent roles in forming and stabilizing the active dimeric enzyme. *Biochemistry* **35**, 1444-1449.
13. Abu-Soud, H. M. & Stuehr, D. J. (1993). Nitric Oxide Synthases Reveal a Role for Calmodulin in Controlling Electron Transfer. **90**, 10769-10772.
14. Siddhanta, U., Presta, A., Fan, B. C., Wolan, D., Rousseau, D. L. & Stuehr, D. J. (1998). Domain swapping in inducible nitric-oxide synthase - Electron transfer occurs between flavin and heme groups located on adjacent subunits in the dimer. *Journal of Biological Chemistry* **273**, 18950-18958.
15. Crane, B. R., Arvai, A. S., Gachhui, R., Wu, C., Ghosh, D. K., Getzoff, E. D., Stuehr, D. J. & Tainer, J. A. (1997). The structure of nitric oxide synthase oxygenase domain and inhibitor complexes. *Science* **278**, 425-431.

16. Klatt, P., Pfeiffer, S., List, B. M., Lehner, D., Glatter, O., Bachinger, H. P., Werner, E. R., Schmidt, K. & Mayer, B. (1996). Characterization of heme-deficient neuronal nitric-oxide synthase reveals a role for heme in subunit dimerization and binding of the amino acid substrate and tetrahydrobiopterin. *Journal of Biological Chemistry* **271**, 7336-7342.
17. Hemmens, B., Gorren, A. C. F., Schmidt, K., Werner, E. R. & Mayer, B. (1998). Haem insertion, dimerization and reactivation of haem-free rat neuronal nitric oxide synthase. *Biochemical Journal* **332**, 337-342.
18. Stuehr, D. J. & Ikeda-Saito, M. (1992). Spectral characterization of brain and macrophage nitric oxide synthases. Cytochrome P-450-like hemeproteins that contain a flavin semiquinone radical. **267**, 20547-20550.
19. Li, H., Raman, C., Glaser, C. B., Blasko, E., Young, T. A., Parkinson, J. F., Whitlow, M. & Poulos, T. L. (1999). Crystal structures of zinc-free and -bound heme domain of human inducible nitric-oxide synthase. *Journal of Biological Chemistry* **274**, 21276-21284.
20. Raman, C., Li, H., Martasek, P., Kral, V., Masters, B. S. S. & Poulos, T. L. (1998). Crystal structure of a constitutive endothelial nitric oxide synthase: a paradigm for pterin function involving a novel metal center. *Cell* **95**, 939-950.
21. Crane, B. R., Arvai, A. S., Ghosh, D. K., Wu, C. Q., Getzoff, E. D., Stuehr, D. J. & Tainer, J. A. (1998). Structure of nitric oxide synthase oxygenase dimer with pterin and substrate. *Science* **279**, 2121-2126.
22. Li, H. & Poulos, T. L. (2005). Structure-function studies on nitric oxide synthases. *Journal of Inorganic Biochemistry* **99**, 293-305.
23. Hurshman, A. R. & Marletta, M. A. (2002). Reactions catalyzed by the heme domain of inducible nitric oxide synthase: evidence for the involvement of tetrahydrobiopterin in electron transfer. *Biochemistry* **41**, 3439-3456.
24. Chen, P.-F., Tsai, A.-l., Berka, V. & Wu, K. K. (1996). Endothelial nitric-oxide synthase: evidence for bidomain structure and successful reconstitution of catalytic activity from two separate domains generated by a baculovirus expression system. *Journal of Biological Chemistry* **271**, 14631-14635.
25. Andrew, P. J. & Mayer, B. (1999). Enzymatic function of nitric oxide synthases. *Cardiovascular Research* **43**, 521-531.
26. Poulos, T. L., Finzel, B. C. & Howard, A. J. (1987). High-resolution crystal structure of cytochrome P450cam. *Journal of Molecular Biology* **195**, 687-700.
27. Crane, B. R., Rosenfeld, R. J., Arvai, A. S., Ghosh, D. K., Ghosh, S., Tainer, J. A., Stuehr, D. J. & Getzoff, E. D. (1999). N-terminal domain swapping and metal ion binding in nitric oxide synthase dimerization. *Embo Journal* **18**, 6271-6281.
28. Venema, R. C., Ju, H., Zou, R., Ryan, J. W. & Venema, V. J. (1997). Subunit interactions of endothelial nitric-oxide synthase: comparisons to the neuronal and inducible nitric-oxide synthase isoforms. *Journal of Biological Chemistry* **272**, 1276-1282.
29. Lee, C. M., Robinson, L. J. & Michel, T. (1995). Oligomerization of Endothelial Nitric-Oxide Synthase - Evidence for a Dominant-Negative Effect of Truncation Mutants. *Journal of Biological Chemistry* **270**, 27403-27406.
30. Ghosh, D. K. & Stuehr, D. J. (1995). Macrophage No Synthase - Characterization of Isolated Oxygenase and Reductase Domains Reveals a Head-to-Head Subunit Interaction. *Biochemistry* **34**, 801-807.

31. Abu-Soud, H. M., Loftus, M. & Stuehr, D. J. (1995). Subunit dissociation and unfolding of macrophage NO synthase: relationship between enzyme structure, prosthetic group binding, and catalytic function. *Biochemistry* **34**, 11167-11175.
32. RodriguezCrespo, I., Gerber, N. C. & deMontellano, P. R. O. (1996). Endothelial nitric-oxide synthase - Expression in Escherichia coli, spectroscopic characterization, and role of tetrahydrobiopterin in dimer formation. *Journal of Biological Chemistry* **271**, 11462-11467.
33. Nishida, K., Harrison, D. G., Navas, J. P., Fisher, A. A., Dockery, S. P., Uematsu, M., Nerem, R. M., Alexander, R. W. & Murphy, T. J. (1992). Molecular-Cloning and Characterization of the Constitutive Bovine Aortic Endothelial-Cell Nitric-Oxide Synthase. *Journal of Clinical Investigation* **90**, 2092-2096.
34. Busse, R. & Fleming, I. (1998). Pulsatile stretch and shear stress: Physical stimuli determining the production of endothelium-derived relaxing factors. *Journal of Vascular Research* **35**, 73-84.
35. Lamas, S., Marsden, P. A., Li, G. K., Tempst, P. & Michel, T. (1992). Endothelial Nitric Oxide Synthase: Molecular Cloning and Characterization of a Distinct Constitutive Enzyme Isoform. **89**, 6348-6352.
36. Sessa, W. C., Barber, C. M. & Lynch, K. R. (1993). Mutation of N-Myristoylation Site Converts Endothelial-Cell Nitric-Oxide Synthase from a Membrane to a Cytosolic Protein. *Circulation Research* **72**, 921-924.
37. Liu, J. W., Garciacardena, G. & Sessa, W. C. (1995). Biosynthesis and Palmitoylation of Endothelial Nitric-Oxide Synthase - Mutagenesis of Palmitoylation Sites, Cysteine-15 and/or Cysteine-26, Argues against Depalmitoylation-Induced Translocation of the Enzyme. *Biochemistry* **34**, 12333-12340.
38. Robinson, L. J., Busconi, L. & Michel, T. (1995). Agonist-Modulated Palmitoylation of Endothelial Nitric-Oxide Synthase. *Journal of Biological Chemistry* **270**, 995-998.
39. Shaul, P. W., Smart, E. J., Robinson, L. J., German, Z., Yuhanna, I. S., Ying, Y., Anderson, R. G. W. & Michel, T. (1996). Acylation Targets Endothelial Nitric-oxide Synthase to Plasmalemmal Caveolae. **271**, 6518-6522.
40. Michel, T., Li, G. K. & Busconi, L. (1993). Phosphorylation and Subcellular Translocation of Endothelial Nitric Oxide Synthase. **90**, 6252-6256.
41. Rodriguez-Crespo, I., Moenne-Loccoz, P., Loehr, T. M. & Ortiz de Montellano, P. R. (1997). Endothelial nitric oxide synthase: modulation of the distal heme site produced by progressive N-terminal deletions. *Biochemistry* **36**, 8530-8538.
42. Liu, J. W., GarciaCardena, G. & Sessa, W. C. (1996). Palmitoylation of endothelial nitric oxide synthase is necessary for optimal stimulated release of nitric oxide: Implications for caveolae localization. *Biochemistry* **35**, 13277-13281.
43. Adak, S., Aulak, K. S. & Stuehr, D. J. (2002). Direct Evidence for Nitric Oxide Production by a Nitric-oxide Synthase-like Protein from Bacillus subtilis. **277**, 16167-16171.
44. Gusarov, I. & Nudler, E. (2005). NO-mediated cytoprotection: Instant adaptation to oxidative stress in bacteria. *Proceedings of the National Academy of Sciences of the United States of America* **102**, 13855-13860.
45. Kers, J. A., Wach, M. J., Krasnoff, S. B., Widom, J., Cameron, K. D., Bukhalid, R. A., Gibson, D. M., Crane, B. R. & Loria, R. (2004). Nitration of a peptide phytotoxin by bacterial nitric oxide synthase. *Nature* **429**, 79-82.

46. Bird, L. E., Ren, J., Zhang, J., Foxwell, N., Hawkins, A. R., Charles, I. G. & Stammers, D. K. (2002). Crystal structure of SANOS, a bacterial nitric oxide synthase oxygenase protein from *Staphylococcus aureus*. *Structure* **10**, 1687-1696.
47. Stuehr, D. J., Santolini, J., Wang, Z. Q., Wei, C. C. & Adak, S. (2004). Update on mechanism and catalytic regulation in the NO synthases. *Journal of Biological Chemistry* **279**, 36167-36170.
48. Wei, C. C., Wang, Z. Q., Arvai, A. S., Hemann, C., Hille, R., Getzoff, E. D. & Stuehr, D. J. (2003). Structure of tetrahydrobiopterin tunes its electron transfer to the heme-dioxy intermediate in nitric oxide synthase. *Biochemistry* **42**, 1969-1977.
49. Adak, S., Wang, Q. & Stuehr, D. J. (2000). Molecular basis for hyperactivity in tryptophan 409 mutants of neuronal NO synthase. *Journal of Biological Chemistry* **275**, 17434-17439.
50. Santolini, J., Adak, S., Curran, C. M. L. & Stuehr, D. J. (2001). A kinetic simulation model that describes catalysis and regulation in nitric-oxide synthase. *Journal of Biological Chemistry* **276**, 1233-1243.
51. Santolini, J., Meade, A. L. & Stuehr, D. J. (2001). Differences in three kinetic parameters underpin the unique catalytic profiles of nitric-oxide synthases I, II, and III. *Journal of Biological Chemistry* **276**, 48887-48898.
52. Abu-Soud, H. M., Ichimori, K., Presta, A. & Stuehr, D. J. (2000). Electron transfer, oxygen binding, and nitric oxide feedback inhibition in endothelial nitric-oxide synthase. *Journal of Biological Chemistry* **275**, 17349-17357.
53. Adak, S., Crooks, C., Wang, Q., Crane, B. R., Tainer, J. A., Getzoff, E. D. & Stuehr, D. J. (1999). Tryptophan 409 controls the activity of neuronal nitric-oxide synthase by regulating nitric oxide feedback inhibition. *Journal Of Biological Chemistry* **274**, 26907-26911.
54. Adak, S. & Stuehr, D. J. (2001). A proximal tryptophan in NO synthase controls activity by a novel mechanism. *Journal of Inorganic Biochemistry* **83**, 301-308.
55. Wilson, D. J. & Rafferty, S. P. (2001). A structural role for tryptophan 188 of inducible nitric oxide synthase. *Biochemical and Biophysical Research Communications* **287**, 126-129.
56. Smith, J. C., Siu, K. M. & RAfferty, S. P. (2004). Collisional cooling enhances the ability to observe non-covalent interactions within the inducible nitric oxide synthase oxygenase domain: dimerization, complexation, and dissociation. *Journal of the American Society for Mass Spectrometry* **15**, 629-638.
57. Dunford, A. J., McLean, K. J., Sabri, M., Seward, H. E., Heyes, D. J., Scrutton, N. S. & Munro, A. W. (2007). Rapid P450 heme iron reduction by laser photoexcitation of Mycobacterium tuberculosis CYP121 and CYP51B1 - Analysis of CO complexation reactions and reversibility of the P450/P420 equilibrium. *Journal of Biological Chemistry* **282**, 24816-24824.
58. Xie, Q.-W., Leung, M., Fuortes, M., Sassa, S. & Nathan, C. (1996). Complementation analysis of mutants of nitric oxide synthase reveals that the active site requires two hemes. *Proceedings of the National Academy of Sciences* **93**, 4891-4896.
59. McDonald, J. K., Taylor, C. M. & Rafferty, S. (2003). Design, preparation, and characterization of mixed dimers of inducible nitric oxide synthase oxygenase domains. *Protein Expression And Purification* **27**, 115-127.

60. Bruice, P. Y. (2001). *Organic Chemistry*. Third Edition edit, Prentice-Hall Inc, Upper Saddle River, NJ.
61. Garrett, R. H. & Grisham, C. M. (1999). *Biochemistry*. Second Edition edit, Brooks/Cole, Pacific Grove, CA.
62. Bray, M. R., Carriere, A. D. & Clarke, A. J. (1994). Quantitation of Tryptophan and Tyrosine Residues in Proteins by 4th-Derivative Spectroscopy. *Analytical Biochemistry* **221**, 278-284.
63. Winter, M. J. (1995). *d-Block Chemistry*. Oxford Chemistry Primers, 27, Oxford University Press, USA, New York, NY|.
64. Peisach, J., Blumberg, W. E., Wittenberg, B. A. & Wittenberg, J. B. (1968). The electronic structure of protoheme proteins: III. configuration of the heme and its ligands. *Journal of Biological Chemistry* **243**, 1871-1880.
65. Rousseau, D. L., Li, D., Couture, M. & Yeh, S.-R. (2005). Ligand-protein interactions in nitric oxide synthase. *Journal of Inorganic Biochemistry* **99**, 306-323.
66. Harris, D. & Bertolucci, M. (1989). *Symmetry and Spectroscopy: An Introduction to Vibrational and Electronic Spectroscopy*, Dover Publications, Mineola, NY.
67. Gao, Y. T., Smith, S. M., Weinberg, J. B., Montgomery, H. J., Newman, E., Guillemette, J. G., Ghosh, D. K., Roman, L. J., Martasek, P. & Salerno, J. C. (2004). Thermodynamics of oxidation-reduction reactions in mammalian nitric-oxide synthase isoforms. *Journal of Biological Chemistry* **279**, 18759-18766.
68. Voegtle, H. L., Sono, M., Adak, S., Pond, A. E., Tomita, T., Perera, R., Goodin, D. B., Ikeda-Saito, M., Stuehr, D. J. & Dawson, J. H. (2003). Spectroscopic characterization of five- and six-coordinate ferrous-NO heme complexes. Evidence for heme Fe-proximal cysteinate bond cleavage in the ferrous-NO adducts of the Trp-409Tyr/Phe proximal environment mutants of neuronal nitric oxide synthase. *Biochemistry* **42**, 2475-2484.
69. Chen, Z. C., Ost, T. W. B. & Schelvis, J. P. M. (2004). Phe393 mutants of cytochrome P450BM3 with modified heme redox potentials have altered heme vinyl and propionate conformations. *Biochemistry* **43**, 1798-1808.
70. Skoog, D. A., Holler, F. J. & Nieman, T. A. (1998). *Principles of Instrumental Analysis*, Harcourt Brace College Publishers, Orlando, FL.
71. Wang, J., Caughey, W. S. & Rousseau, D. L. (1996). Resonance Raman Scattering: a Probe of Heme Protein-bound Nitric Oxide. In *Methods in Nitric Oxide Research* (Feelisch, M. & Stamler, J. S., eds.), pp. 428-449. John Wiley & Sons Ltd.
72. Chartier, F. J. & Couture, M. (2004). Stability of the heme environment of the nitric oxide synthase from *Staphylococcus aureus* in the absence of pterin cofactor. *Biophysical Journal* **87**, 1939-1950.
73. Vogel, K. M., Kozlowski, P. M., Zgierski, M. Z. & Spiro, T. G. (1999). Determinants of the FeXO (X = C, N, O) vibrational frequencies in heme adducts from experiment and density functional theory. *Journal of the American Chemical Society* **121**, 9915-9921.
74. Jordan, T., Eads, J. C. & Spiro, T. G. (1995). Secondary and Tertiary Structure of the a-State of Cytochrome-C from Resonance Raman-Spectroscopy. *Protein Science* **4**, 716-728.
75. Jentzen, W., Ma, J. G. & Shelnutt, J. A. (1998). Conservation of the conformation of the porphyrin macrocycle in hemoproteins. *Biophysical Journal* **74**, 753-763.

76. Pufahl, R. A., Wishnok, J. S. & Marletta, M. A. (1995). Hydrogen peroxide-supported oxidation of N^G-hydroxy-L-arginine by nitric oxide synthase. *Biochemistry* **34**, 1930-1941.
77. Sudhamsu, J. & Crane, B. R. (2006). Structure and reactivity of a thermostable prokaryotic nitric-oxide synthase that forms a long-lived oxy-heme complex. *Journal of Biological Chemistry* **281**, 9623-9632.
78. Chartier, F. J. M. & Couture, M. (2007). Interactions between substrates and the haem-bound nitric oxide of ferric and ferrous bacterial nitric oxide synthases. *Biochemical Journal* **401**, 235-245.
79. Li, D., Stuehr, D. J., Yeh, S.-R. & Rousseau, D. L. (2004). Heme distortion modulated by ligand-protein interactions in inducible nitric-oxide synthase. *Journal of Biological Chemistry* **279**, 26489-26499.
80. Adak, S., Bilwes, A. M., Panda, K., Hosfield, D., Aulak, K. S., McDonald, J. F., Tainer, J. A., Getzoff, E. D., Crane, B. R. & Stuehr, D. J. (2002). Cloning, expression, and characterization of a nitric oxide synthase protein from Deinococcus radiodurans. **99**, 107-112.
81. Clague, M. J., Wishnok, J. S. & Marletta, M. A. (1997). Formation of N^{δ}-cyanoornithine from N^G-hydroxy-L-arginine and hydrogen peroxide by neuronal nitric oxide synthase: Implications for mechanism. *Biochemistry* **36**, 14465-14473.
82. Green, L. C., Wagner, D. A., Glogowski, J., Skipper, P. L., Wishnok, J. S. & Tannenbaum, S. R. (1982). Analysis of Nitrate, Nitrite, and [N-15]-Labeled Nitrate in Biological-Fluids. *Analytical Biochemistry* **126**, 131-138.
83. Toal, S. J. & Trogler, W. C. (2006). Polymer sensors for nitroaromatic explosives detection. *Journal of Materials Chemistry* **16**, 2871-2883.
84. McDonald, J. K. (2002). Expression and Purification of Mixed Dimers of the Oxygenase Domain of Inducible Nitric Oxide Synthase, Queen's University.
85. Couture, M., Stuehr, D. J. & Rousseau, D. L. (2000). The ferrous dioxygen complex of the oxygenase domain of neuronal nitric-oxide synthase. *Journal of Biological Chemistry* **275**, 3201-3205.
86. Fan, B., Wang, J., Stuehr, D. J. & Rousseau, D. L. (1997). NO synthase isozymes have distinct substrate binding sites. *Biochemistry* **36**, 12660-12665.
87. Wang, J., Stuehr, D. J. & Rousseau, D. L. (1997). Interactions between substrate analogues and heme ligands in nitric oxide synthase. *Biochemistry* **36**, 4595-4606.
88. Fishel, L. A., Villafranca, J. E., Mauro, J. M. & Kraut, J. (1987). Yeast Cytochrome-C Peroxidase - Mutagenesis and Expression in Escherichia-Coli Show Tryptophan-51 Is Not the Radical Site in Compound-I. *Biochemistry* **26**, 351-360.
89. Goodin, D. B., Mauk, A. G. & Smith, M. (1987). The Peroxide Complex of Yeast Cytochrome-C Peroxidase Contains 2 Distinct Radical Species, Neither of Which Resides at Methionine-172 or Tryptophan-51. *Journal of Biological Chemistry* **262**, 7719-7724.
90. Wang, J., Stuehr, D. J. & Rousseau, D. L. (1995). Tetrahydrobiopterin-deficient nitric oxide synthase has a modified heme environment and forms a cytochrome P 420 analog, Vol. 34, pp. 7080-7087.
91. Yoshioka, S., Takahashi, S., Ishimori, K. & Morishima, I. (2000). Roles of the axial push effect in cytochrome P450cam studied with the site-directed

mutagenesis at the heme proximal site. *Journal of Inorganic Biochemistry* **81**, 141-151.
92. Wang, J., Stuehr, D. J., Ikeda-Saito, M. & Rousseau, D. L. (1993). Heme coordination and structure of the catalytic site in nitric oxide synthase. *Journal of Biological Chemistry* **268**, 22255-22258.
93. Hoffman, B. M. & Gibson, Q. H. (1978). Photosensitivity of Liganded Hemoproteins and Their Metal-Substituted Analogs. *Proceedings of the National Academy of Sciences of the United States of America* **75**, 21-25.
94. Couture, M., Adak, S., Stuehr, D. J. & Rousseau, D. L. (2001). Regulation of the properties of the heme-NO complexes in nitric-oxide synthase by hydrogen bonding to the proximal cysteine. *Journal of Biological Chemistry* **276**, 38280-38288.
95. Obayashi, E., Tsukamoto, K., Adachi, S., Takahashi, S., Nomura, M., Iizuka, T., Shoun, H. & Shiro, Y. (1997). Unique binding of nitric oxide to ferric nitric oxide reductase from Fusarium oxysporum elucidated with infrared, resonance Raman, and X-ray absorption spectroscopies. *Journal of the American Chemical Society* **119**, 7807-7816.
96. Hu, S. Z. & Kincaid, J. R. (1991). Resonance Raman Characterization of Nitric-Oxide Adducts of Cytochrome-P450cam - the Effect of Substrate Structure on the Iron Ligand Vibrations. *Journal of the American Chemical Society* **113**, 2843-2850.
97. Nakamura, M., Ohgo, Y. & Ikezaki, A. (2008). Electronic ground states of low-spin iron(III) porphyrinoids. *Journal of Inorganic Biochemistry* **102**, 433-445.
98. Wang, J. L., Stuehr, D. J. & Rousseau, D. L. (1995). Tetrahydrobiopterin-Deficient Nitric-Oxide Synthase Has a Modified Heme Environment and Forms a Cytochrome P-420 Analog. *Biochemistry* **34**, 7080-7087.
99. Wells, A. V., Li, P., Champion, P. M., Martinis, S. A. & Sligar, S. G. (1992). Resonance Raman investigations of Escherichia coli-expressed Pseudomonas putida cytochrome P450 and P420. *Biochemistry* **31**, 4384-4393.
100. Ueno, T., Nishikawa, N., Moriyama, S., Adachi, S., Lee, K., Okamura, T., Ueyama, N. & Nakamura, A. (1999). Role of the invariant peptide fragment forming NH center dot center dot center dot S hydrogen bonds in the active site of cytochrome P-450 and chloroperoxidase: Synthesis and properties of Cys-containing peptide Fe(III) and Ga(III) (octaethylporphinato) complexes as models. *Inorganic Chemistry* **38**, 1199-1210.
101. Li, H. Y., Igarashi, J., Jamal, J., Yang, W. P. & Poulos, T. L. (2006). Structural studies of constitutive nitric oxide synthases with diatomic ligands bound. *Journal of Biological Inorganic Chemistry* **11**, 753-768.
102. Ogura, T., Yoshikawa, S. & Kitagawa, T. (1989). Raman Absorption Simultaneous Measurements for Cytochrome-Oxidase Compound-a at Room-Temperature with a Novel Flow Apparatus. *Biochemistry* **28**, 8022-8027.
103. Presta, A., Weber-Main, A. M., Stankovich, M. T. & Stuehr, D. J. (1998). Comparative effects of substrates and pterin cofactor on the heme midpoint potential in inducible and neuronal nitric oxide synthases. *Journal of the American Chemical Society* **120**, 9460-9465.
104. Stuehr, D. J. (1997). Structure-function aspects in the nitric oxide synthases. *Annual Review of Pharmacology and Toxicology* **37**, 339-359.

105. Hoard, K. F. (2002). Design and Isolation of Endothelial Nitric Oxide Synthase Oxygenase Domain Mixed Dimers, Trent University.

Appendix A: Vectors

Three vector backbones were used in this project: pET 23a (Figure 42), and pET 30b (Figure 43), and pET 9h. The pET 9h and pET 30b vectors conferred kanamycin resistance, and pET 23a conferred ampicillin resistance. The pET 23a and pET 30b vectors possessed C-terminal His_6 tags, and pET 9h possessed a C-terminal Glu_7 tag.

The $eNOS_{oxy}$ coding sequences coding sequences are flanked by restriction sites for Nde1 and Xho1. The pET 9a (Figure 44) vector contains a restriction site for Xho1, and thus the removal of this restriction site through site directed mutagenesis produced the pET 9h vector.[105]

pET-23a-d(+) Vectors

TB051 12/98

	Cat. No.
pET-23a DNA	69745-3
pET-23b DNA	69746-3
pET-23c DNA	69747-3
pET-23d DNA	69748-3

The pET-23a-d(+) vectors carry an N-terminal T7• Tag® sequence plus an optional C-terminal His• Tag® sequence. These vectors differ from pET-21a-d(+) by the "plain" T7 promoter instead of the T7*lac* promoter and by the absence of the *lacI* gene. Unique sites are shown on the circle map. Note that the sequence is numbered by the pBR322 convention, so the T7 expression region is reversed on the circular map. The cloning/expression region of the coding strand transcribed by T7 RNA polymerase is shown below. The f1 origin is oriented so that infection with helper phage will produce virions containing single-stranded DNA that corresponds to the coding strand. Therefore, single-stranded sequencing should be performed using the T7 terminator primer (Cat. No. 69337-3).

pET-23a(+) sequence landmarks	
T7 promoter	303-319
T7 transcription start	302
T7• Tag coding sequence	207-239
Multiple cloning sites	
(*Bam*H I - *Xho* I)	158-203
His• Tag coding sequence	140-157
T7 terminator	26-72
pBR322 origin	1450
bla coding sequence	2211-3068
f1 origin	3200-3655

The maps for pET-23b(+), pET-23c(+) and pET-23d(+) are the same as pET-23a(+) (shown) with the following exceptions: pET-23b(+) is a 3665bp plasmid; subtract 1bp from each site beyond *Bam*H I at 198. pET-23c(+) is a 3664bp plasmid; subtract 2bp from each site beyond *Bam*H I at 198. pET-23d(+) is a 3663bp plasmid; the *Bam*H I site is in the same reading frame as in pET-23c(+). An *Nco* I site is substituted for the *Nde* I site with a net 1bp deletion at position 238 of pET-23c(+). As a result, *Nco* I cuts pET-23d(+) at 234, and *Nhe* I cuts at 229. For the rest of the sites, subtract 3bp from each site beyond position 239 in pET-23a(+). *Nde* I does not cut pET-23d(+). Note also that *Sty* I is not unique in pET-23d(+).

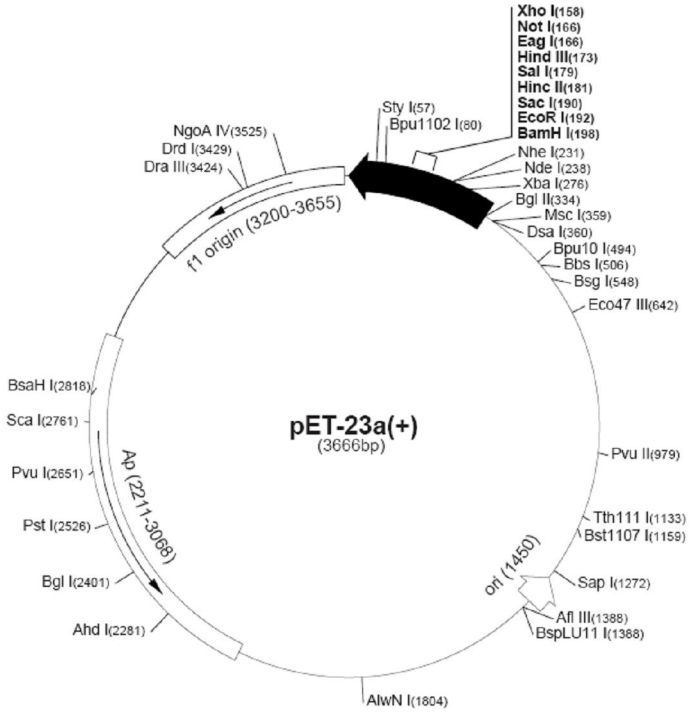

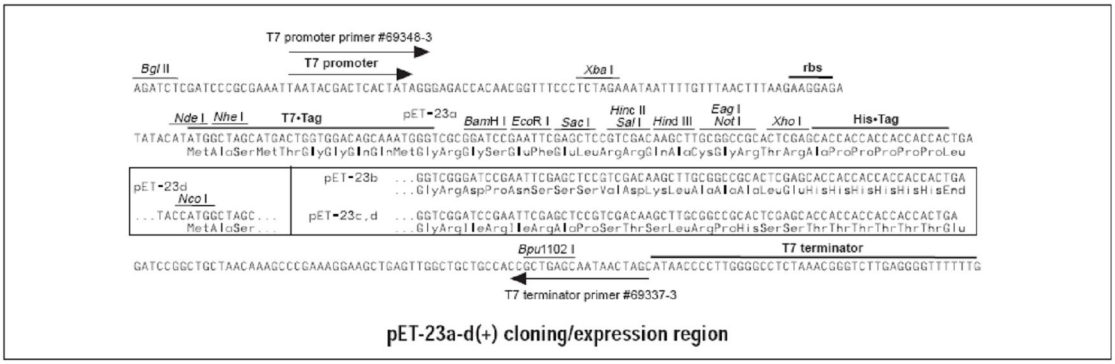

Figure 42. The vector map for pET 23a.

(Novagen. Available at http://www.emdbiosciences.com/docs/docs/PROT/TB051.pdf)

pET-30a-c(+) Vectors

TB095 12/98

	Cat. No.
pET-30a DNA	69909-3
pET-30b DNA	69910-3
pET-30c DNA	69911-3

The pET-30a-c(+) vectors carry an N-terminal His• Tag®/thrombin/S• Tag™/enterokinase configuration plus an optional C-terminal His• Tag sequence. Unique sites are shown on the circle map. Note that the sequence is numbered by the pBR322 convention, so the T7 expression region is reversed on the circular map. The cloning/expression region of the coding strand transcribed by T7 RNA polymerase is shown below. The f1 origin is oriented so that infection with helper phage will produce virions containing single-stranded DNA that corresponds to the coding strand. Therefore, single-stranded sequencing should be performed using the T7 terminator primer (Cat. No. 69337-3).

pET-30a(+) sequence landmarks	
T7 promoter	419-435
T7 transcription start	418
His• Tag coding sequence	327-344
S• Tag coding sequence	249-293
Multiple cloning sites	
(*Nco* I - *Xho* I)	158-217
His• Tag coding sequence	140-157
T7 terminator	26-72
lacI coding sequence	826-1905
pBR322 origin	3339
Kan coding sequence	4048-4860
f1 origin	4956-5411

The maps for pET-30b(+) and pET-30c(+) are the same as pET-30a(+) (shown) with the following exceptions: pET-30b(+) is a 5421bp plasmid; subtract 1bp from each site beyond *Bam*H I at 198. pET-30c(+) is a 5423bp plasmid; add 1bp to each site beyond *Bam*H I at 198.

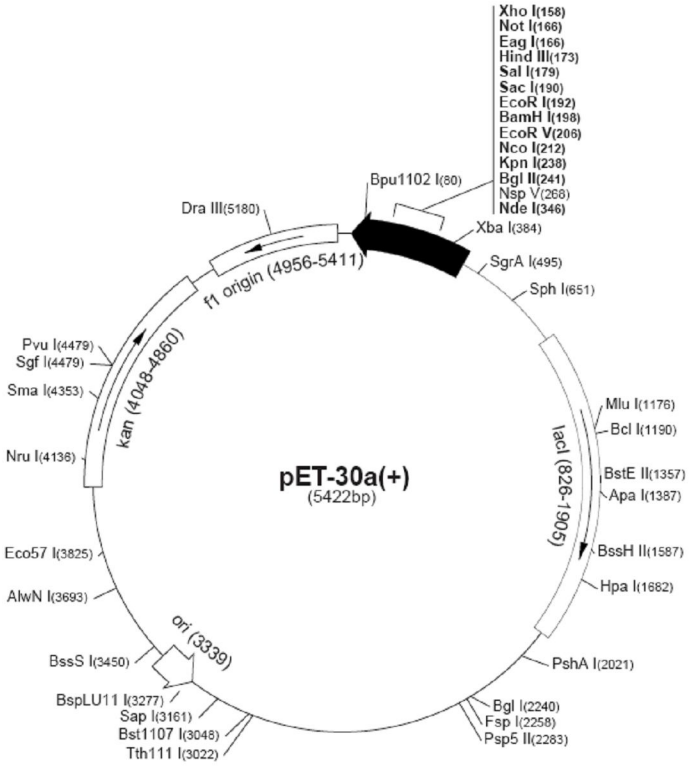

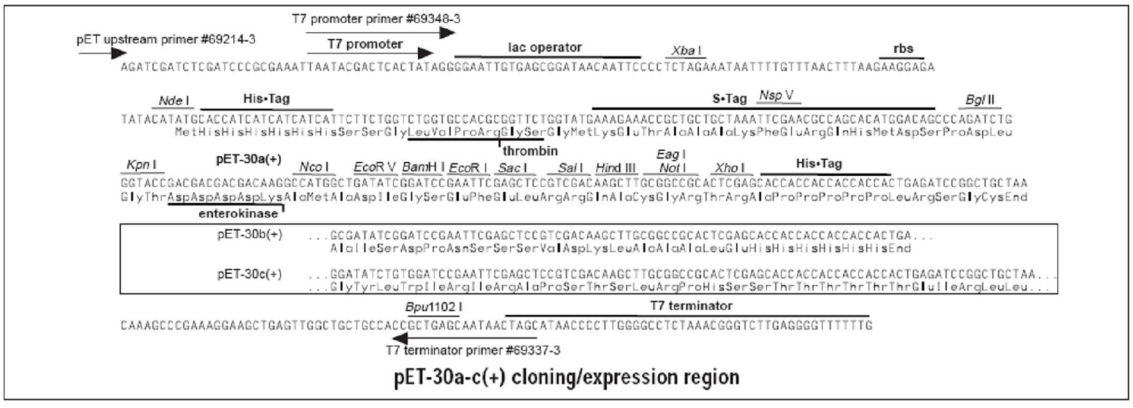

Figure 43. The vector map for pET 30b.

(Novagen. Available at http://www.emdbiosciences.com/docs/docs/PROT/TB095.pdf)

pET-9a-d Vectors

	Cat. No.
pET-9a DNA	69431-3
pET-9b DNA	69432-3
pET-9c DNA	69433-3
pET-9d DNA	69434-3

The pET-9a-d(+) vectors carry an N-terminal T7•Tag® sequence and *Bam*H I cloning site. These vectors are the precursors to many pET family vectors. Unique sites are shown on the circle map. Note that the sequence is numbered by the pBR322 convention, so the T7 expression region is reversed on the circular map. The cloning/expression region of the coding strand transcribed by T7 RNA polymerase is shown below.

pET-9a sequence landmarks

T7 promoter	615-631
T7 transcription start	614
T7•Tag coding sequence	519-551
T7 terminator	404-450
pBR322 origin	2814
kan coding sequence	3523-4335

The maps for pET-9b, pET-9c and pET-9d are the same as pET-9a (shown) with the following exceptions: pET-9b is a 4340bp plasmid; subtract 1bp from each site beyond *Bam*H I at 510. pET-9c is a 4339bp plasmid; subtract 2bp from each site beyond *Bam*H I at 510. pET-9d is a 4338bp plasmid; the *Bam*H I site is in the same reading frame as in pET-9c. An *Nco* I site is substituted for the *Nde* I site with a net 1bp deletion at position 550 of pET-9c. As a result, *Nco* I cuts pET-9d at 546. For the rest of the sites, subtract 3bp from each site beyond position 551 in pET-9a. *Nde* I does not cut pET-9d.

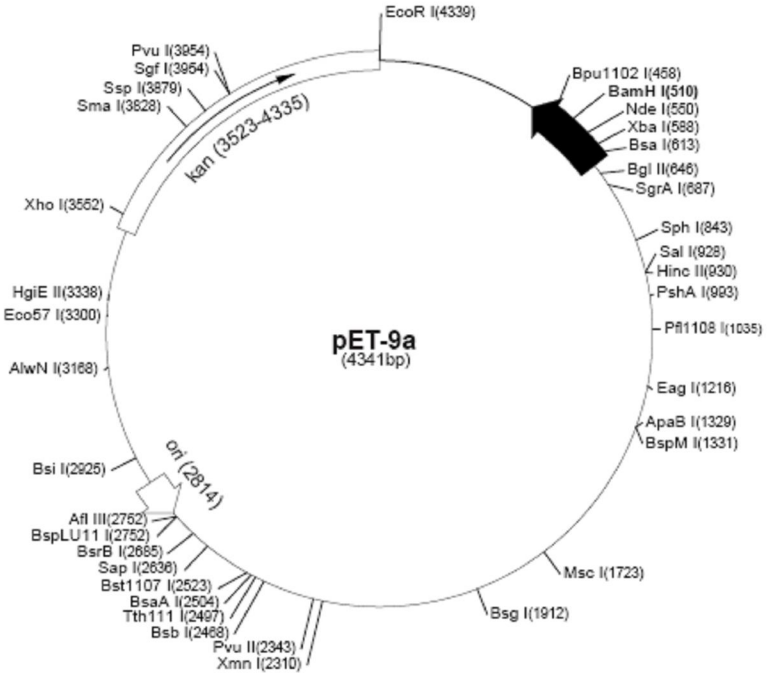

Figure 44. The vector map for pET 9a, from which pET 9h was previously derived. (Novagen. Available at http://www.emdbiosciences.com/docs/docs/PROT/TB040.pdf)

Appendix B: Buffer Recipes

eNOS Ni-NTA Lysis Buffer

50 mM Tris-HCl (pH 7.5)
500 mM NaCl
10% (v/v) glycerol
5 mM L-arginine
(1 mM H_4B)

eNOS Ni-NTA Wash Buffer

50 mM Tris-HCl (pH 7.5)
500 mM NaCl
10% (v/v) glycerol
5 mM L-arginine

eNOS Ni-NTA Elution Buffer

50 mM Tris-HCl (pH 7.5)
500 mM NaCl
10% (v/v) glycerol
5 mM L-arginine
200 mM imidazole

saNOS Ni-NTA Lysis Buffer

50 mM HEPES (pH 7.5)
150 mM NaCl
5 mM L-arginine

saNOS Ni-NTA Wash Buffer

50 mM HEPES (pH 7.5)
150 mM NaCl
5 mM L-arginine
20 mM imidazole

saNOS Ni-NTA Elution Buffer

20 mM imidazole
50 mM HEPES (ph 7.5)
150 mM NaCl
5 mM L-arginine
200 mM imidazole

saNOS AEC Starting Buffer

25 mM Bis-Tris (pH 6.5)
100 mM NaCl

saNOS AEC Elution Buffer

25 mM Bis-Tris (pH 6.5)
1 M NaCl